



# **BRNO UNIVERSITY OF TECHNOLOGY**

VYSOKÉ UČENÍ TECHNICKÉ V BRNĚ

## **FACULTY OF CIVIL ENGINEERING**

FAKULTA STAVEBNÍ

## **INSTITUTE OF CHEMISTRY**

ÚSTAV CHEMIE

# **MODIFICATION OF THE PROPERTIES OF ALKALI ACTIVATED ALUMINOSILICATES BY POLYMER ADMIXTURES**

MODIFIKACE VLASTNOSTÍ ALKALICKY AKTIVOVANÝCH ALUMINOSILIKÁTŮ POLYMERNÍMI  
PŘISADAMI

## **DOCTORAL THESIS**

DIZERTAČNÍ PRÁCE

### **AUTHOR**

AUTOR PRÁCE

**Ing. Olesia Mikhailova**

### **SUPERVISOR**

VEDOUCÍ PRÁCE

**doc. RNDr. PAVEL ROVNANÍK, Ph.D.**

**BRNO 2022**

## ABSTRACT

Currently, the concrete industry utilizes Portland cement (PC) widely, whose production has a significant environmental impact, while it is also a non-sustainable process. Efforts towards a greener building industry involve employing several aluminosilicate materials that can be either by-products obtained from other industrial activities, such as granulated blast furnace slag, silica fume, and fly ash, or materials derived from less energy-intensive industrial processes, such as metakaolin. Using these materials in the preparation of building materials also contributes to reduced production costs.

Activation of aluminosilicate materials by alkaline activators leads to high-strength materials that can be considered an alternative to ordinary Portland cement (OPC). Despite the numerous advantages of alkali-activated aluminosilicates (AAA), a major drawback is the significant autogenous and drying shrinkage that might occur during the material's hardening. This phenomenon leads to microcracking and deterioration of mechanical fracture properties. Polymer admixtures can modify the properties of the fresh and hardened AAA material and overcome the abovementioned problems.

This thesis investigates the influence of polymer admixtures, in different amounts by weight of the aluminosilicate binder, on reducing shrinkage and fragility and increasing fracture toughness. Polyethylene glycol (PEG), Polypropylene glycol (PPG), and different types of commercial polymers of the Vinnapas<sup>®</sup> - family of dispersible polymer powders were selected as polymer admixtures. Their effect on the properties of the obtained materials was compared with that of powder shrinkage reducer Peramin SRA 40. The specimens were tested for flexural and compressive strength, and their microstructure was investigated employing mercury intrusion porosimetry and scanning electron microscopy

One of the chapters of the thesis deals with the study of different analytical techniques for the characterization of main reaction products in alkali activated slag (AAS), such as X-ray diffraction, Fourier-transformed infrared spectroscopy, and Confocal Raman microscopy techniques. This study was carried out during the internship program "Erasmus+" in Madrid, Instituto de Cerámica y Vidrio, Spain.

The results showed several correlations between the admixtures' type/amount and the aluminosilicates binder's properties. The study reveals that incorporating organic polymers into AAA systems affects the composite's rheology and ultimate mechanical properties. In AAS systems – 1 % of PPG is the most effective admixture in reducing linear shrinkage, specimens with 1 % of Peramin SRA and 1 and 2 % of PPG have the best mechanical fracture properties. The most brittle specimens are the mixture with 1 % of PEG 1000 and 2 % of Peramin SRA. In geopolymer systems, the additions of PEG 400 and Vinnapas<sup>®</sup> 7016F introduce the best mechanical performance.

## KEYWORDS

Alkali activated materials, geopolymers, slag, metakaolin, polymer admixtures

## ABSTRAKT

V současné době se v betonářském průmyslu ve velké míře používá portlandský cement (PC), jehož výroba má značný dopad na životní prostředí a zároveň se jedná o neudržitelný proces. Snahy o ekologičtější stavebnictví zahrnují využití několika aluminosilikátů, které mohou být buď odpadními produkty získanými z jiných průmyslových výroby, jako je granulovaná vysokopecní struska, popílek a křemičitá dýmka, nebo materiály pocházející z energeticky méně náročných průmyslových procesů, jako je metakaolin. Použití těchto materiálů při výrobě stavebních materiálů rovněž přispívá ke snížení výrobních nákladů.

Aktivace aluminosilikátových materiálů alkalickými aktivátory vede k získání vysoce pevných materiálů, které lze považovat za alternativu běžného PC. Navzdory mnoha výhodám alkalicky aktivovaných aluminosilikátů (AAA) existuje zásadní nevýhoda, která se týká výrazného autogenního smršťování a smršťování při vysoušení, k němuž může docházet během tuhnutí materiálu. Tento jev vede k mikrotrhlinám a zhoršení mechanických lomových vlastností. Polymerní příměsi mohou modifikovat vlastnosti čerstvého a vytvrzeného materiálu AAA a překonat výše uvedené problémy.

Tato disertační práce se zabývá vlivem polymerních přísad v různých hmotnostních množstvích aluminosilikátového pojiva na snižování smrštění a křehkosti a na zvýšení lomové houževnatosti. Jako polymerní příměsi byly vybrány polyetylen glykol (PEG), polypropylen glykol (PPG) a různé typy komerčních polymerů z řady dispergovatelných polymerních prášků Vinnapas<sup>®</sup>. Jejich vliv na vlastnosti získaných materiálů byl porovnáván s vlivem práškového přípravku proti smrštění Peramin SRA 40. Vzorky byly testovány na pevnost v ohybu a tlaku a jejich mikrostruktura byla zkoumána pomocí rtuťové porozimetrie a skenovací elektronové mikroskopie.

Jedna z kapitol práce se zabývá studiem různých charakterizačních technik vzniku hlavních reakčních produktů v alkalicky aktivované strusce, jako jsou RTG difrakční analýza, Fourierovou transformovanou infračervenou spektroskopií a techniky Konfokální Ramanovy mikroskopie. Tato studie byla provedena během stáže v rámci programu "Erasmus+" v Madridu, Instituto de Cerámica y Vidrio, Španělsko.

Výsledky tohoto výzkumu ukázaly několik závislostí mezi typem a množstvím přísad a vlastnostmi aluminosilikátového pojiva. Studie ukazuje, že přidání organických polymerů do systémů AAA ovlivňuje reologii a konečné mechanické vlastnosti kompozitu. V systémech AAS - 1 % PPG je nejúčinnější přísadou při snižování lineárního smršťování, vzorky s 1 % Peramin SRA a 1 a 2 % PPG mají nejlepší mechanické lomové vlastnosti. Nejkréhčí jsou vzorky s 1 % PEG 1000 a 2 % Peraminu SRA. V případě geopolymerních systémů přinášejí nejlepší mechanické vlastnosti přísady PEG 400 a Vinnapas<sup>®</sup> 7016F.

## KLÍČOVÁ SLOVA

Alkalicky aktivované materiály, geopolymery, struska, metakaolin, polymerní přísady

## **BIBLIOGRAPHIC CITATION**

Ing. Olesia Mikhailova *Modification of the properties of alkali activated aluminosilicates by polymer admixtures*. Brno, 2022. 84 s., Doctoral thesis. Brno University of Technology, Faculty of Civil Engineering, Institute of Chemistry. Supervisor doc. RNDr. Pavel Rovnaník, Ph.D.

## **DECLARATION OF CONFORMITY OF THE PRINTED AND ELECTRONIC FORM OF THE FINAL THESIS**

I declare that the electronic form of the submitted doctoral thesis titled Modification of the properties of alkali activated aluminosilicates by polymer admixtures is identical to the submitted printed form.

Brno, 31. 8. 2022

---

Ing. Olesia Mikhailova

## **DECLARATION OF AUTHORSHIP OF THE FINAL THESIS**

I declare that this doctoral thesis titled Modification of the properties of alkali activated aluminosilicates by polymer admixtures is my own work and the result of my own original research. I have clearly indicated the presence of quoted or paraphrased material and provided references for all sources.

Brno 31. 8. 2022

---

Ing. Olesia Mikhailova

## **ACKNOWLEDGEMENT**

I would like sincerely thank doc. RNDr. Pavel Rovnaník, Ph.D., for supervising my work, for his support and advice during my doctoral program, and for including me as a team member in his research projects.

I would also like to thank the other colleagues from the Institute of Chemistry and other doctoral students from our faculty for their help, cooperation, and support.

Next, I would also like to thank the Ceramic and Glass Institute (ICV-CSIC) team in Madrid, Spain, where I spent three months during my Erasmus Internship. I appreciated working as a part of their team. Special thanks go to M. Torres-Carrasco.

Finally, I would like to thank my family and friends for supporting me emotionally and believing in me whenever I needed it.

# CONTENT

1	INTRODUCTION.....	3
2	THEORETICAL PART .....	4
2.1	HISTORICAL REVIEW .....	4
2.2	ALKALI AKTIVATED SLAG .....	6
2.2.1	<i>Ground blast furnace slag (GBFS)</i> .....	6
2.2.2	<i>Reaction mechanism and hydration products</i> .....	7
2.2.3	<i>Characterization of main reaction products in alkali-activated slag materials</i> ....	10
2.3	METAKAOLIN BASED GEOPOLYMERS .....	10
2.3.1	<i>Metakaolin</i> .....	10
2.3.2	<i>Reaction mechanism and hydration products</i> .....	11
2.4	ACTIVATORS .....	13
2.5	POLYMER ADMIXTURES .....	15
2.5.1	<i>Classification of admixtures</i> .....	15
2.5.2	<i>Polymer admixtures as modifiers in cementitious binders</i> .....	18
2.5.3	<i>Polymer admixtures as modifiers in alkali-activated aluminosilicates</i> .....	25
3	AIM OF THESIS.....	28
4	ALKALI ACTIVATED SLAG.....	29
4.1	MATERIALS, PREPARATION AND TESTING .....	29
4.1.1	<i>Materials</i> .....	29
4.1.2	<i>Alkaline activators</i> .....	29
4.1.3	<i>Aggregates</i> .....	29
4.1.4	<i>Polymer admixtures</i> .....	29
4.1.5	<i>Preparation of AAS mortars: Mixing, molding, curing</i> .....	30
4.1.6	<i>Compressive and flexural strength tests</i> .....	31
4.1.7	<i>Shrinkage tests</i> .....	31
4.1.8	<i>Acoustic emission</i> .....	31
4.1.9	<i>Mechanical fracture properties</i> .....	31
4.1.10	<i>Porosimetry</i> .....	32
4.1.11	<i>The scanning electron microscope - microstructure assessment</i> .....	32
4.1.12	<i>Infrared spectroscopy</i> .....	32
4.1.13	<i>Rheology tests - workability assessment.</i> .....	32
4.1.14	<i>Isothermal calorimetry - reaction kinetics</i> .....	33
4.1.15	<i>X-ray diffraction (XRD) - phase assemblage</i> .....	33
4.1.16	<i>Thermogravimetric analysis (TG) - phase assemblage</i> .....	33
4.1.17	<i>Confocal Raman Microscopy (CRM) - phase distribution</i> .....	33
4.2	RESULTS AND DISCUSSION .....	34
4.2.1	<i>Determination of the main reaction products of AAS: FTIR, XRD, TG and Confocal Raman Microscopy</i> .....	34
4.2.2	<i>Stability of admixtures</i> .....	42
4.2.3	<i>Rheological tests</i> .....	47
4.2.4	<i>Isothermal calorimetry</i> .....	50
4.2.5	<i>Mechanical properties</i> .....	52
4.2.6	<i>Shrinkage</i> .....	54
4.2.7	<i>Porosity</i> .....	55
4.2.8	<i>Fracture tests</i> .....	55

4.2.9	<i>Acoustic emission</i> .....	58
4.2.10	<i>Microstructure</i> .....	58
4.2.11	<i>Efflorescence</i> .....	59
5	METAKAOLIN GEOPOLYMER.....	60
5.1.1	<i>Mortars preparation</i> .....	60
5.1.2	<i>Mechanical properties</i> .....	60
5.1.3	<i>Porosity</i> .....	62
5.1.4	<i>Microstructure</i> .....	64
5.1.5	<i>Efflorescence</i> .....	64
6	CONCLUSIONS.....	69
7	LITERATURE .....	71
	LIST OF USED ABBREVIATIONS .....	82
	LIST OF SELECTED PUBLICATIONS .....	83
	ABOUT AUTHOR .....	84

# 1 INTRODUCTION

Concrete is the most widely used construction material in the world. The production of PC used in concrete requires a significant amount of energy input and causes various environmental problems (e.g. emission of greenhouse gases such as CO<sub>2</sub>) [1, 2].

Each year concrete industry produces approximately 12 billion tons of concrete and uses about 1.6 billion tons of PC worldwide [3]. Cement production is increasing by about 3 % annually [4]. In addition, cement production consumes considerable amounts of raw materials (limestone and clay). Indeed, with the manufacture of 1 ton of cement, approximately 0.94 tons of CO<sub>2</sub> are emitted into the atmosphere [5].

In light of these problems, the scientific community seeks new processes, technologies and materials to provide the construction industry with alternative binders.

One alternative is the use of alkaline activation. Nowadays, alkaline activation is a globally growing technology involving a chemical reaction between a solid aluminosilicate precursor and an alkaline activator at room temperature, giving a hardened product. Industrial by-products, such as granulated blast furnace slag (derived from the steel-making industry), fly-ash (derived from coal combustion), and calcined natural clays (metakaolin) are used, among others, as main precursors for the production of alkali-activated materials [6].

In addition, there are numerous advantages of this AAA system, such as lower heat of hydration [7], early development of higher strength [8, 9], better resistance to chemical attack [10, 11] and chloride diffusion [12], freeze-thaw resistance [13], fire resistance [14, 15], and stronger aggregate–matrix interface formation [16, 17]. On the contrary, the AAA system presents some drawbacks such as rapid setting periods [18], higher shrinkage values [19], higher formation of salt efflorescence [20], higher carbonation [21], and a tendency to crack during setting [22, 23].

Researchers have tried to solve some of these problems by using different additives in the AAA system. Consequently, one of the main objectives of this thesis is to investigate the influence of different types of admixtures on the properties of AAA mortars considering their different dosage aiming to increase the toughness and reduce the brittleness of the hardened AAA mortars.

In conclusion, it should be noted that granulated blast furnace slag and metakaolin are suitable precursors to produce alkali-activated materials that can perform as a sole binder in the production of mortars and concretes. These materials can show high strength, low permeability, high resistance to acidic attack and good retention of mechanical strength when exposed to high temperature, with comparable or even superior performance to what has been identified for reference materials based on Portland cement.

## 2 THEORETICAL PART

### 2.1 HISTORICAL REVIEW

The development of alkali activated binders had a significant contribution in the 1940s with the work of Belgian scientist Purdon [24], who tested more than 30 different blast furnace slags activated by NaOH solution as well as by combinations of  $\text{Ca}(\text{OH})_2$  and different sodium salts and achieved rates of strength development and final strengths comparable to those of Portland cement [25]. Victor Glukhovskiy, a Ukrainian scientist at the KICE (Kyiv Institute of Civil Engineering in the former USSR), discovered that sodium aluminosilicate hydrates (zeolites) are created from rocks and clay minerals during alkali treatment. He called these materials “soil silicate concretes” and “soil cement” [26]. The word soil is used because it seems like a ground rock, and the word cement due to its cementitious capacity. The “soil cement” was obtained from ground aluminosilicate mixed with rich in alkalis industrial wastes [27].

In 1972, a technology based on geosynthesis, natural kaolinite/quartz blended with mixed solid sodium hydroxide and water, was developed at CORDI laboratory in Saint-Quentin, France [28]. A significant contribution to the development and implementation of geopolymer composites was provided by the extensive research by Prof. Waltraud M. Kriven [29].

Investigations in the field of alkaline activation had an exponential increase after the research results by the French author Davidovits [27]. He developed and patented binders obtained from the alkaline activation of metakaolin, describing them with the term “geopolymer” in 1978.

In the Czech Republic, the research of alkali-activated materials (AAM) as a structural material was introduced by prof. Brandštetr from the Brno University of Technology in the early 1980s [30].

František Škvára from the Institute of Chemical Technology, Prague Department of Glass and Ceramics, has investigated the problems associated with alkaline activation since 1973. The attention has been focused on processes of alkaline activation of Portland cements, ground Portland cement clinker, blast-furnace slags, kaolinite materials and other inorganic wastes [31]. Table 1 presents the most important historical events in the development of AAM [32].

**Table 1.** Bibliographic listing of some important events in the history.

Author	Year	Significance
Feret	1939	Slags used for cement
Purdon	1940	Alkali-slag combinations
Glukhovskiy	1959	Theoretical basis and development of alkaline cements
Glukhovskiy	1965	First called “alkaline cement”
Davidovits	1979	“Geopolymer” term
Lanoton and Roy	1984	Ancient building materials characterized
Davidovits and Sawyer	1985	Patent of 'Pyrament' cement

Krivenko	1986	DSc Thesis. $R_2O-RO-SiO_2-H_2O$
Malck <i>et al.</i>	1986	Slag cement-low level radioactive wastes forms
Davidovits	1987	Ancient and modern concretes compared
Majundar <i>et al.</i>	1989	$C_{12}A_7$ – slag activation
Talling and Brandštetr	1989	Alkali-activated slag
Wu <i>et al.</i>	1990	Activation of slag cement
Roy <i>et al.</i>	1991	Rapid setting alkali-activated cements
Roy and Silsbee	1992	Alkali-activated cements: an overview
Palomo and Glasser	1992	CBC with metakaolin
Roy and Malek	1993	Slag cement
Glukhovsky	1994	Ancient, modern and future concretes
Krivenko	1994	Alkaline cements
Wang and Scrivener	1995	Slag and alkali-activated microstructure
Shi	1996	Strength, pore structure and permeability of alkali-activated slag
Femandez-Jimenez and Puertas	1997	Kinetic studies of alkali-activated slag cements
Katz	1998	Microstructure of alkali-activated fly ash
Davidovits	1999	Chemistry of copolymeric systems, technology
Roy	1999	Opportunities and challenges of alkali-activated cements
Palomo	1999	Alkali-activated fly ash - a cement for the future
Gong and Yang	2000	Alkali-activated red mud-slag cement
Puertas	2000	Alkali-activated fly ash/slag cement
Bakharev	2001–2002	Alkali-activated slag concrete
Duxson <i>et al.</i>	2007	Geopolymer technology: the current state of the art
Provis and van Deventer	2009	Geopolymers: structure, processing, properties and industrial applications

## 2.2 ALKALI AKTIVATED SLAG

### 2.2.1 Ground blast furnace slag (GBFS)

Slags are by-products of the metallurgical industry and consist mainly of lime, calcium, and magnesium aluminosilicates. The most common slag is produced in the iron and steel industry, so-called blast-furnace slag [33], defined as the glassy granular material formed when molten blast-furnace slag is rapidly chilled by immersion in water [34].

Blast-furnace slag is formed as a liquid at 1350–1550 °C during iron production; limestone reacts with matter rich in SiO<sub>2</sub> and Al<sub>2</sub>O<sub>3</sub> associated with the ore or present in ash from the coke. Cooling rapidly enough to the temperature below 800 °C forms a glass, a latent hydraulic cement. Cooling is most often affected by spraying droplets of the molten slag with high-pressure jets of water. This gives a wet, sandy material which, when dried and the ground, is called ground granulated blast-furnace slag (GBFS) and often contains over 95% of glass [35] with a fineness of 400 to 700 m<sup>2</sup>/kg Blaine [36]. Fig. 1 shows the slag particles observed with SEM.

The major oxides in the GBFS are lime (CaO), silica (SiO<sub>2</sub>), alumina (Al<sub>2</sub>O<sub>3</sub>), magnesia (MgO) and some others (SO<sub>3</sub>, FeO or Fe<sub>2</sub>O<sub>3</sub>, TiO<sub>2</sub>, K<sub>2</sub>O, Na<sub>2</sub>O, etc.) in minor amounts. While the oxide composition can vary from one blast furnace to another, the slag from one blast furnace remains relatively consistent. Compared to the typical oxide composition of clinker, GBFS generally contains less lime, more silica, alumina and magnesia than clinker. Typical blast-furnace slag contains alkalines (Na<sup>+</sup>, K<sup>+</sup>) at a mild level, and if quenched with sea water, the alkali level could be relatively high [37].

The composition of the slag must be controlled within relatively narrow limits to ensure satisfactory and economic operation of the blast furnace and depends on that of the ore. It, therefore, varies considerably between plants, but that of a given plant is unlikely to vary much unless the source of the ore is changed [38]. Table 2 gives mean values and deviations for slags typical of those produced in Western Europe. For a broader range of steel-producing countries, the contents of major components are MgO, 0–21 %; Al<sub>2</sub>O<sub>3</sub>, 5– 33 %; SiO<sub>2</sub>, 27–42 %; and CaO. 30–50 %.

**Table 2.** Chemical compositions of some blast-furnace slags [39].

	Mean	Minimum	Maximum		Mean	Minimum	Maximum
Na <sub>2</sub> O	0.39	0.25	0.50	TiO <sub>2</sub>	0.55	0.49	0.65
MgO	5.99	3.63	8.66	MnO	0.64	0.34	1.31
Al <sub>2</sub> O <sub>3</sub>	13.29	10.26	16.01	FeO	1.24	0.29	9.32
SiO <sub>2</sub>	33.48	31.96	37.29	S <sup>2-</sup>	0.94	0.68	1.25
P <sub>2</sub> O <sub>5</sub>	0.13	0.00	0.34	F <sup>-</sup>	0.16	0.06	0.31
SO <sub>3</sub>	0.04	0.00	0.19	Cl <sup>-</sup>	0.02	0.003	0.05
K <sub>2</sub> O	0.70	0.44	0.98	Ign. Loss	0.42	0.00	1.04
CaO	42.24	37.92	44.38	Total	99.68		

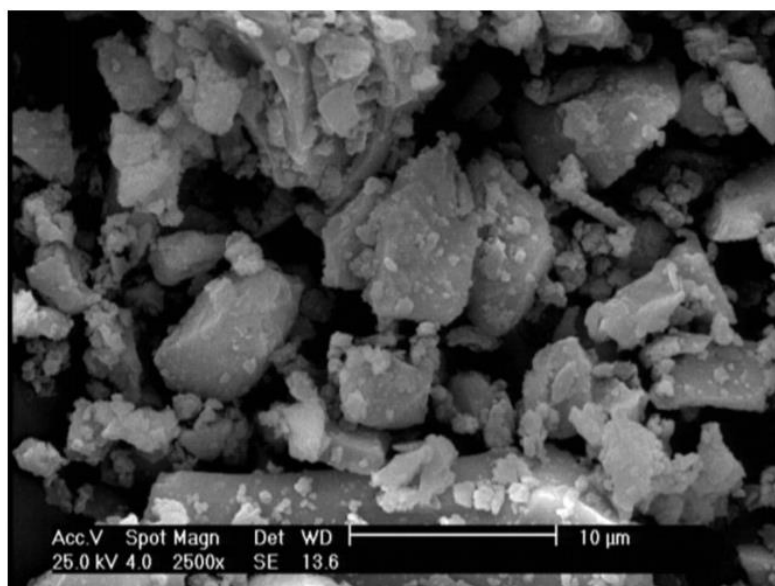


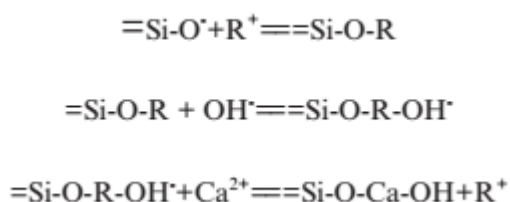
**Fig. 1** SEM photo of slag particles [40].

### 2.2.2 Reaction mechanism and hydration products

The slag is known for its latent hydraulic property, i.e., it is reactive with water, but only at such a slow rate that it is normally mixed with activators, which can remarkably accelerate the reaction of slag [41]. The most commonly used activators for GBFS are sulfates, Portland cement, sodium silicate, calcium hydroxide, and sodium hydroxide. A big portion of these activators contains alkali metal (e.g., Li, Na, K); thus, they are called alkali activators. The materials from GBFS and alkali activators are denoted as alkali-activated slag (AAS). Typical AAS consists of GBFS with 3.5–5.5 % (in mass) of  $\text{Na}_2\text{O}_{\text{eq}}$  added, usually water glass [42, 43].

Several research studies have shown that slag reactivity in alkaline activation processes depends mainly on its component phases and vitreous structure. Some authors [44] think that the vitreous phase content should be over 90% for slag activation to be highly effective; others [45] conclude that slag with a low vitreous content (30 to 65%) may be suitable for these purposes.

Glukhovskiy and Krivenko [45, 46] proposed a model that would explain the alkaline activation of  $\text{SiO}_2$ - and  $\text{CaO}$ -rich materials such as blast furnace slag through the series of reactions summarised below in sequence.



In that sequence, the alkaline cation ( $\text{R}^+$ ) acts as a mere catalyzer in the initial phases of hydration via cationic exchange with the  $\text{Ca}^{2+}$  ions. These same authors believed that the alkaline cations are taken up into the structure as the reactions advance.

Fernández-Jiménez et al. [45] reported that the nature of the anion in the solution also plays an instrumental role in alkaline activation, especially in the early stages of hydration and in particular

concerning paste setting. Their model for the reaction mechanisms (based on a model proposed by Glasser in 1990) is depicted in Fig. 2.

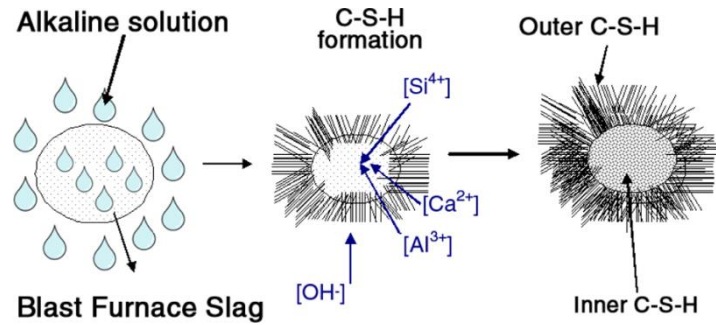


**Fig. 2** Reaction mechanism in an alkali-activated slag particle [45].

In alkaline cements developed from materials with high calcium content, such as blast furnace slag, activation generates reaction products that resemble those precipitating during Portland cement hydration. The main reaction product formed is a C-A-S-H (the structure is presented in Fig. 3) gel whose composition (lower Ca/Si ratio: 1–1.2) and structure vary from the typical C-S-H formed from OPC. Several secondary products may form, including hydrotalcite, calcite and bases such as AFm, depending on activator type and concentration, slag structure and composition, and the curing conditions under which the paste hardens [47, 48]. The microstructure of the gels formed during slag activation has been explored by several authors [49, 50].

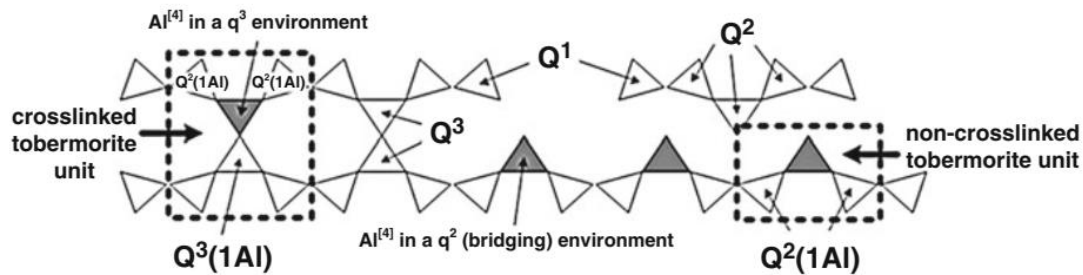


**Fig. 3** Generalized structure of the C-(N)-A-S-H type gel [51].

Several formulations of the reaction mechanism of alkaline activation of GGBS have been proposed in the literature. According to Krivenko [52], alkaline cations play a catalytic role in the early stages of hydration in a process involving interchange with  $\text{Ca}^{2+}$  cations. However, in the later stage, they are combined into the structure to form zeolite-like phases. Jiang [53] found that the role of alkali hydroxides was twofold, to provide  $\text{OH}^-$  ions at the initial stage and to become part of the reaction products at a later stage. Taylor [54] stated that the role of alkalis in alkali-activated slag is similar to that in blended GGBS–OPC cement, i.e. to maintain the supply of  $\text{OH}^-$  anions in the system. The coating formed on the surface of slag grains after they were mixed with water will prevent further hydration. An alkaline environment is needed to break down this layer. In blended slag–OPC, this alkaline environment will be maintained by the  $\text{Ca}(\text{OH})_2$  from the hydration of OPC. However, as the level of replacement increases, the quantity of  $\text{Ca}(\text{OH})_2$  is insufficient; therefore, an external source of alkalis is needed.

As observed in many experiments [55–59], a hydrated calcium silicate gel, namely C-S-H ( $\text{Ca-Si-OH}$ , see Fig. 3), is the most abundant product in hardened AAS pastes. The Ca/Si ratio in

C-S-H is generally close to that of the unhydrated slag [60]. According to Taylor [61], this type of C-S-H gel is C-S-H(I) with Ca/Si ratios below 1.5, whereas in Portland cement, it is C-S-H(II) with Ca/Si ratios of approximately 2. Brough and Atkinson [62] further examined this hydration product; they found that the inner product regions of hydrates of AAS mortars contained C-S-H gel with Ca/Si ratio of  $\sim 0.9$  mixed with a high Mg hydrotalcite. In contrast, the outer product regions have Ca/Si ratio of  $\sim 0.7$  and lower Mg hydrotalcite.

Shi and Day [63] studied the evolution of the AAS binder's hydration using a calorimetric method. They proposed three models of hydration of AAS cements, as shown in Fig. 4. The type I model: one peak occurs during the first few minutes, and no more peaks appear after that. An example is the hydration of slag in water or in  $\text{Na}_2\text{HPO}_4$  solution at both 25 and 50 °C. Type II: only the initial peak appears before the induction period, and one accelerated hydration peak appears after the induction period. Hydration of slag activated by NaOH at 25 and 50 °C belongs to this type. Type III two peaks, the initial and the additional initial peaks, appear after the induction period. This type of hydration includes the slag activated by  $\text{Na}_2\text{SiO}_3$  and  $\text{Na}_2\text{CO}_3$  at 25 °C and NaF at both 25 and 50 °C [54].

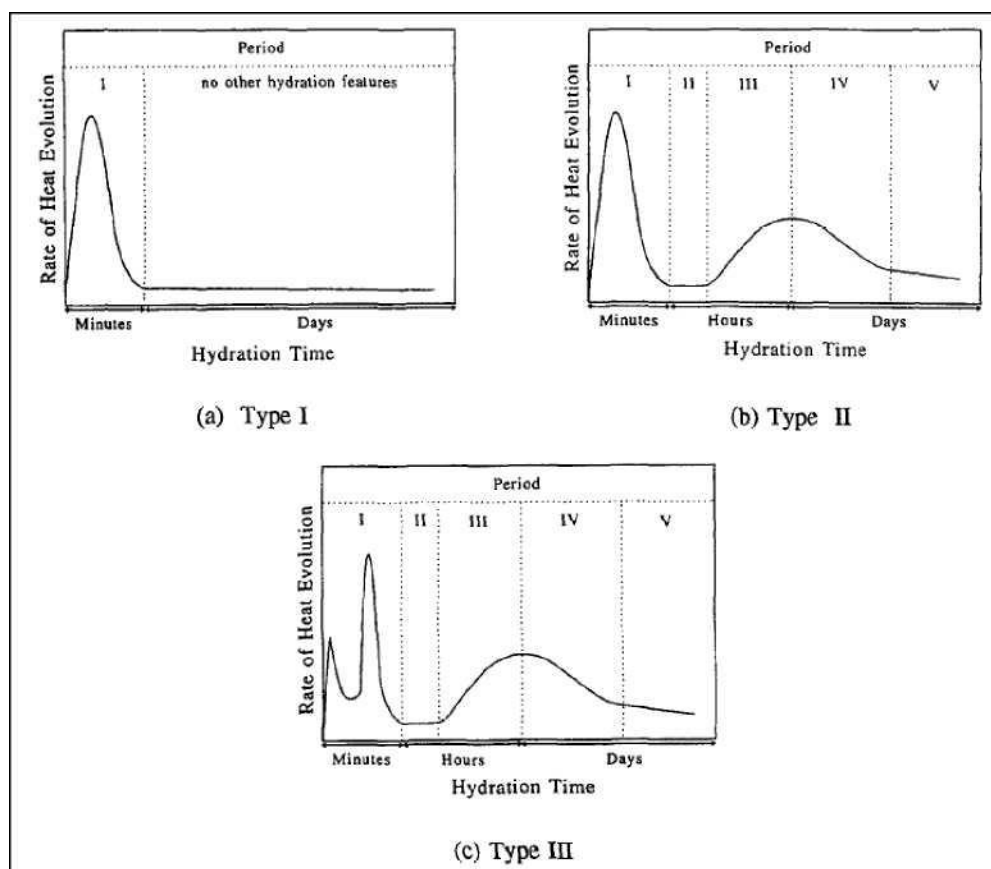


**Fig. 4** Schematic representation of hydration models of alkali slag cements [63].

Brough and Atkinson [62] studied the microstructure of AAS gel; they found that after early hydration, the microstructure of AAS gel consisted of a homogeneous gel and considerable microcracking, especially against the aggregate interface. However, when complete hydration has occurred, the degree of drying shrinkage cracking is significantly reduced at a later age. Under SEM observation, the microstructure of AAS was very smooth, homogeneous, and interconnected solid

in all samples. Pores between grains look very tortuous, and some of them appear isolated from each other.

### 2.2.3 Characterization of main reaction products in alkali-activated slag materials

The main reaction product formed in OPC concrete is C-S-H gel, which significantly influences the strength, durability, and other physical and chemical properties of hydrated OPC [64]. In materials with high calcium content, such as blast furnace slag, activation generates reaction products that resemble those precipitating during OPC hydration. The main reaction product is a silicoaluminate calcium hydrate gel (CaO(-Al<sub>2</sub>O<sub>3</sub>)-SiO<sub>2</sub>-H<sub>2</sub>O), commonly called C-A-S-H gel, that confers high mechanical properties of the material. Several secondary products may form, including hydroxalite and calcite, depending on activator type and concentration, slag structure and composition, and the curing conditions under which the paste hardens [51].

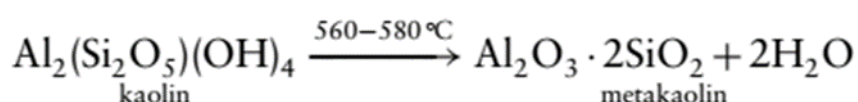
C-A-S-H gels can be regarded as a new phase of aluminum in the C-S-H structure gel, and it is the principal binding phase in hardened OPC pastes and concretes. It is generally believed that the C-A-S-H gels and the C-S-H gels have a similar tobermorite structure [49, 65]. However, the low crystallinity of the C-A-S-H phase is a limiting factor to understand. Its structure, and the effects of Ca, Si and Al cations in the reactivity of the alkali-activated binder have been evaluated by several characterization techniques, such as X-ray diffraction (XRD) [66, 67], Fourier-transform infrared spectroscopy (FTIR) [68], differential thermal analysis (DTA), thermogravimetry (TG), <sup>29</sup>Si and <sup>27</sup>Al MAS NMR [69] and Raman spectroscopy [70].

## 2.3 METAKAOLIN BASED GEOPOLYMERS

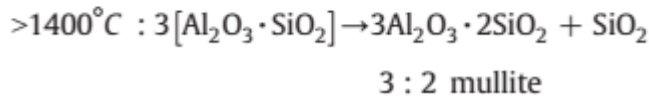
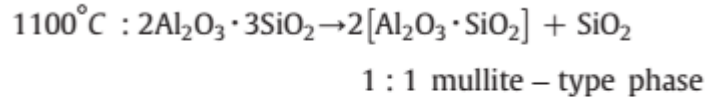
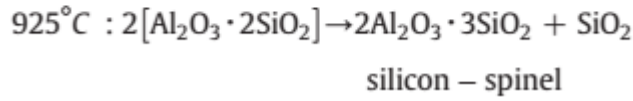
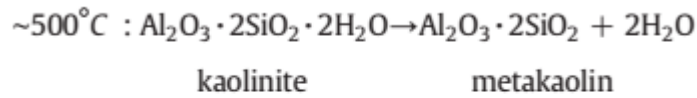
### 2.3.1 Metakaolin

Metakaolin is a highly reactive amorphous aluminosilicate produced by the calcination and dehydroxylation of kaolinitic clay. Metakaolin consists of porous, angular-shaped, platy particles with a mean size ranging from 0.5 to 20 μm [71].

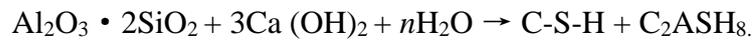
Metakaolin is obtained by heating kaolin-containing clays expressed as follows:



Research has indicated that the metakaolin produced under the heating temperature of 600 to 900 °C shows the highest pozzolanic reactivity. If the temperature exceeds 900 °C, crystalline mullite Al<sub>6</sub>Si<sub>2</sub>O<sub>13</sub> or spinel MgAl<sub>2</sub>O<sub>4</sub> and amorphous silica will form. At higher temperatures, there is the formation of cristobalite. And then, the reactivity of metakaolin decreases [72]. The exothermal dehydroxylation reactions are represented below [73].



Metakaolin can react with lime and produce both C-S-H and hydrated gehlenite:



The chemical composition of metakaolin depends on the composition of the raw materials from which metakaolin is produced. In the Czech Republic, the main raw materials are kaolins and shales from the North Bohemian Basin. The kaolinite content ranges between 80–95%, and the most important impurities are Fe<sub>2</sub>O<sub>3</sub> and TiO<sub>2</sub> [74]. A typical range of composition of metakaolin in Czech Republic is shown in Table 3.

**Table 3.** Chemical composition of metakaolins produced in the Czech Republic [74].

Component	SiO <sub>2</sub>	Al <sub>2</sub> O	Fe <sub>2</sub> O <sub>3</sub>	TiO <sub>2</sub>	CaO	MgO	Na <sub>2</sub> O	K <sub>2</sub> O	LOI
<b>Composition (%)</b>	52,0– 59,0	37,5– 42,5	0,5– 3,5	0,5– 1,4	0,1– 0,4	0,2– 0,5	0,01– 1,0	0,6– 1,7	0,4– 3,1

However, pozzolanic activity and other properties depend not only on the chemical composition but also on the particle size. The finer the particles are milled, the larger the surface area, and the more reactive they are. Metakaolin can react with alkalis and form cementing materials [75].

### 2.3.2 Reaction mechanism and hydration products

Geopolymers are also referred to as alkali activated aluminosilicate binders. They comprise three classes of inorganic polymers that, depending on the ratio of silica to alumina (silica/alumina), are based on the following three different monomeric units: (–Si–O–Al–O–), polysialate, SiO<sub>2</sub>/Al<sub>2</sub>O<sub>3</sub>=2; (–Si–O–Al–O–Si–O–), polysialatesiloxo, SiO<sub>2</sub>/Al<sub>2</sub>O<sub>3</sub>= 4; (–Si–O–Al–O–Si–O–Si–O–), polysialatedisiloxo, SiO<sub>2</sub>/Al<sub>2</sub>O<sub>3</sub>=6 [76].

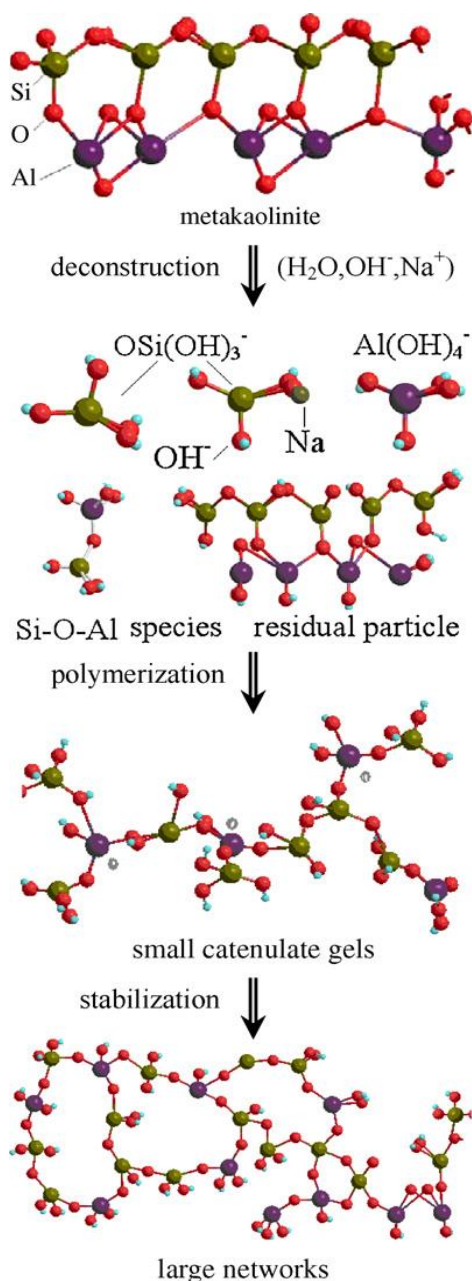


**Fig. 5** Sketch of the geopolymerization process, including the deconstruction of MK by the activation of alkaline solution [78].

Calcining temperatures range from 500 to 750 °C for 2 to 10 hours and result in the formation of X-ray amorphous metakaolin. However, the calcination process can sometimes result in crystalline phases such as spinel, cristobalite, and mullite that are deleterious for processing geopolymers due to their lower reactivity in alkaline solutions [79]. Fig. 6 shows the structure of a layered, uncreated aluminosilicate source that might be present in geopolymers due to incomplete reaction [80, 81].

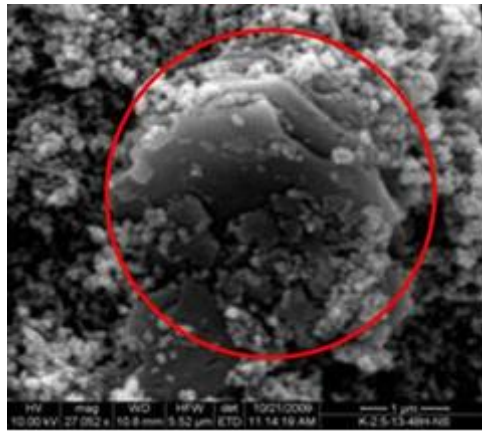


**Fig. 6** Layered, uncreated aluminosilicate source in geopolymer [81].

## 2.4 ACTIVATORS

The slag is known for its latent-hydraulic property, i.e. it is reactive with water, but only at such a slow rate that it is typically mixed with other substances called activators, which can remarkably accelerate the reaction of slag. The most commonly used activators for GGBFS are sulfates, Portland cement, sodium silicate, calcium hydroxide, and in rare cases, sodium hydroxide. A significant portion of these activators contain alkali metals (e.g. Li, Na, K); thus, they are called alkali activators. The composed materials made from GGBFS and alkali activators are denoted as alkali-activated slag (AAS) [41].

Activators are the second essential component in alkaline design and development. Activators used are mostly alkali silicates, hydroxides, carbonates or mixtures thereof, but, also other additions like sodium aluminates or cement kiln dust can be applied. The most commonly used ones are listed below, where M is the alkali metal Na or K [82]:

1. caustic alkalis: MOH;
2. non-silicate weak acid salts:  $M_2CO_3$ ,  $M_2SO$ ,  $M_3PO_4$ , MF, etc.;
3. silicates:  $M_2O \cdot nSiO_2$ ;
4. aluminates:  $M_2O \cdot nAl_2O_3$ ;
5. aluminosilicates:  $M_2O \cdot Al_2O_3 \cdot (2-6)SiO_2$ ;
6. non-silicate strong acid salts:  $M_2SO_4$ .

While common activators include NaOH,  $Na_2SO_4$ , water glass,  $Na_2CO_3$ ,  $K_2CO_3$ , KOH,  $K_2SO_4$  and cement clinker, the most utilized alkaline activators are a mixture of sodium or potassium hydroxides (NaOH, KOH) and sodium water glass ( $nSiO_2 \cdot Na_2O$ ) or potassium water glass ( $nSiO_2 \cdot K_2O$ ). Water glass, also called sodium silicate or soluble glass, is a compound containing sodium oxide ( $Na_2O$ ) and silica (silicon dioxide,  $SiO_2$ ) that forms a glassy solid with the advantageous property of being soluble in water [83].

Glass from the silicate furnace is dissolved in water at an elevated temperature, 120 °C, in an autoclave and under pressure to yield a solution. At room temperature, the glass is hardly soluble. Water glass can be produced as solid lumps or powders or as a clear, syrupy liquid [84].

The activation process of slag varies with the chemical properties and phase compositions of slags and the type and concentration of activators. Slags have a variable composition depending on the raw materials and the industrial process; hence, each slag responds differently to the activation process. For every slag, it is necessary to plan a research program to determine the most suitable

activator type and content. Sodium hydroxide and sodium silicate (water glass) are the most commonly used activators. Sodium silicate is also considered the most effective activator. The most important parameters of water glass are the ratio of  $\text{SiO}_2/\text{Na}_2\text{O}$  and  $\text{Na}_2\text{O}$  content [85].

In the slag activation, the water glass is believed to contribute to strength development: as an alkaline activator and an inducer of a high silica primary gel formation. This gel forms when soluble silicates react with the  $\text{Ca}^{2+}$  ions in the slag to form a C-S-H/C-A-S-H-type, silica-rich, calcium silicate hydrate. The reaction products formed often exhibit high strength, significant drying shrinkage, and short setting times, while the formation of  $\text{Q}_3(\text{nAl})$  units in their structure is also favoured [46]. Depending on slag nature and fineness, and curing conditions, the optimal  $\text{Na}_2\text{O}$  content is regarded to be around 4 % of slag weight, and the optimal  $\text{SiO}_2/\text{Na}_2\text{O}$  molar ratio on the order of 0.75–1.25 for acid slag, 0.9–1.3 for neutral slag and 1.0–1.5 for basic slag [86]. In the water glass activation of aluminosilicates, the soluble silica induces the development of a microstructure that resembles many types of glass (absence of pores and a uniform and compact microstructure) [87].

For basic slag, alkaline activators from the first 3 groups can be used independently of the hardening conditions. For neutral and acid slag, activators from the first and third groups ensure hardening under normal conditions. In combination with activators from groups 1 or 3, activators from group 2 can be used for neutral and acid slag. Although  $\text{NaOH}$ ,  $\text{NaSO}_4$  and  $\text{Na}_2\text{CO}_3$  are often used as activators of slag and can be effective, most research has found that activation with sodium silicate or sodium silicate blended with  $\text{NaOH}$  has given the best strength [54].

The dosage of the activator in terms of %  $\text{Na}_2\text{O}$  is defined as the ratio of the  $\text{Na}_2\text{O}$  content of the alkaline activator to the mass of the binder (GGBS for AAS or fly ash for FA-based geopolymer). In contrast, the activator modulus ( $M_s$ ) is the mass ratio of the  $\text{SiO}_2$  to the  $\text{Na}_2\text{O}$  in the alkaline activator [88]. Wang found that both dosage and modulus of activator significantly influence the strength of AAS mortar. In an activator containing sodium silicate or blended sodium silicate and sodium hydroxide, there is a competing effect of the dosage and modulus of the activator, which results in an optimum value for both the dosage and modulus of the activator [54].

The silicate modulus ( $M_s$ ) is the  $\text{SiO}_2/\text{M}_2\text{O}$  molar ratio. Theoretically, silica  $\text{SiO}_2$  and metal oxide  $\text{M}_2\text{O}$  can be combined in all proportions. The practical range for commercial silicates is determined by their solubility and instability at room temperature. Therefore, the  $M_s$  ranges in practice from 0.4 to 4.0 for sodium silicates [89].

The viscosity of alkali silicate solutions changes very little regardless of the ratio when the  $\text{Na}_2\text{O}$  concentration is smaller than about 7 % but increases drastically with the ratio if the  $\text{Na}_2\text{O}$  concentration is higher than approx. 7 %. For a given temperature, the viscosity of a sodium silicate solution increases as the concentration and modulus of the solution increase, as shown in Fig. 7. For a given modulus, there is a “threshold” concentration, above which the viscosity of the solution starts to increase drastically [90].

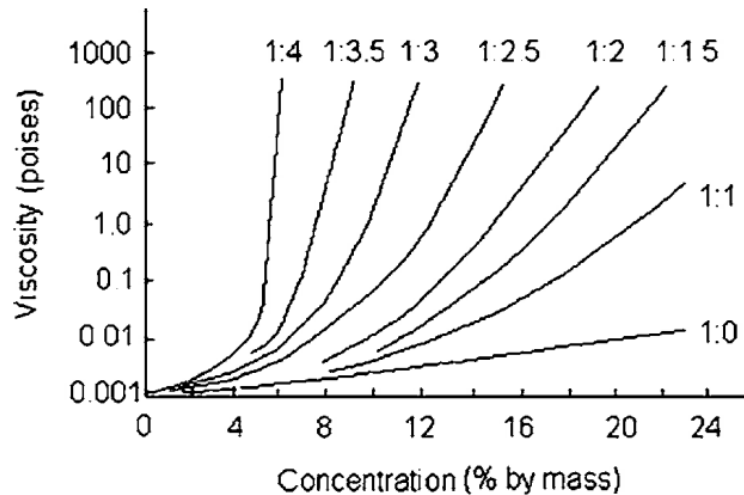


**Fig. 7** Effect of concentration of  $\text{Na}_2\text{O}$  and silicate modulus on the viscosity of sodium silicate solution at  $20\text{ }^\circ\text{C}$  (numbers in the figure are molar ratios).

## 2.5 POLYMER ADMIXTURES

### 2.5.1 Classification of admixtures

Concrete admixtures are ingredients in concrete other than Portland cement, water, and aggregates that are added to the mixture immediately before or during mixing [91]. Concrete admixtures are liquid or powder additives. They are added to the concrete mix in small quantities. Dosage is usually defined based on cement content. Concrete admixtures significantly impact the fresh and/or hardened concrete properties. Admixtures can act chemically and/or physically [92]. The permitted dosage of admixtures according to EN 206-1 is  $\leq 5\%$  by weight of the cement [93].

Concrete admixtures can be divided by Mindess et al. according to their physico-chemical mechanisms or actions into four different categories [94]:

1. Air-entraining agents (ASTM C260) that are added primarily to improve the frost resistance of concrete;
2. Chemical admixtures (ASTM C494 and BS 5075) that are water-soluble compounds added primarily to control the setting and early hardening of fresh concrete or to reduce its water requirements;
3. Mineral admixtures that are fine solids added to concrete to improve durability or to provide additional cementing properties;
4. Miscellaneous admixtures, which include all those materials that do not come under one of the previous categories, many of which have been developed for specialized applications.

Types of admixtures per American Concrete Institute Committee report and IS 9103:1999 [95]. The standard states the following types:

- Accelerating admixtures;
- Retarding admixtures;
- Water-reducing and set controlling admixtures;
- Air-entraining admixtures;
- Superplasticizing admixtures;

- Admixtures for flowing concrete;
- Miscellaneous admixtures.

Accelerating admixture accelerates the rate of hydration (setting) and strength development of concrete at an early age. Calcium chloride ( $\text{CaCl}_2$ ) is the chemical most used accelerating admixture, especially for nonreinforced concrete [96].

Retarding admixtures are used to delay the rate of setting of concrete. Retarders do not decrease the initial temperature of concrete. High temperatures of fresh concrete ( $30\text{ }^\circ\text{C}$ ) are often the cause of an increased rate of hardening that makes placing and finishing difficult. The bleeding rate and bleeding capacity of concrete are increased with retarders. Retarding admixtures help extend the setting time of concrete. However, they are often also used in attempts to decrease slump loss and extend workability, especially prior to placement at elevated temperatures [97].

Water-reducing admixtures, the name itself defines that they are used to minimize the water demand in a concrete mix. Workability is the crucial property of concrete which is improved with the addition of water. However, if more water is added than required, concrete's strength and durability properties are affected. In addition to increasing workability, it also improves the strength of concrete, good bond between concrete and steel, prevents cracking, segregation, honeycombing, bleeding, etc. Admixture of this type, when used as workability aids on water reducers, does not adversely affect the shrinkage [91].

Water-reducing admixtures are also called plasticizers, and these are classified into three types: plasticizers, mid-range plasticizers and superplasticizers. Standard plasticizer reduces the water demand by up to 10%, mid-range plasticizers reduce the water demand by up to 15%, while super plasticizers reduce the water demand by up to 30% [98].

Air-entraining admixtures are generally used to improve workability, ease placing, increase durability and resistance to frost action and reduce bleeding. The common air-entraining agents are natural wood resins, neutralized vinsol resins, polyethylene oxide polymers and sulfonated compounds [99].

Superplasticizer – admixture which permits a high reduction in the water content of a given mix without affecting the consistence, or increases the slump/flow considerably without affecting the water content; or produces both effects simultaneously [100].

There are many miscellaneous concrete additives for use as pumping aids and as damp-proofing, permeability-reducing, gas-forming agents. Pumping aids are used to decrease the viscosity of harsh or marginally pumpable mixes. Organic and synthetic polymers, fly ash, bentonite, or hydrated lime may be used for this purpose. Damp-proofing admixtures include soaps, stearates, and other petroleum products. They are intended to reduce the passage of water and water vapor through concrete. Gas-forming admixtures are used to form lightweight concrete. They are also used in masonry grout, where the grout should expand and bond to the concrete masonry unit. This is typically an aluminum powder [91].

A **polymer-based** (or polymeric) admixture, also called a cement modifier, is defined as an admixture that consists of a polymeric compound as a main ingredient effective at modifying or improving the properties such as strength, deformability, adhesion, waterproofness and durability of cement mortar and concrete. Such a polymeric compound is a polymer latex, re-dispersible polymer powder, water-soluble or liquid polymer [101].

Plasticizers or mid-range water-reducing admixtures are **natural polymers**, as lignosulphonates were the first water-reducing admixtures used in concrete as a plasticizer. Lignosulphonate is among the cheapest concrete admixtures available on the market [94].

**Synthetic linear polymers** are a category which includes some of the most commonly used superplasticizers, such as polynaphthalene sulphonates, polymelamine sulphonates and vinyl copolymers [102].

Fig. 8 shows the classification of polymer-based or polymeric admixtures. In general, polymer-based admixtures are classified into four main types, i.e., polymer latex (or polymer dispersion), re-dispersible polymer powder, water-soluble polymer and liquid polymer [103].

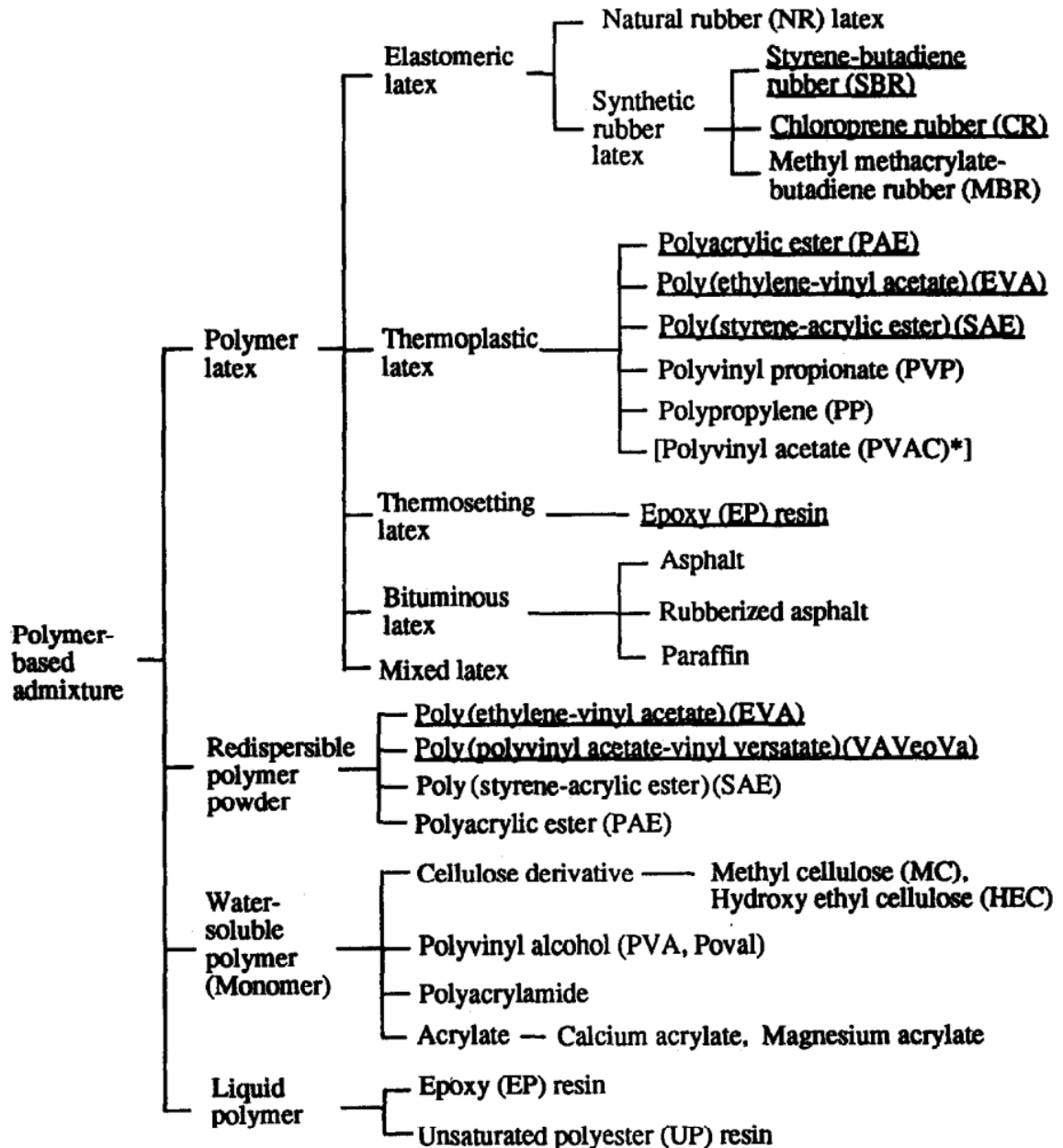


Fig. 8 Classification of polymer-based (or polymeric) admixtures [103].

## 2.5.2 Polymer admixtures as modifiers in cementitious binders

Portland cement concrete is one of the most versatile and cost-effective construction materials. Polymer-modified concrete was developed in the 1960s to overcome some of the limitations of concrete, such as low tensile and flexural strength, high porosity and low resistance to certain chemicals. The relatively high cost of monomers has limited the commercial viability of specific polymer-modified concrete [104].

Nevertheless, ordinary concretes encounter serious problems, including low tensile and flexural strength, low strain capacity, brittleness, permeability, and long-term durability, which need to be improved. The advancement in polymer admixtures has offered alternative solutions to overcome a range of those limitations [105].

Polymers can be incorporated into concrete in two ways: they can be added to the concrete in its fresh state (e.g., latexes), or they can be impregnated into the hardened concrete and cured in a specialized place (e.g., methyl methacrylate monomer) [106].

Polymers are usually added to cement in the ratio of about liquid monomer particles in 0.05 to 0.20 kg of pure polymer per kilogram of cement, which is specified as the polymer/cement ratio [107].

Polymer modification of hydraulic cementitious mixtures is governed by cement hydration and polymer coalescence. Generally, cement hydration occurs first. The polymer particles become concentrated in the void spaces as the cement particles hydrate and the mixture sets and hardens. Figures 9 and 10 indicate the type of change that occurs during polymer modification [108–110]. With continuous water removal by the cement hydration, evaporation, or both, the polymer particles coalesce into a polymer film interwoven in the hydrated cement resulting in a mixture or co-matrix that coats the aggregate particles and lines the interstitial voids. Unlike conventional cementitious mixtures, the polymer-modified cementitious mixture does not produce bleeding water. During its fresh state, polymer-modified mixtures are more sensitive to plastic-shrinkage cracking than unmodified mortar or concrete because of the water-reducing influence of the polymer's surfactant system. This phenomenon (plastic-shrinking cracking) is caused by water evaporation at the surface. Two things can happen, both of which contribute to the problem. The polymer particles may coalesce before noticeable cement hydration occurs, and the cement paste may shrink before sufficient tensile strength develops to restrain crack formation. Care should be taken to restrict this surface evaporation by using various cover systems. Because latex particles are typically greater than 100 nm in diameter, they cannot penetrate the small capillaries in the cement paste that may be as small as 1 nm. Therefore, latex can be most effective in larger capillaries and voids. Some of the polymers used in Portland cement mixtures contain reactive groups that may react with calcium and other metallic ions in the cement and with the silicate and other chemical radicals at the surface of the aggregates [111]. Such reactions would improve the interparticle bonds and hence, the strength of the mixture. Hardened Portland cement paste is predominantly an agglomerated structure of calcium silicates, aluminates, and hydroxide bound together by relatively weak van der Waals forces.

Consequently, microcracks are induced in the paste by stresses such as those caused by the evaporation of excess mixing water (drying shrinkage). Polymer modification helps in two ways. Not only do the polymer particles reduce the rate and extent of moisture movement by blocking the passages, but when microcracks form, the polymer films ridge the cracks and restrict propagation. This phenomenon is depicted in Fig. 11 [108].

An optimum balance of mortar properties is generally obtained by incorporating approximately 15 % polymer solids by weight of Portland cement. The correlation between polymer and performance properties is shown in Fig. 13 [112].

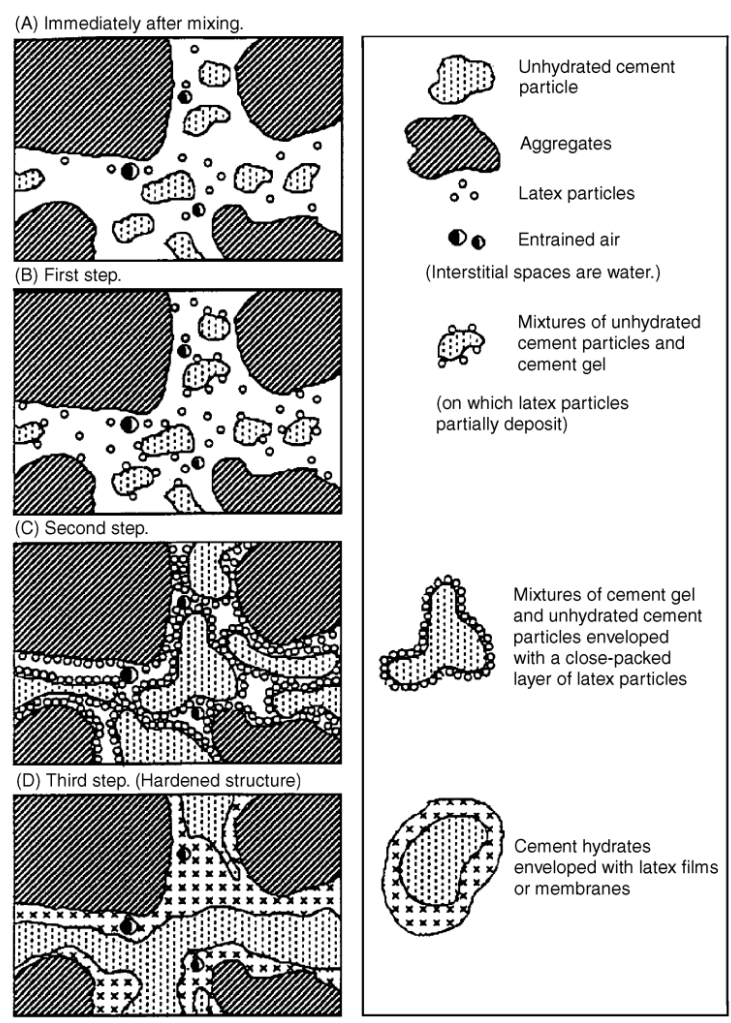


**Fig. 9** Model of formation of latex-cement comatrix [108].

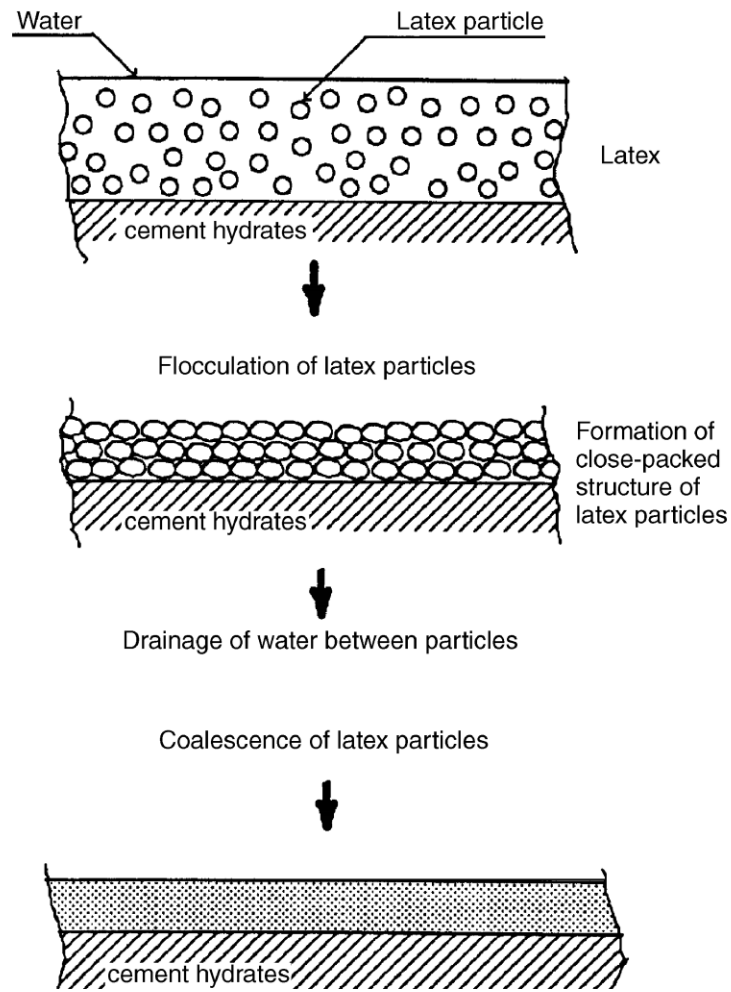
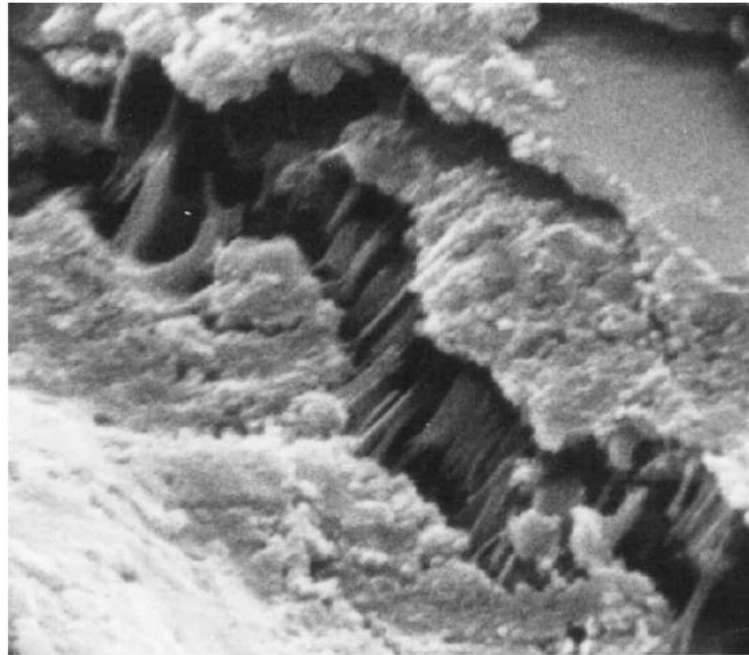


**Fig. 10** Model of formation of polymer film on cement hydration [109].



*Latex-modified concrete*



*Portland cement concrete*

**Fig. 11** Micrographs of latex-modified and portland cement concrete (magnification 12000×) [108].

**Polymeric latexes** are widely used to modify cement-based concretes' physical and mechanical properties [113]. Latex is an aqueous dispersion of spherical polymer particles which are generally incorporated into cement mixture by a mixture-proportioning method as an admixture.

Polymer latex consists of small (0.05 to 1.0  $\mu\text{m}$  – diameter) spherical particles held in suspension using surface-active agents. Polymer latexes are generally copolymer systems (see Fig. 12) of two or more polymers with the possible addition of plasticizers or other modifiers, and typically contain around 50 % solids by weight [114].

Research has shown that latexes involve their properties, including flexibility, damping ability, chemical resistance and barrier effect to the concretes [115]. The film formation of latex results from the coalescence of latex particles when water is consumed by cement hydration and evaporation. This latter is the reason for the decreased water permeability of latex modified concretes. The durability of concrete is directly related to its permeability. The different gases and chemical substances can penetrate pores and cracked areas and attack the concrete and reinforcement elements. The incorporation of latexes improves the chloride penetration resistance of the concrete and reduces the general ionic permeability [116]. Polymer latexes affect concretes' mechanical properties by forming latex films and membranes on the concrete's capillary pores [113]. The latexes reduce the concrete water content due to the presence of a high-range superplasticizing agent in latex constituents, producing concrete with improved mechanical properties [101].

The main elastomeric polymers used in latexes are natural rubber, styrene-butadiene, polyacrylonitrile butadiene and polychloroprene. The main thermoplastic polymers used are [117]:

1. polyvinyl acetate or copolymers of vinyl acetate with monomers such as vinyl chloride, vinylidene chloride, dibutylmaleate and vinylpropionate;
2. polystyrene or copolymers of styrene with different acrylate monomers;
3. polyvinylchloride or copolymers of vinylchloride with monomers such as vinylidene chloride and vinylpropionate
4. polyacrylates and their copolymers.

The effect of the latex on mortar or concrete will increase the bond of a fresh mortar with existing concrete surfaces with the amount of polymer added. However, a polymer/cement ratio of about 0.10 to 0.20 is generally used in practice [118]. Most types of latexes have a plasticizing effect on PC mortars, similar to concrete plasticizers.

**Redispersible polymers** are polymers in powder form that are used to modify hydraulic cement mixtures. Such powders are referred to as re-dispersible because they convert to latex after mixing with water. In 1953, a patent was applied for using these polymer powders as polymer modifiers for hydraulic cementitious mixtures [119]. Like latexes, these polymers are made by emulsion polymerization, and the resultant latex is converted to powder form, usually by a process known as spray drying. The commercially available re-dispersible powders are vinyl acetate homopolymers, vinyl acetate copolymers, and acrylic copolymers.

Redispersible powders are usually free-flowing white powders with ash contents of 5 to 15%. The ash content that primarily comes from the anti-blocking aid varies depending on the type of material. The bulk density of the powder is relatively low, being less than 25% of Portland cement. The particle size of the powder averages about 0.08 mm; however, these particles are agglomerates that break up on redispersing in water to give typical latex-particle sizes (1 to 5 mm).

The mixture proportioning of cement mixtures modified by re-dispersible powder polymers is similar to that of other polymer-modified systems, considering that the polymer admixture is free of water.

#### **Water soluble polymers**

These types of polymers are usually added to mortars or concrete in the form of aqueous solutions. Water soluble polymers have been divided into two categories – synthetic and natural. Synthetic water-soluble polymers are substances that dissolve, disperse or swell in water and, thus, modify the physical properties of aqueous systems in the form of gelation, thickening or emulsification/stabilization. These polymers usually have repeating units or blocks of units; the

polymer chains contain hydrophilic groups that are substituents or are incorporated into the backbone. The hydrophilic groups may be nonionic, anionic, cationic, or amphoteric (or zwitterionic) [120]].

Water soluble polymers are usually used with a very low polymer/cement ratio; the fresh mix workability was significantly improved compared to typical cement mortar mixtures due to the impact of polymeric materials on plasticizers and air-entraining agents. The modified mortar structure demonstrates greater water retaining capacity than normal cement structures [121]. Moreover, well spreading of cement mortar and an increase in direct tensile strength is achieved due to improvement in bond strength between cement grains and aggregate among cement mortar. A significant decrease in interfacial transition zone thickness nearby aggregate particles and meaningful reduction in  $\text{Ca(OH)}_2$  crystal could be achieved due to the use of polymers and by potentially replacing those with the C-S-H phase. Addition of water-soluble polymers reduces bleeding and improves the homogeneity of mortar or concrete by controlling segregation of fresh mixtures [122]. On the other hand, water-soluble polymers have often decreased the mechanical properties of mortar and concrete because of the increased air entrainment [120].

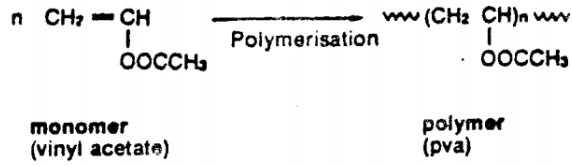
The most popular synthetic water-soluble polymers are polyethylene glycol (PEG), polyvinyl alcohol (PVA) and methylcellulose.

Fu and Chung [123] studied the effect of small additions of methylcellulose (0.2% – 0.8% by weight of cement). The tensile strength was increased by up to 72%, the tensile ductility by up to 620%, while the compressive strength was decreased by up to 30% and the compressive ductility by up to 34% . The addition of methylcellulose (0.4% by weight of cement) or latex (20% by weight of cement) to cement paste gave similarly significant increases in the shear bond strength between stainless steel fibers and cement paste, despite the low concentration, and therefore, lower cost of methylcellulose compared to latex. The microstructure of the interfacial transition zone is influenced by modification with water-soluble polymers. Because of the alteration of the microstructure of the interfacial transition zone, the admixing of small amounts of water-soluble polyvinyl alcohol was reported to have doubled the pullout strength and friction of steel fibers in cement paste by Chu et al. [124] .

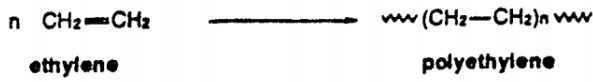
**Liquid resins** are thermosetting type polymers such as polyester and epoxies, which can also be added to mortars and concretes in a liquid form. Liquid resins have several advantages over latexes. Epoxy resins have been widely used as admixtures in the concrete industry due to their high inherent strength, high bond strength and chemical resistant properties [125].

Usually, epoxy resins require a hardener, which is generally amines or organic acids, to initiate the curing process and to form crosslinked networks. However, some studies have pointed out that epoxy resin can be cured in the presence of hydroxide ions or alkalis (i.e.  $\text{Ca(OH)}_2$ ) formed from the hydration of Portland cement [125]. Hardener-free epoxy-modified cements can provide a self-healing or self-repairing function for microcracks [126]. It is estimated that a degree of crosslinking of epoxy resin (without a hardener) of about 50 % is achieved with a polymer content of 20% in the cement. The excess of unhardened resin remains initially in the pores of the hardened cement paste. As microcracks are formed, the resin is gradually released to crosslink and harden with  $\text{Ca(OH)}_2$ , which is present in the cement. This phenomenon can fill and repair the microcracks. Besides the self-repairing property, studies have shown that epoxy cement mortars without a hardener maintain some chemical and mechanical properties that are much better than conventional epoxy cement mortars with a hardener.

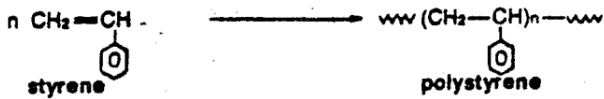
**Polyvinyl acetate (pva)**



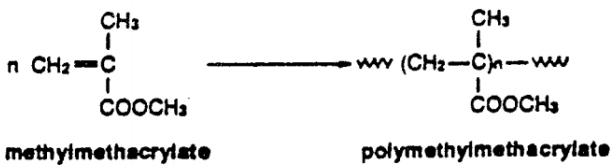
**Polyethylene**



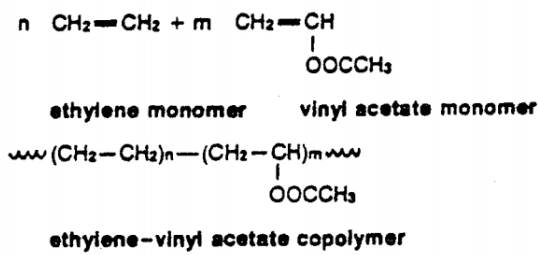
**Polystyrene**



**Polymethylmethacrylate (acrylics, typically perspex)**



**Ethylene vinyl acetate (EVA)**



**Styrene-butadiene (SBR)**

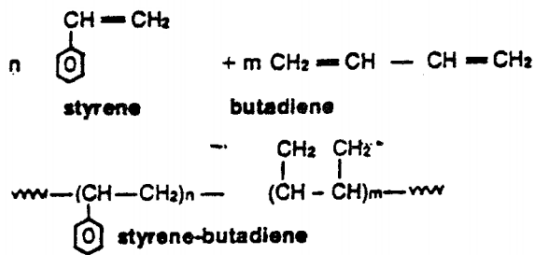


**Fig. 12** Structures of some polymers used for polymer admixtures [112].

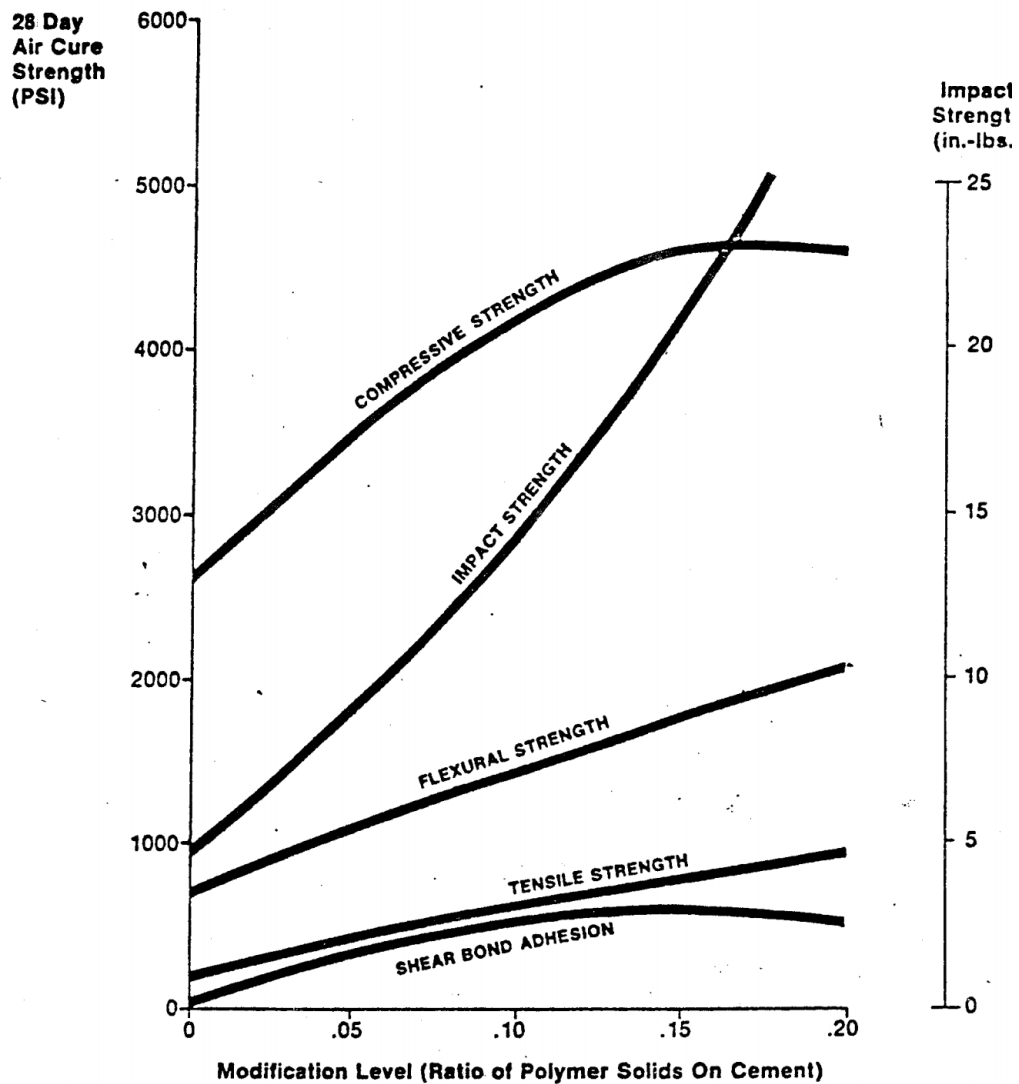


Fig. 13 Performance properties versus the level of polymer modification [112].

### 2.5.3 Polymer admixtures as modifiers in alkali-activated aluminosilicates

Despite the advantages of AAS mortars, they have a significant disadvantage – a high value of shrinkage followed by the formation of microcracks. This effect is caused both autogenously and by drying shrinkage, resulting in volume contraction, microcracking and deterioration of tensile and bending properties [127]. Therefore, using various types of polymer admixtures can overcome these problems.

Modern admixtures are less based on the use of industrial by-products but rather on synthetic molecules or polymers specially produced for the concrete industry [94]. Modern admixtures modify one or several properties of fresh and hardened concrete by correcting some of the technological weaknesses of PC and hydraulic binders [128].

According to the literature review, the use of polymer admixtures in geopolymer systems is rather limited in this field of study.

Bakharev et al. [129] studied the effect of superplasticizer, air-entraining agent, and water-reducing and shrinkage-reducing admixtures to improve the shrinkage properties and workability of AAS concretes. The superplasticizers are based on modified naphthalene formaldehyde polymers, water-reducing admixtures based on lignosulphonates and air-entraining admixture with a soluble salt of an alkyl- or aryl- sulphonate. They showed that air-entraining admixture is the most suitable for use in AAS concrete, as it improves workability, reduces shrinkage, and does not deteriorate later strength. Shrinkage-reducing admixtures were effective in reducing shrinkage cracking.

Also, the effect of shrinkage-reducing admixtures based on polypropylene glycol was presented by M. Palacios and F. Puertas [130]. The concentrations of shrinkage-reducing agents were 1 and 2 % by slag mass. The results showed that adding a 1 % shrinkage-reducing agent did not significantly modify the compressive strength or the flexural strength of the specimens because, after 28 days, the flexural strength was 25 % higher than the flexural strength of mortar without admixture. The addition of a 2 % shrinkage-reducing admixture increased the compressive strength and flexural strength. Especially flexural strength was increased by approximately 75 % at 7 days and more than 100% at 28 days related to the mortars without shrinkage-reducing admixture.

Bilim et al. [131] examined the effect of shrinkage-reducing and set-retarding admixtures on some properties of AAS pastes and mortars. Shrinkage-reducing and set-retarding admixtures reduced both compressive and flexural strength of AAS mortars at the age of 2 days. However, after 2 days set-retarding admixtures had no impact on the flexural and compressive strength values of AAS mortars. In contrast, shrinkage-reducing admixtures increased AAS's flexural strength without changing the compressive strength behavior. Also, V. Bílek studied the using shrinkage-reducing admixtures as possible solutions for chemical and autogenous shrinkage of AAS [132].

Geopolymers also have many advantages compared to OPC, such as high early strength [133], good fire and acid resistance and good durability [134, 135]. Additionally, they have generally low apparent porosity, which gives them very low water permeability and, thus, very good resistance in freezing-thawing cycles [136]. However, disadvantages also exist. Geopolymers present a typical brittle mechanical behavior with the consequent low ductility and low fracture toughness [137]. These characteristics can limit their applications as structural materials. In order to improve these drawbacks of geopolymer materials, organic polymers are often incorporated into their structure [134].

Polyethylene glycol (PEG) is a polyether compound with many applications in industrial manufacturing. PEG is one of the most well-known water-soluble polymers, and it can also be dissolved in many organic solvents, including aromatic hydrocarbons. PEG is used as a plasticizer to increase lubricity and acts as a water retention agent in ceramic mass, adhesives, binders, and soldering fluxes with good spreading properties [138].

In a study by Catauroa et al. [139], the influence on the mechanical strength of the different percentages of PEG added to geopolymer was investigated. In the absence of PEG, the tests showed overall strength regularity with ageing time due to the chemical composition of a sample. PEG-free samples can reach final mechanical strength faster than hybrid systems. The stretching effect of PEG, which generally provides the characteristic of elasticity to the base material and the longer time required to reach the final structural strength, justifies the increase of flexural and compressive strengths with ageing time.

Lamanna et al. [56] concluded that polymer-modified mortars had improved compressive strength compared to unmodified ones, and polymer helps restrain micro-crack propagation. They

also found that total porosity decreases with the addition of organic polymer, which may contribute to improved durability.

In the study by Shrotri, which was described in the book written by Davidovits [89], we analysed the dynamic mechanical behavior of geopolymers-organic polymer composites in the forms of cured plaques and uncured slurries. Organic polymer PEG in a small quantity was added to the geopolymer system to modify its behavior. The geopolymer composite showed remarkable flexibility without cracking, as shown in Fig. 14. Plaques produced without organic polymer were brittle and cracked easily.

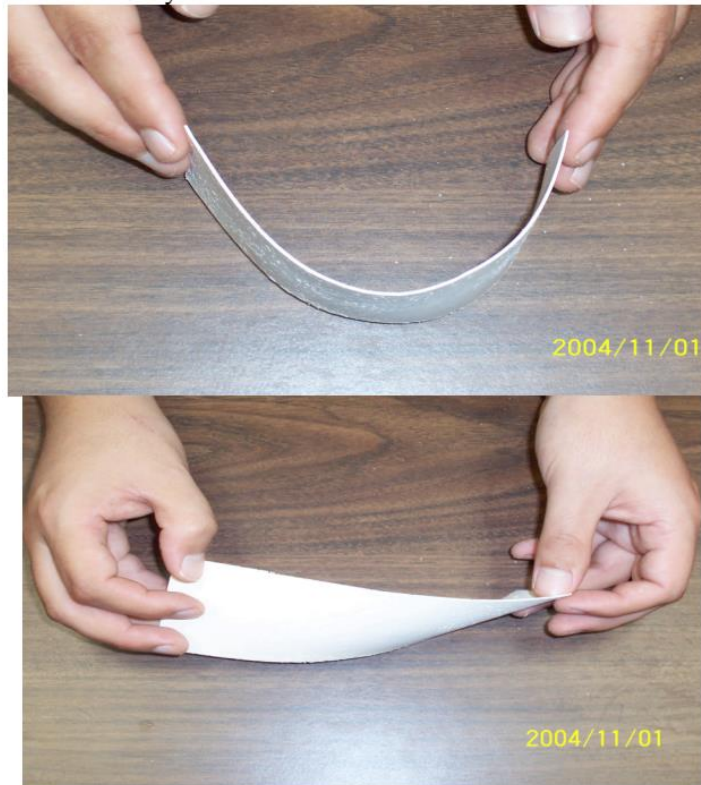


**Fig. 14** Polymer – geopolymer composite [89].

### 3 AIM OF THESIS

The literature review showed that raw materials for the production of alkali activated aluminosilicate materials and/or geopolymers include blast furnace slag, fly ash and metakaolin. Their mechanical properties depend on hardness, tensile strength, toughness, setting periods, and shrinkage values. Modification of the properties is done by polymer admixtures as they are used for ordinary PC because of their ability to prevent the formation of cracks during shrinkage and improve toughness. However, limited research has been done on modifying AAS with polymer-based admixtures. Therefore, the present study aims to show how various additives (e.g., polymer admixtures, shrinkage reducing admixture) in different dosages influence the mechanical properties of alkali-activated aluminosilicate materials. Moreover, the main target of the study is to find suitable types of polymer admixtures at optimal dosage to produce high-quality composite material having good physical-mechanical properties with high durability and toughness and low brittleness, as the main disadvantages of AAS and geopolymers. Another task was to study the microstructure of alkali-activated slag and geopolymers, focusing on the highly porous structure and the identification of hydration products, taking into consideration the factors influencing the hydration of slag.

To fulfil the goal of the thesis, locally produced raw materials from the Czech Republic were chosen – ground granulated blast furnace slag for AAS mortars and metakaolin for geopolymer mortars. The modifiers as admixtures were also chosen for their excellent ability to improve concrete properties, namely shrinkage cracking resistance and compressive and flexural strength. The water-soluble polymers, shrinkage-reducing admixtures, PPG, PEG and various types of commercial Vinnapas<sup>®</sup> were chosen.

In order to investigate mechanical properties, compressive and flexural strength tests were performed. The compositions that presented the best mechanical properties underwent further tests, such as Mercury intrusion porosimetry and Scanning electron microscopy to describe the microstructure of mortars. For pastes' mixtures, the rheological properties were studied using a stress-controlled rotational rheometer. Isothermal calorimetry tests were also performed to measure the influence of admixtures on the hydration process in AAS pastes. Besides the technical properties of AAM mortars, the stability of selected admixtures in AAS suspensions (in alkaline medium) was studied by IR technique.

Based on the test results and type of the modifiers (polymer admixtures) used, the composition of mixtures was optimized to produce a material with the best performance properties.

## 4 ALKALI ACTIVATED SLAG

### 4.1 MATERIALS, PREPARATION AND TESTING

#### 4.1.1 Materials

Czech ground-granulated blast-furnace slag (Kotouč Štramberk, spol. s r.o.) was used as the primary precursor for alkali-activated slag mortars. The chemical composition of the slag is given in Table 4. The specific surface of the slag was 380 m<sup>2</sup>/kg. The particle sizes determined through laser granulometry are  $d_{10} = 1.72 \mu\text{m}$ ,  $d_{50} = 11.81 \mu\text{m}$ , and  $d_{90} = 39.38 \mu\text{m}$ .

**Table 4.** Chemical analysis of blast furnace slag, [%].

SiO <sub>2</sub>	Fe <sub>2</sub> O <sub>3</sub>	Al <sub>2</sub> O <sub>3</sub>	CaO	MgO	SO <sub>3</sub>	Na <sub>2</sub> O	K <sub>2</sub> O	MnO	Cl	LOI
39.66	0.47	6.45	40.12	9.5	0.72	0.33	0.55	0.65	0.05	1.25

#### 4.1.2 Alkaline activators

The commercial solid sodium water glass SUSIL MP 2.0 (27% SiO<sub>2</sub>; 8% Na<sub>2</sub>O and 65% H<sub>2</sub>O by weight) with a SiO<sub>2</sub>/Na<sub>2</sub>O ratio of 2.0 was used as an alkaline activator for the slag.

#### 4.1.3 Aggregates

Quartz sand with a maximum grain size of 2.5 mm was used as aggregate. It was composed of three different fractions (PG 1–3) mixed in the ratio of 1:1:1 to obtain a standard mixture for testing mortars.

#### 4.1.4 Polymer admixtures

In this study, eleven types of commercial polymer admixtures were used:

- polyethylene glycol (PEG) 400;
- PEG 1000;
- PEG 6000;
- PEG 20000;
- polypropylene glycol (PPG);
- Peramin SRA;
- VINNAPAS<sup>®</sup> 5023 L;
- VINNAPAS<sup>®</sup> 5111 L;
- VINNAPAS<sup>®</sup> 7016 F;
- VINNAPAS<sup>®</sup> 7220 E;

VINNAPAS<sup>®</sup> 5023 L and VINNAPAS<sup>®</sup> 5111 L are dispersible polymer powders based on vinyl acetate and ethylene copolymers with good defoaming properties. VINNAPAS<sup>®</sup> 7016 F is a plasticizing dispersible polymer powder based on vinyl ester, ethylene and methyl methacrylate with an instant plasticizing effect. VINNAPAS<sup>®</sup> 7220 E is a semi-flexible polymer powder based on vinyl esters, ethylene and acrylic acid ester for good workability and excellent tensile adhesion strength after water immersion [140].

PEG is one of the most well-known water-soluble polymers and was used with different molar masses. The chemical formula of PEG is  $C_{2n}H_{4n+2}O_{n+1}$ .

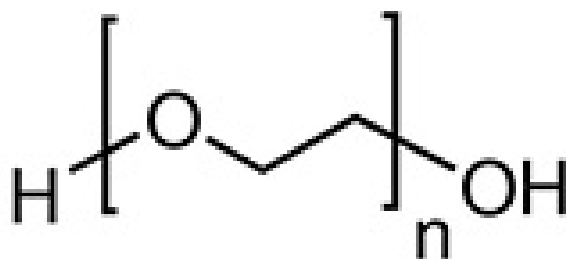


**Fig. 15** Chemical structure of PEG.

PPG is the polymer of propylene glycol. It is used as a rheology modifier. Linear formula is  $H[OCH(CH_3)CH_2]_nOH$ .

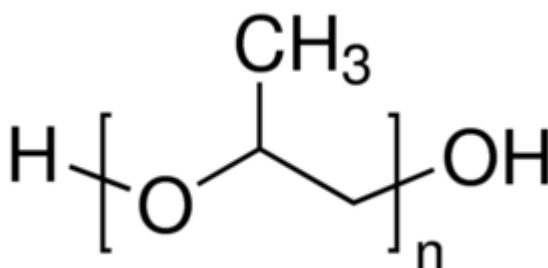


**Fig. 16** Chemical structure of PPG.

Peramin SRA is a polyol-based additive in powder form, which mainly reduces drying shrinkage. The chemical structure is derived from cyclo-aliphatic ether alcohol. The typical dosage of Peramin<sup>®</sup> SRA 40 varies between 1–5 % by weight of the binder.

Active matter %: 58–64

Bulk density: 0.55–0.75

Particle size (% > 600  $\mu\text{m}$ ): < 3

pH (5% solution): 6–8.

It is composed of silicon dioxide, 5-ethyl-1,3-dioxane-5-methanol and 2,2-dimethylpropane-1,3-diol [141].

#### **4.1.5 Preparation of AAS mortars: Mixing, molding, curing**

The reference AAS mortar mix design comprised of slag (450 g), activator (90 g), aggregates (1350 g) and total water (175 ml). The activator and polymer admixtures were dispersed and partially dissolved in water before mixing with slag. Finally, quartz aggregate was added to prepare fresh mortar. AAS mortars were poured into prismatic moulds (40 × 40 × 160 mm) and removed from the moulds after 24 hours. Then the specimens were cured under wet conditions for 27 days.

AAS mortars with and without admixtures were prepared with an aggregate/binder ratio of 3/1. Each type of PEG was added at dosages of 0.5, 1, 2, 5, 7, and 10 % by mass of slag. Each type of Vinnapas<sup>®</sup> was added at dosages of 0.5, 1, 1.5 and 2 % by mass of slag. PPG a Peramin SRA – at the dosage of 0.5 and 1 % by mass of slag.

The activator and admixtures were added to water and then mixed with metakaolin. Then quartz sand was added into the fresh mortar during mixing.

#### 4.1.6 Compressive and flexural strength tests

The effect of the type of polymer admixtures was evaluated by compressive and flexural strength. These tests assess the mechanical performance and the stability, respectively, of the produced materials in function of the additive used.

Flexural and compressive strengths of the specimens were measured at the age of 28 days. Flexural strengths were determined by using a standard three-point-bending test, while compressive strengths were measured on both residual pieces obtained from the flexural strength test. Mortar specimens were made in prismatic molds with dimensions: of  $40 \times 40 \times 160$  mm according to EN 196-1.

#### 4.1.7 Shrinkage tests

Shrinkage is one of the main harmful properties of AAS. Three shrinkage moulds ( $40 \times 40 \times 160$  mm) with steel inserts were used to determine of linear shrinkage of AAS mortar. The specimens were removed from moulds after 4 hours and then put into special apparatus (Fig.18) to measure the linear shrinkage during 28 days. The shrinkage was determined by the continual measurement of linear change in the sample's dimension.



Fig. 17 Measuring the linear shrinkage of AAS mortar specimens.

#### 4.1.8 Acoustic emission

The acoustic emission (AE) measurements were performed during the fracture experiments to assess the material's internal structure. The guard sensor eliminated mechanical and electrical noise. Four acoustic emission sensors were attached to the surface of the specimen with beeswax. Acoustic emission signals were taken by measuring equipment DAKEL XEDO with four acoustic emission sensors IDK-09 with 35 dB preamplifier.

#### 4.1.9 Mechanical fracture properties

The fracture mechanics experiments were carried out on the Heckert FP 10/1 mechanical testing machine with the measuring range of 0–1200 N. During the fracture experiments, the load vs displacement diagrams were recorded using induction sensors connected to the HBM SPIDER 8 device. The effective crack extension method was used to evaluate the  $P-d$  diagrams. The modulus

of elasticity values was obtained from the first (almost) linear part of the corrected  $P - d$  diagrams. The effective fracture toughness values were determined using the Effective Crack Model, which combines linear elastic fracture mechanics and the crack length approach.

#### **4.1.10 Porosimetry**

Total porosity and pore size distribution were determined in mortar specimens for pore and void structure through mercury intrusion porosimetry using Micromeritics Poresizer 9310 porosimeter. The specimen is put into a tared penetrometer tube and weighed. The tube is evacuated and filled with Hg at the minimum pressure. Then the pores with diameters larger than 300  $\mu\text{m}$  are filled, and the bulk volume of the sample is obtained. When the pressure is gradually increased, the Hg penetrates smaller and smaller capillaries. The filled pore volume can be computed from the capacitance of the penetrometer. Then the penetrometer is detached, weighed, and inserted in the high-pressure site where hydraulic pressure is applied. With some tens of increments, the pressure is gradually raised to the maximum of 207 MPa, and the pores down to about 6 nm are filled.

#### **4.1.11 The scanning electron microscope - microstructure assessment**

The microstructure assessment of mortars was investigated with a Tescan MIRA3 XMU scanning electron microscope, applying an acceleration voltage of 30 kV. The samples used were dried and sputtered with gold.

#### **4.1.12 Infrared spectroscopy**

The stability of admixtures was evaluated using attenuated total reflectance infrared spectroscopy (ATR IR). Infrared spectroscopy is one of the most common instrumental techniques used to study the molecular structure of organic polymers. Infrared spectroscopy is a technique based on the vibrations of the atoms of a molecule. An infrared spectrum is commonly obtained by passing infrared radiation through a sample and determining what fraction of the incident radiation is absorbed in particular energy. The energy at which any peak in an absorption spectrum appears corresponds to the frequency of vibration of a part of a sample molecule.

Admixture stability of the admixtures mentioned above was measured in the form of their 1 % solutions in alkaline media. Alkaline media was prepared by mixing water and NaOH. The solution's pH was measured with S20 SevenEasy™ pH Mettler Toledo (pH=12.42). Totally fourteen solutions with different admixtures were prepared. The solutions were placed in plastic containers and then kept dry for 24 hours using an infrared lamp at ambient temperature. After drying thin films were formed.

Infrared spectra were obtained using Perkin Elmer Frontier™ spectrometer with UATR accessory, which uses diamond crystal and enables measurement in the range of 4000–500  $\text{cm}^{-1}$ . Original polymer admixtures were used as a reference to compare and evaluate the structural changes after alkaline treatment.

For the investigation of hydration products of the alkali-activated slag, Perkin Elmer Spectrum 100 FTIR spectrometer was used. The samples were measured in the transmission mode in the range of 400–4000  $\text{cm}^{-1}$ .

#### **4.1.13 Rheology tests - workability assessment.**

Rheological investigations were performed employing a Discovery HR-1 (TA Instruments) hybrid rheometer, and TRIOS 4.0.2.30774 software was used for data evaluation. The measurements were performed in a Peltier Concentric Cylinder system with a DIN rotor at 25 °C. The standard gap for the DIN cylinder system (5.917 mm) was employed. Rheological properties were measured using 2 program methods – *Flow Sweep* and *Flow Ramp*.

The *Flow Sweep* procedure is based on measuring shear stress at changing shear rates. The rheological properties of AAS pastes were determined from curves at increasing and decreasing shear rates in the range of 0.1–100 s<sup>-1</sup>. The paste was pre-sheared for 60 s at 100 s<sup>-1</sup>. After a rest period of 60 s, the rheological measurements were started. The testing routine consisted of a shear rate increase (from 0.1 to 100 s<sup>-1</sup>) applied through 30 steps with 15 s of measuring time at each shear rate followed by a decrease of shear rate at the same conditions. The results were expressed as shear rate vs shear stress.

With the *Flow Ramp* method, shear stress at a constant shear rate in AAS paste was measured. This procedure started with pre-shearing at 100 s<sup>-1</sup> for 1 min, then ramping at the constant shear rate of 100 s<sup>-1</sup> for 30 min. The results were expressed as shear stress vs time.

The reference AAS paste mix design comprised slag (300 g) and activator (60 g). Modified AAS pastes contain different polymer admixtures at dosages 0.5, 1, 1.5 and 2 % by slag mass. The activator and polymer admixtures were dispersed and partially dissolved in water before mixing with slag. Rheology measurements were performed on pastes with a water-to-slag ratio of 0.4. For both program measurements, the pastes were initially mixed by hand in a plastic bowl with a spatula for approx. 2–3 minutes, depending on the polymer dosage (lower dosages required more time), and then they were inserted into the cup of the coaxial cylinder device mounted on the rheometer.

#### **4.1.14 Isothermal calorimetry - reaction kinetics**

TAM Air calorimeter (TA Instruments) was employed to measure the generated heat during the reaction process of AAS pastes when different dosages of polymer admixtures were used. For this purpose, several mixtures were prepared, containing slag (4 g), activator (0.8 g), water (2 g) and different types of Vinnapas<sup>®</sup> at dosages 0.5, 1, 1.5 and 2 % by mass of slag. Each composition was mixed in identical glass vials at 25 °C and then placed into a calorimeter. Heat flow was measured at 25 °C for approx. 116 h for each sample.

#### **4.1.15 X-ray diffraction (XRD) - phase assemblage**

The XRD patterns for the samples were recorded on a Bruker AXS D8 Advance diffractometer fitted with a Lynxeye super speed RX detector, a 2.2 kW Cu anode, and no monochromator. The instrument was set at 40 kV and 30 mA and the sample was not rotated during scanning. The scanning range, from 5 to 60 °, was covered in 24 minutes.

#### **4.1.16 Thermogravimetric analysis (TG) - phase assemblage**

The TG test was performed by adapting the ASTM E1131:2008 standard on thermogravimetric and compositional analysis of solids and liquids. The Setaram simultaneous thermal analyzer, model Labsys Evo with a balance accurate to 0.1 mg, was used. The dynamic heating ramp varied between 40 °C and 800 °C. The heating rate was 10 °C/min, and alumina crucibles were used. The reference material was  $\alpha$ -alumina ( $\alpha$ -Al<sub>2</sub>O<sub>3</sub>). The test was conducted under N<sub>2</sub> atmosphere. All the tests were performed using approximately 50 mg of ground sample.

#### **4.1.17 Confocal Raman Microscopy (CRM) - phase distribution**

Confocal Raman measurements have been accomplished using a 532 nm excitation laser (green laser) and a 100X objective lens (N.A. 0.9) with an area of focus over the sample at a 20 mW laser power. The scan area was 35 × 35  $\mu$ m, 20 × 20  $\mu$ m, and 15 × 15  $\mu$ m, the parameter of the Raman image: was 50 × 50 pixels, integration time per pixel was 1.2 s. All measurements were carried out in the samples to identify the modification of the phases present in the anhydrous blast furnace slag and the new phases formed after the activation with sodium silicate hydrate. Collected Raman spectra were analyzed using Witec Control Plus Software (Witec, Ulm, Germany). For the

treatment of the results obtained by Confocal Raman microscopy, “cosmic rays remove” (CRR) and “background subtraction” (BSub) were performed.

## 4.2 RESULTS AND DISCUSSION

### 4.2.1 Determination of the main reaction products of AAS: FTIR, XRD, TG and Confocal Raman Microscopy

The low crystallinity of C-A-S-H gel, which is the main product formed in AAS, does not allow its detection with XRD, while other methods, such as FTIR and TG, do not give accurate information about its presence. In order to gain more insights into this phase, the Confocal Raman Spectroscopy was used complementary to XRD, FTIR, and TG.

FTIR spectrum of the anhydrous slag is illustrated in Fig. 19. The absorption band at ca.  $930\text{ cm}^{-1}$  in the anhydrous slag is attributed to the Si–O vibration in the  $\text{SiO}_4$  units. In addition, the absorption band ca.  $508\text{ cm}^{-1}$  is associated with  $\nu_4$  [Si–O–Si] bond vibrations, and the absorption band ca.  $669\text{ cm}^{-1}$  is due to the stretching vibrations of Al–O bonds in the  $\text{AlO}_4$  groups. The presence of carbonate in this material is evident due to the absorption band at ca.  $1420\text{ cm}^{-1}$  attributed to  $\nu_3[\text{CO}_3^{2-}]$ . Carbonation occurred due to the high content of CaO included initially in the slag.

Figure 18a presents the FTIR spectra of AAS pastes at 1, 2, 7, and 28 days. It is observed that the main absorption band (related to the Si–O–Si vibrations) moves towards higher wavenumbers with time due to the formation of calcium silicoaluminate hydrated compound, C-A-S-H gel (Figure 18b). This displacement is typical for alkaline activated slag pastes with silicon-rich solutions, indicating the formation of silicon-rich gel, though without becoming a silica gel [34]. The absorption band at ca.  $450\text{ cm}^{-1}$  (observed in the anhydrous slag at ca.  $508\text{ cm}^{-1}$ ) is assigned to the vibrations of  $\delta$  Si–O–Si bonds,  $\nu_4$ , due to the formation of the C-A-S-H gel, while the absorption band observed ca.  $669\text{ cm}^{-1}$  is due to the Al–O vibrations in the  $\text{AlO}_4$  groups (Figure 18c). Absorption bands at ca.  $1420\text{ cm}^{-1}$  also appear, attributed to  $\text{CO}_3^{2-}$ ,  $\nu_3$ , confirming the carbonation or weathering of the pastes.

The  $\nu_{\text{as}}$ , located ca.  $967\text{ cm}^{-1}$ , shows a decrease in intensity compared to the Si–O–Si bonds of anhydrous blast furnace slag. This development results from aluminum and calcium incorporation in the Si–O chains during the formation of the main reaction product (C-A-S-H gel). Garcia-Lodeiro et al. [35, 36] suggested that the displacement of sodium by calcium in the (N,C)-A-S-H gels does not imply relevant changes in the position of the absorption band; however, the variation in its shape likely marks the precipitation of new phases that are not typical components of C-S-H gels.

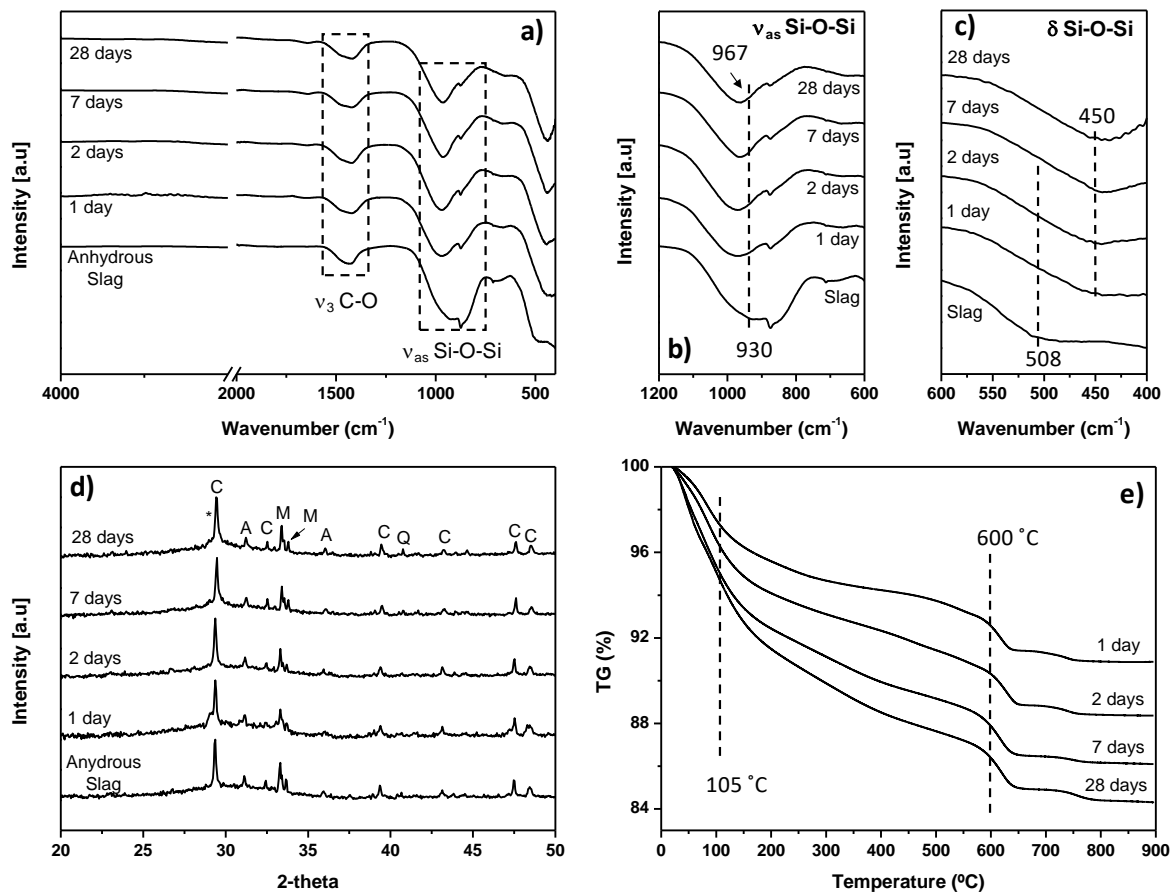


**Fig. 18** Determination of the blast furnace slag and the main reaction products at 1, 2, 7 and 28 days by FTIR, XRD and TG. **a)** FTIR spectra of the anhydrous blast furnace slag and AAS pastes; **b)** main absorption band associated with Si-O-Si in the range 600-1200  $\text{cm}^{-1}$ . There is a shift of the main absorption band from 930 to 967  $\text{cm}^{-1}$ , indicative of the formation of C-A-S-H gel (rich in silicon); **c)** absorption band associated to  $\delta$  Si-O-Si. There is an FTIR shift towards lower wavenumbers, indicative of the formation of the C-A-S-H gel; **d)** XRD patterns for the anhydrous blast furnace slag and AAS pastes. The main phases present are calcite ( $\text{CaCO}_3$ , C), akermanite ( $\text{Ca}_2\text{Mg}(\text{Si}_2\text{O}_7)$ , A), mullite (M) and quartz ( $\text{SiO}_2$ , Q). In addition, the main reaction product is the C-A-S-H gel (\*) located at  $2\theta$  values in the same region of the main calcite diffraction peak; **e)** TG analysis of AAS pastes with the mass losses (%) evolution vs temperature up to 900  $^\circ\text{C}$ .

The diffractogram of the anhydrous blast furnace slag (Figure 18d) shows a small amorphous halo with a maximum of around  $2\theta = 30\text{--}32^\circ$ . This halo coincides with the region in which the characteristic diffraction peaks of akermanite appear ( $\text{Ca}_2\text{Mg}(\text{Si}_2\text{O}_7)$ ) at values close to  $2\theta = 31.1^\circ$ ,  $28.9^\circ$ , and  $51.8^\circ$ , which constitutes one of the main phases found in the slag. In addition, crystalline diffraction peaks attributed to the quartz ( $2\theta = 21.8^\circ$ ,  $27.7^\circ$  and  $40.8^\circ$ ), calcite ( $2\theta = 29.4^\circ$ ,  $47.4^\circ$  and  $48.5^\circ$ ), and mullite (due to the aluminum content of the slag), were observed. The formation of C-A-S-H gel is indicated by the wide bump around  $29^\circ$ , overlapping with the main diffraction peak of calcite ( $\text{CaCO}_3$ ) due to its low structural order (C-A-S-H is largely amorphous). Thus, XRD is inadequate to quantitatively assess the formation of C-A-S-H gel in the studied systems. Thermogravimetry analysis (TG) may provide more information [142].

The mass loss values determined during the thermogravimetry analysis of the alkaline activated slag are associated with the chemically combined water that is proportional to the amount of reaction products formed. Hence, higher mass loss points to a higher reaction degree of the slag. Table 6 shows the mass loss values of mass losses calculated from TG curves in the temperature range 105–600 °C for AAS pastes of different ageing (1, 2, 7 and 28 days) (see Figure 18e). However, these data can be used mainly to compare the effect of different curing times on AAS paste, without providing significant information about the reaction degree. The obtained data refer to water lost in a wide temperature range, related to the amorphous nature of the gel, i.e. the water may occupy multiple places within the amorphous structure of the gel, including bonds with different cations involved or even interposition places. The nanometric nature of the formed bonds allows for several binding of water in the systems; the energy required for water removal confirms this fact. Consequently, considering the water determined as an indicator of the quantity of the gel formed would lead to an underestimation of its actual quantity.

**Table 5.** Mass losses by TG between 105–600 °C

Temperature (°C)	1 day	2 days	7 days	28 days
105–600	4.9 %	6.3 %	7.6 %	8.9 %

From Table 5 it can be observed that the water loss occurs mainly in the temperature interval of 105–600 °C, being higher for longer ageing times. Therefore, this indicates that the formation of the main reaction product (C-A-S-H gel) has gradually occurred.

FTIR, XRD and TG provided relative information at each studied age of the reaction degree of alkaline activated slag. However, the low crystallinity of the main reaction product (C-A-S-H gel) prevents the retrieval of information related to its formation, distribution throughout the sample, the extent of carbonation, etc. That is why we must resort to more sophisticated techniques, such as <sup>29</sup>Si and <sup>27</sup>Al s NMR, BSEM/EDX, TEM or Confocal Raman Microscopy (CRM). The latter allows for investigating the AAS pastes' structure and microstructural evolution during the alkaline activation process.

Figure 19a reports the Raman spectrum for the anhydrous slag, contributed by different phases which have a characteristic Raman cross-section; thus, this technique is not affected by the amount of the phases in the sample. The presence of different phases in the average Raman spectrum of the main phases is shown in Figure 20c. In the region 800–1000 cm<sup>-1</sup> of the average spectrum, the presence of a weak and broad Raman peak at ca. 885 cm<sup>-1</sup> is observed, attributed to the symmetric stretching of Si–O–Si,  $\nu_1$ , of the anhydrous slag, corresponding to the presence of the main Raman bands associated with the presence of mullite at ca. 800 and 950 cm<sup>-1</sup> [143]. Another phase contributing to the Raman spectrum is the crystalline akermanite (Ca<sub>2</sub>Mg(Si<sub>2</sub>O<sub>7</sub>)), giving rise to the bands located at 666 cm<sup>-1</sup> and 911 cm<sup>-1</sup>. Further, the Raman bands observed at 350–500 cm<sup>-1</sup> and 400–600 cm<sup>-1</sup> are attributed to  $\nu_2$ -type internal deformations and  $\nu_4$ -type asymmetric bending vibrations of SiO<sub>4</sub> tetrahedra, respectively. An intense and narrow Raman band at ca. 1096 cm<sup>-1</sup> and the less intense Raman band at ca. 283 cm<sup>-1</sup> are distinguished, both attributed to the presence of calcium carbonate.

Figure 19b shows the Raman spectrum of the commercial sodium silicate solution, in which four well-distinguished zones are observed: the band at ca. 525 cm<sup>-1</sup> is associated with the stretching modes of Si–O–Si (Q<sup>3</sup>); the band at ca. 1041 cm<sup>-1</sup> is attributed to the symmetric stretching of Q<sup>3</sup> (Q<sup>3</sup>-SS); the band at ca. 1647 cm<sup>-1</sup> is due to the bending vibrations of water; the very wide and intense band at ca. 3400 cm<sup>-1</sup> is associated to the stretching vibrations of OH<sup>-</sup> groups.

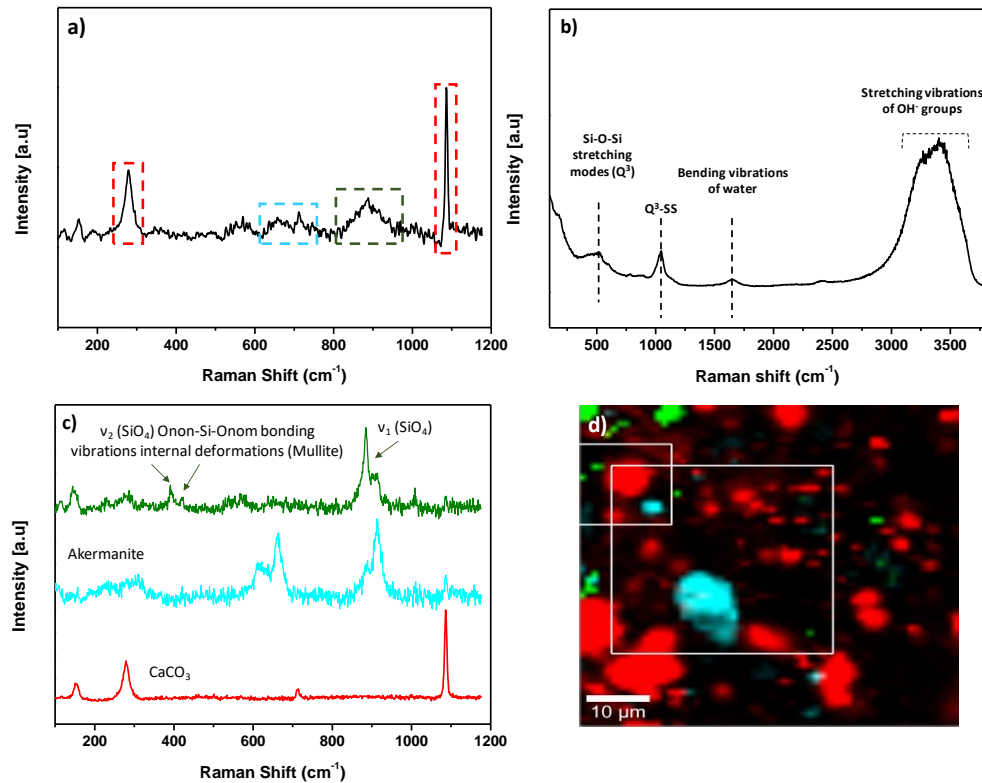


**Fig. 19** **a)** Average Raman spectrum of the anhydrous blast furnace slag; **b)** Average Raman spectrum of sodium silicate solution (water glass solution); **c)** average Raman spectra of the main phases present in the anhydrous blast furnace slag: calcium carbonate ( $\text{CaCO}_3$  in red), akermanite ( $\text{Ca}_2\text{Mg}(\text{Si}_2\text{O}_7)$ , in cyan) and the symmetric stretching bonds of  $\text{SiO}_4$  from slag, in green; **d)** Surface Raman image by CRM of the anhydrous blast furnace slag used in this study. The main phases present in the blast furnace slag are  $\text{CaCO}_3$  in red, akermanite ( $\text{Ca}_2\text{Mg}(\text{Si}_2\text{O}_7)$ ) in cyan and the symmetric stretching bonds of  $\text{SiO}_4$  ( $\nu_1$  Si-O-Si) of the anhydrous slag and for the presence of mullite, in green. The boxes represent the different regions of the sample where the analysis has been made.

Besides detecting different phases, CRM provides a microstructural view of the phase distribution, evident in Figure 19d, which is indicated by the corresponding colors assigned to each of them. The mean particle size ( $d_{50}$ ) of the slag was  $19 \mu\text{m}$ ; however, due to the confocality of the instrument, only a small portion of the sample ( $0.7 \mu\text{m}$ ) is located at the focal plane. Therefore, Figure 19d shows the abundant presence of  $\text{CaCO}_3$  in red, which has particle size lower than  $10 \mu\text{m}$ , representing a portion of the particles. Carbonate phases formed in the sample due to the calcium content of slag, which reacted with  $\text{CO}_2$ . In addition, the presence of akermanite ( $\text{Ca}_2\text{Mg}(\text{Si}_2\text{O}_7)$ ) is indicated with cyan colour, while the symmetric stretching bonds of  $\text{SiO}_4$  ( $\nu_1$  Si-O-Si) of mullite (green color) found in anhydrous slag are also detected.

Fig. 20 shows the average Raman spectra of the anhydrous blast furnace slag and the alkali-activated slag at different hydration ages (1, 2, 7 and 28 days). The alkali activation of slag by the solution of sodium silicate (or water glass solution) results in the detection of Raman bands associated with the main reaction products, in addition to those corresponding to the main phases of the anhydrous slag still present in the samples. More specifically, the newly appearing band at ca.  $673 \text{ cm}^{-1}$  is a band associated with the formation of C-A-S-H gel, assigned to  $\text{Q}^2$  Si-O-Si symmetric bending vibrations. Although the C-A-S-H gel is poorly crystalline, the CRM

measurement conditions applied in the test (532 nm excitation laser; a 100X objective lens, N.A. 0.9; and 20 mW laser power) allow for detecting its signal at each age. The peak at ca.  $673\text{ cm}^{-1}$  is better resolved 1 and 2 days after mixing (Fig. 21b) than at more advanced ages (7 and 28 days), indicating that the amount of C-A-S-H gel formed increased with time. Moreover, the intensity of this band coincides with the presence of akermanite,  $\text{Ca}_2\text{Mg}(\text{Si}_2\text{O}_7)$ , a characteristic phase of the anhydrous slag, having its main band at ca.  $666\text{ cm}^{-1}$  (Figure 20c). As the reaction time evolved, the amount of C-A-S-H gel in the system increased, being highest at the ages of 7 and 28 days, as observed both in the average spectra (see Fig. 20b) and in the different micrographs obtained (Fig. 20c).

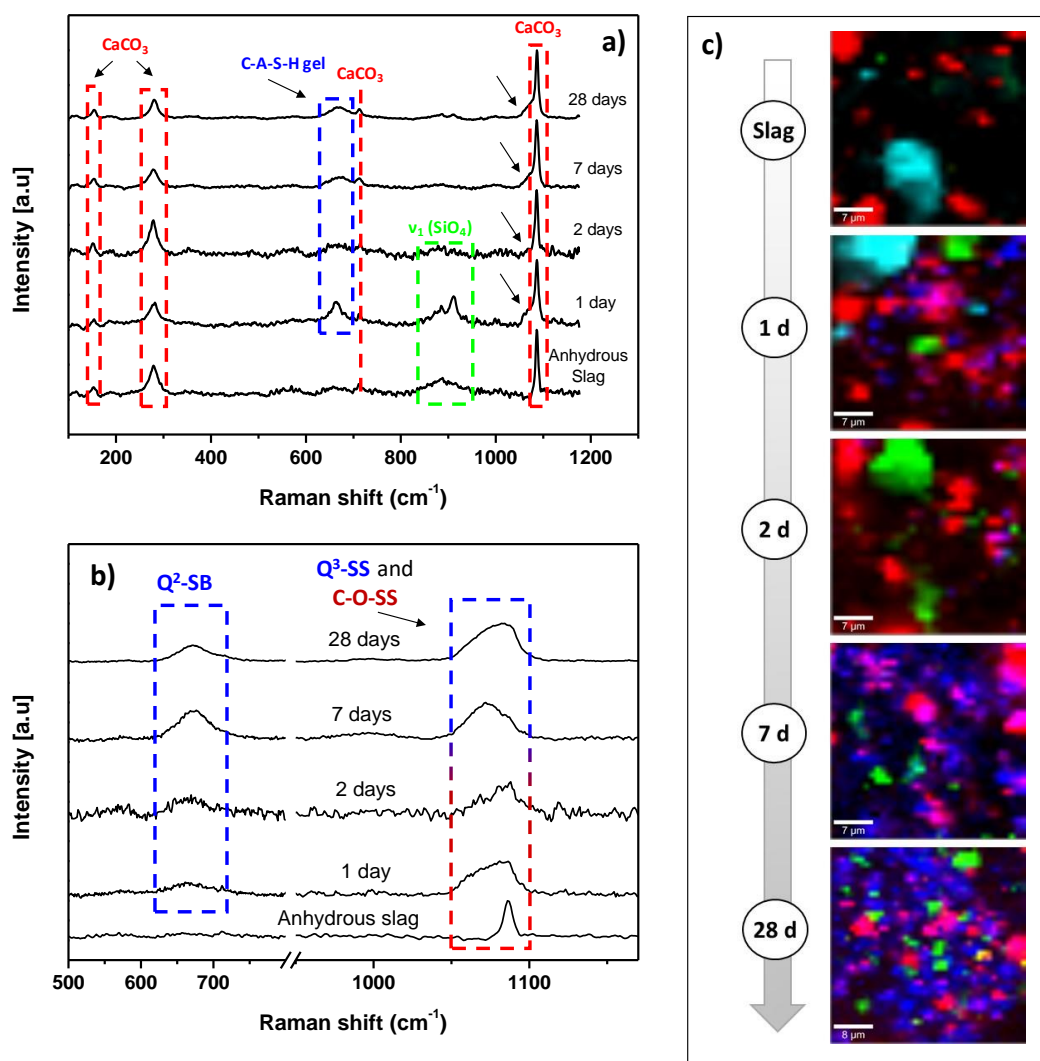


**Fig. 20** a) Average Raman spectra of the anhydrous blast furnace slag and the alkali-activated slag at different ages (1, 2, 7 and 28 days) obtained by Confocal Raman Microscopy (CRM). b) Average Raman spectra of the region where C-A-S-H gel Raman bands are located at different activation times. The main Raman band of the C-A-S-H gel is located at ca.  $666\text{ cm}^{-1}$ , attributed to Si-O-Si symmetric bending  $\text{Q}^2$  ( $\text{Q}^2\text{-SB}$ ); and a Raman band ca.  $1040\text{ cm}^{-1}$ , associated with the symmetric stretching of  $\text{Q}^3$  ( $\text{Q}^3\text{-SS}$ ) and symmetric stretching of C-O group in  $\text{CaCO}_3$  precipitates (C-O-SS); c) Raman images by CRM of the evolution of the main phases of anhydrous slag (akermanite, in cyan and the symmetric stretching bonds of  $\text{SiO}_4$  from slag, in green), calcite ( $\text{CaCO}_3$ , in red) and the formation of the main reaction product in this system (C-A-S-H gel, in blue).

Another aspect to be highlighted from the results of CRM is the presence of carbonates in the samples ( $\text{CaCO}_3$ ). In the average Raman spectrum of the anhydrous slag, the presence of a calcite-like crystalline carbonate is unequivocal. The Raman spectrum of calcite possesses several bands: ca. 180 and 280  $\text{cm}^{-1}$  are due to the relative translations between the cation and anionic groups; the vibration mode  $\nu_4$  at ca. 711  $\text{cm}^{-1}$  is attributed to symmetric  $\text{CO}_3$  deformation; the vibration mode  $\nu_1$  at ca. 1085  $\text{cm}^{-1}$  corresponds to the symmetric stretching of C–O group in  $\text{CaCO}_3$  that precipitates as calcite [143–145]. However, these Raman bands, considered indicators of the presence of calcite in slag, remain practically unaltered during the alkaline activation with sodium silicate. From the beginning of the reaction, some regions of slag are partially carbonated, especially those at the surface of the reaction product, due to their high crystallinity and opacity. In addition, as the reaction evolves with time, the calcium included in slag dissolves in the silicate solution, contributing to a calcium enrichment of the solution, and, therefore, calcite forms due to the available atmospheric  $\text{CO}_2$  [146].

As regards the main silicate phases, inherited either from the raw material (slag) or from the liquid activator (sodium silicate or water glass solution), they are also maintained throughout the hydration process, acting both as the source of silicates for the formation of the C-A-S-H gel. However, this behavior does not account for akermanite, only detected in the anhydrous slag and at 1 and 2 days after activation. The presence of akermanite at early ages obscures the detection of the C-A-S-H gel since the Raman bands of both compounds overlap in the same spectral region. The extensive formation of well-crystallized akermanite in early ages intensifies its Raman signal compared to the low-intensity Raman signal of the C-A-S-H gel. Subsequently, at 1 and 2 days, the presence of C-A-S-H gel is hardly observed. At a later age, gel precipitation occurs in the solution (Fig 21), growing differently compared to the C-S-H gel forming during the hydration of Portland cement. In such a system, C-S-H gel grows around the  $\text{C}_3\text{S}$  particles forming layers [147]. However, in the alkali-activated slag systems, the growth of the C-A-S-H gel is random. At early ages, the hydration products grew in the space between the slag grains originally occupied by alkaline solution, indicating that gel forms through a dissolution/precipitation mechanism. SEM is not appropriate for detecting the amorphous C-A-S-H gel when the activator is a water glass solution because of the homogeneity of their mixture. On the contrary, CRM allows for distinguishing the C-A-S-H gel and, thus, observing its growth and structural evolution.

The main Raman band of the C-A-S-H gel appears at ca. 666  $\text{cm}^{-1}$ . Additionally, Raman bands of this phase emerge in the regions 350–500  $\text{cm}^{-1}$  and 400–600  $\text{cm}^{-1}$ , which is generally attributed to  $\nu_2$ -type internal deformation and  $\nu_4$ -type asymmetric bending vibrations of  $\text{SiO}_4$  tetrahedra, respectively. In the average Raman spectrum, it is possible to observe the evolution of the Raman band at ca. 1080  $\text{cm}^{-1}$  with the activation time. In addition to the presence of calcite, another Raman band is attributed to symmetric stretching of  $\text{Q}^3$  groups, which form as the result of polymerization of the C-A-S-H gel chains. In this region, the main Raman bands of the sodium silicate solution also contributes to line widening (see Fig. 21b).

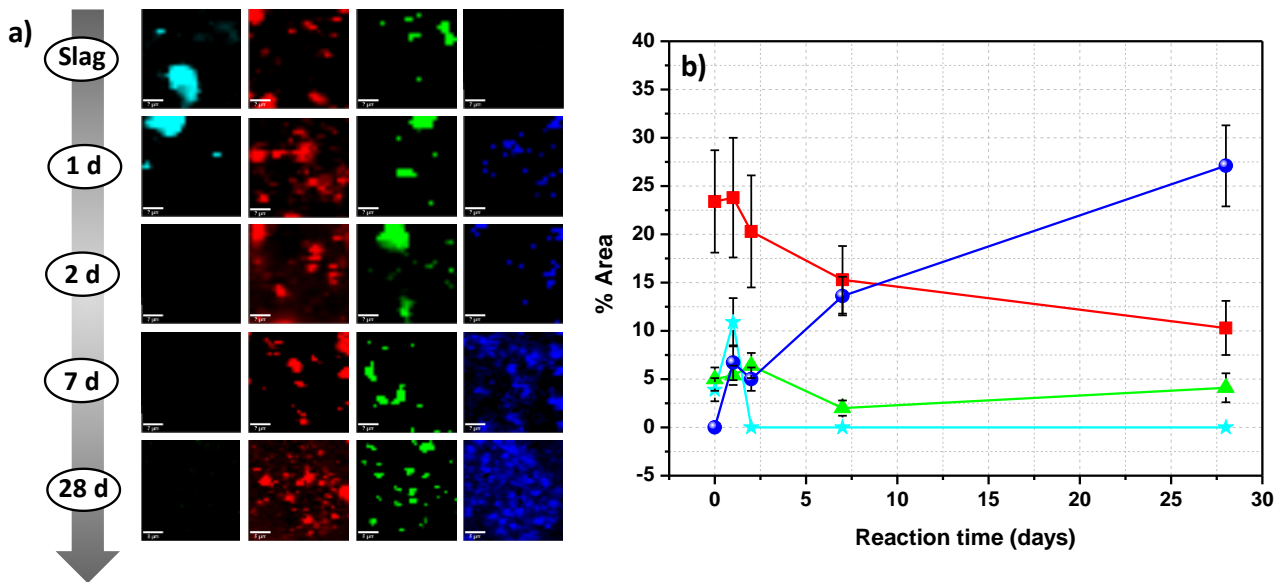


**Fig. 21 a)** Raman images by CRM of the evolution of the main phases present in the alkali-activated slag at different ages (1, 2, 7 and 28 days): akermanite (in cyan), calcite ( $\text{CaCO}_3$ , in red), the symmetric stretching bonds of  $\text{SiO}_4$  from slag (in green), and the presence of C-A-S-H gel (in blue); **b)** quantitative determination of the presence of the main phases present during the alkali-activation of blast furnace slag: akermanite (in cyan), calcite (in red), the symmetric stretching bonds of  $\text{SiO}_4$  (in green) and the C-A-S-H gel (in blue).

From a quantitative standpoint, using CRM allows for more detailed information on each of the phases present in the alkaline activated system. Fig. 21 shows the evolution of phase content with time. On the other hand, as the reaction of slag with the sodium silicate occurs, carbonates dissolve too. Besides the carbonates that are initially present in the systems, newly formed carbonates appear in the regions close to those where C-A-S-H gel forms, indicative of the susceptibility of the C-A-S-H gel to carbonation.

In Fig. 22, the quantification of the main reaction product is reported based on the obtained Raman spectra. Although the high amount of carbonates in the system can suppress the Raman signal corresponding to the C-A-S-H gel due to their crystal order, the use of the CRM technique gives a high degree of reliability in the quantification of the gel at different ages. Unlike the quantification obtained by DTA/TG, which is established from the water loss associated with the C-A-S-H gel in a temperature range between 105–600 °C, the amount of C-A-S-H gel forming is detected in situ with CRM without destroying the sample. When working at room temperature, the amount of water chemically bound to the gel cannot be determined; however, the information obtained is much more representative and concise regarding the composition of the amorphous material. A comparison of the C-A-S-H gel content in the AAS paste, as derived from DTA/TG and CRM, is illustrated in Fig. 22. Since CRM allows for determining the area where C-A-S-H gel is present, the amount of gel detected is more than three times higher than that determined from DTA/TG. The values obtained from CRM are more realistic, and not affected by the C-A-S-H gel's low crystallinity.

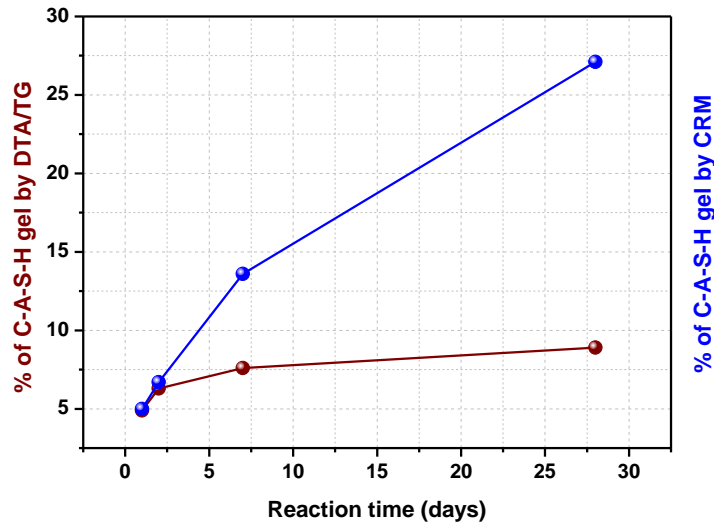


**Fig. 22** Quantitative determination of the presence of C-A-S-H gel determined by Confocal Raman Microscopy and by DTA/TG.

The results show that using Confocal Raman Microscopy (CRM) is a feasible technique for characterising alkali activated materials. The results obtained from conventional characterization techniques (FTIR, XRD, or DTA/TG) allowed for obtaining information about the phases of the slag and the main reaction product, i.e. the C-A-S-H gel. However, due to the poor crystallinity of the C-A-S-H gel, XRD cannot provide detailed information about its structure. Regarding the degree of reaction of the activated pastes with the sodium silicate solution, DTA/TG technique is more informative. Since the water that is chemically bound in the C-A-S-H gel can be determined through the weight loss of the material occurring in the temperature range 105–600 °C, the extent of C-A-S-H gel formation can be assessed. However, this technique underestimates the degree of reaction and does not provide any information concerning the C-A-S-H gel's composition and morphology.

CRM, combining the high spectral resolution of Raman spectroscopy with the high spatial resolution of Confocal Microscopy, illustrates the distribution of the main phases present in the alkali-activated system at different ages. Despite the poor crystallinity of the C-A-S-H gel, the hydration of slag at different ages can be easily assessed. Furthermore, the phases formed can be quantified with good accuracy. In addition, CRM allowed for highlighting the differences between the growth of C-A-S-H gel in AAS paste and of a C-S-H gel in OPC systems. In contrast to C-S-H gel that grows on the surface of  $C_3S$  grains, the growth of C-A-S-H gel occurs randomly in the medium, always in regions where the calcium, included in the slag, is dissolved.

CRM is an alternative technique for the microstructural characterization of alkali-activated materials or geopolymers. It allows for revealing the mechanisms involved during the activation process, leading to the formation of new phases. At the same time, it likely facilitates the understanding of durability-related phenomena in these systems, such as carbonation, freeze-thaw resistance or chemical attack.

#### 4.2.2 Stability of admixtures

All organic admixtures used in the experiments were tested for their stability in a highly alkaline environment. The changes in chemical structure were evaluated through infrared spectroscopy. The IR spectra compare the original unexposed admixtures and admixtures after 1 day of exposure to alkaline media (Figs. 23–32).

IR spectra depicted in Figs. 23–27 showed that the chemical structure of the PEG and PPG admixtures are not significantly affected by the treatment in highly alkaline media of NaOH. In the IR spectra of PEG 400 (Fig. 23), the H<sub>2</sub>O bending band at 1638 cm<sup>-1</sup> attributed to the trapped water has been observed as a new feature. Furthermore, the band at 3461 cm<sup>-1</sup> corresponding to the stretching vibrations of the OH group became broader.

Almost no significant structural changes were also observed in the spectra of the Peramin SRA admixture (Fig. 28). Only two new features appeared in the spectrum of exposed admixture: a broader band at 1427 cm<sup>-1</sup> and a sharp band at 874 cm<sup>-1</sup>. The band at 1427 cm<sup>-1</sup> was assigned to  $\nu_{as}CO$  mode in carbonate anion, and the sharp band at 874 cm<sup>-1</sup> corresponds with the bending  $\delta CO_3$  mode. The presence of carbonate species leads to the assumption that partial carbonation of alkaline solution occurred.

The qualitative analyses of the structural changes of different types of Vinnapas<sup>®</sup> admixtures are presented in Figures 29–32. Significant structural changes were observed using IR spectroscopy in all Vinnapas<sup>®</sup> samples that were treated with NaOH solution. The three characteristic bands between 3700 and 3500 cm<sup>-1</sup>, which correspond to vibrations of O–H groups, diminished. A broad band around 3300 cm<sup>-1</sup> that is associated with adsorbed water split into three bands. There are also small changes in the intensity of the peaks at 2937 and 2864 cm<sup>-1</sup> (correspond to C–H bonds of CH<sub>2</sub>) in the IR spectrum of all types of Vinnapas<sup>®</sup> (Figs. 29–32). A very strong band at 1730 cm<sup>-1</sup> (corresponds to C=O stretching of ester) is present in all IR spectra. However, more intense bands were observed in alkaline media only for Vinnapas<sup>®</sup> 5023 L and 7220 E (Figs. 29 and 32), whereas for Vinnapas<sup>®</sup> 5023 L and 7022 E, the intensity of the C=O band in alkaline media was slightly lower.

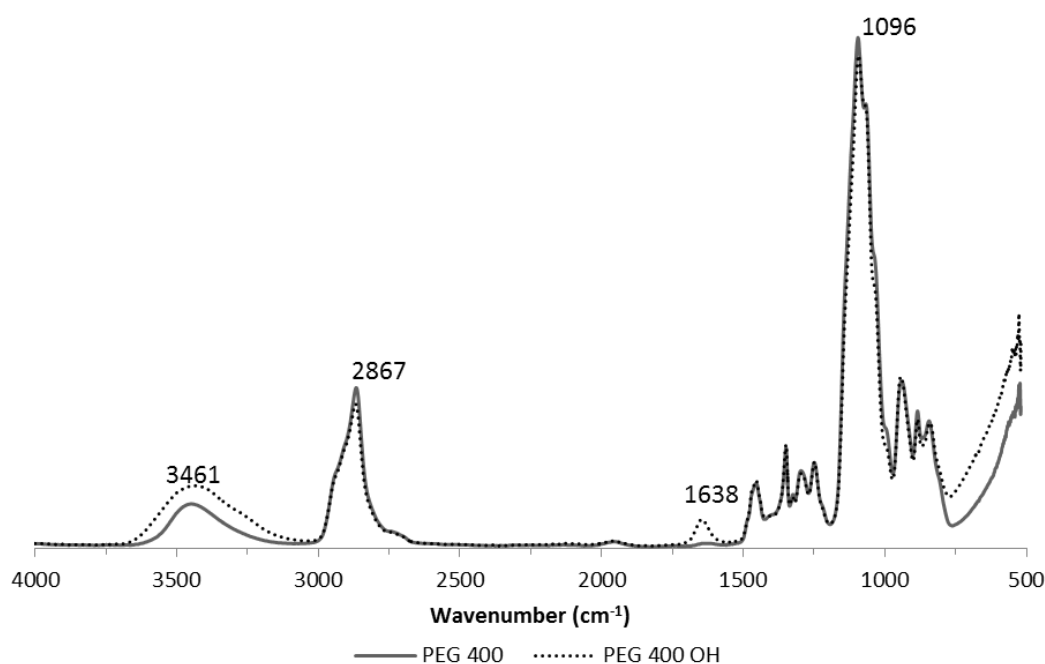


**Fig. 23** Infrared spectra of PEG 400 and its solution in alkaline media.

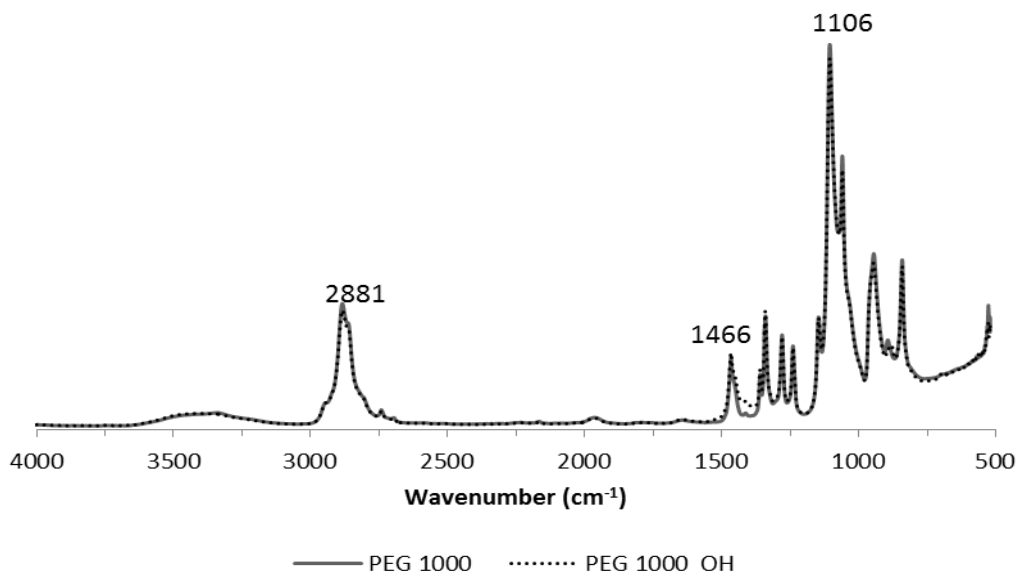


**Fig. 24** Infrared spectra of PEG 1000 and its solution in alkaline media.

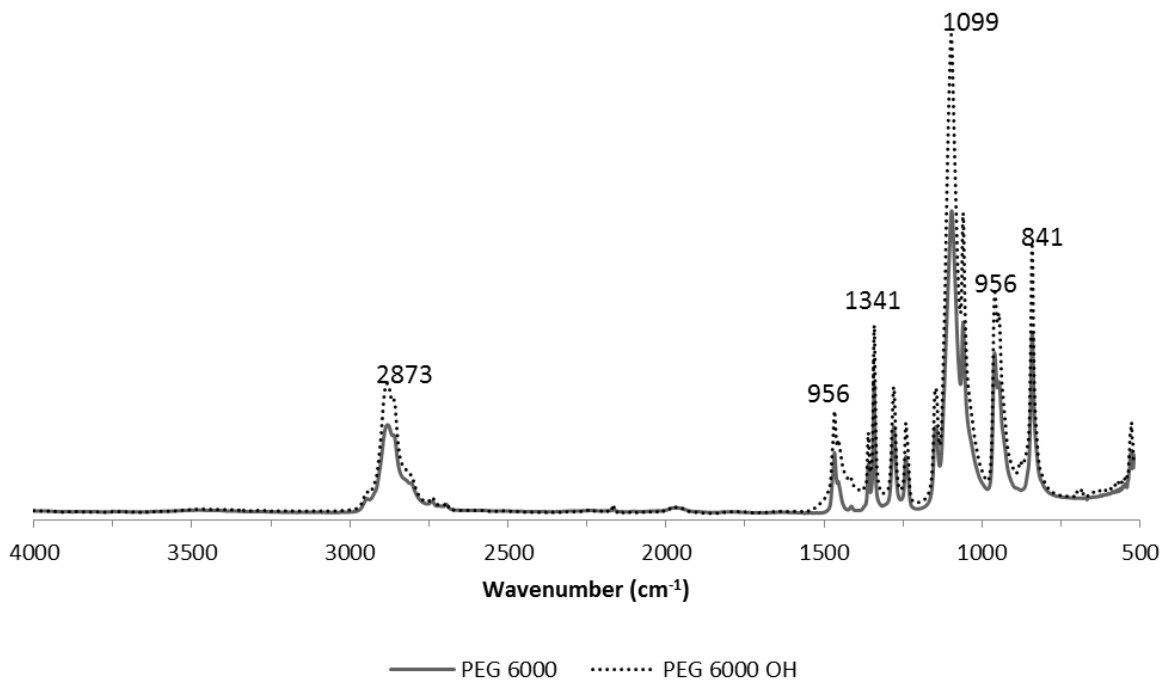


**Fig. 25** Infrared spectra of PEG 6000 and its solution in alkaline media.

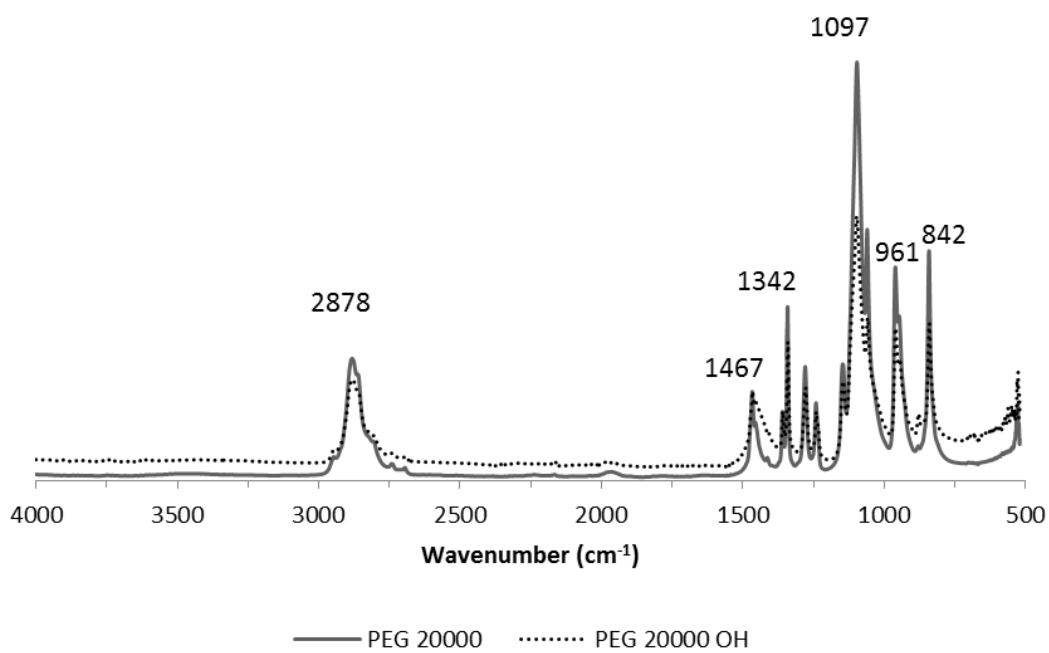


**Fig. 26** Infrared spectra of PEG 20000 and its solution in alkaline media.

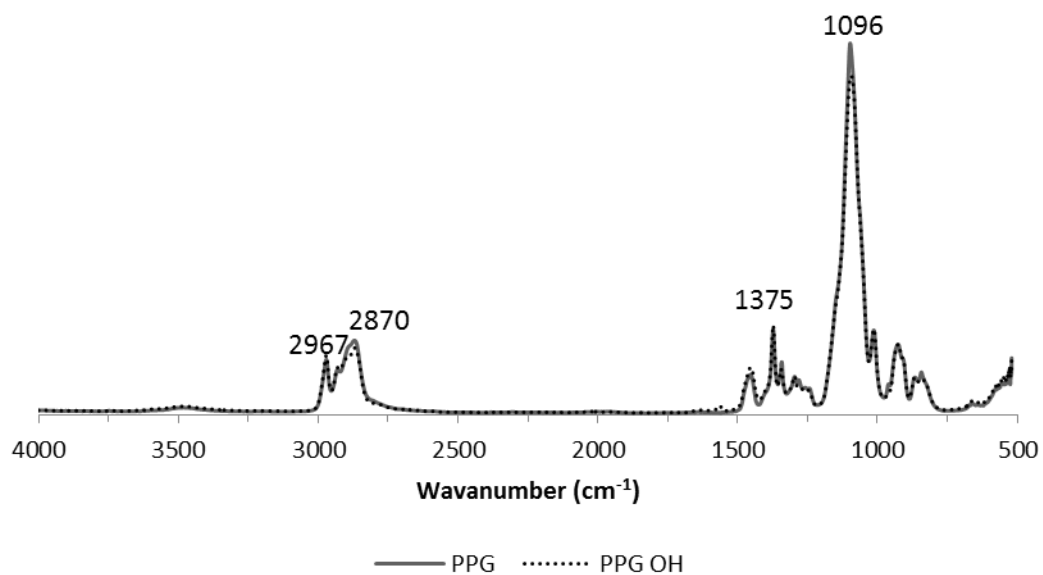


**Fig. 27** Infrared spectra of PPG and its solution in alkaline media.

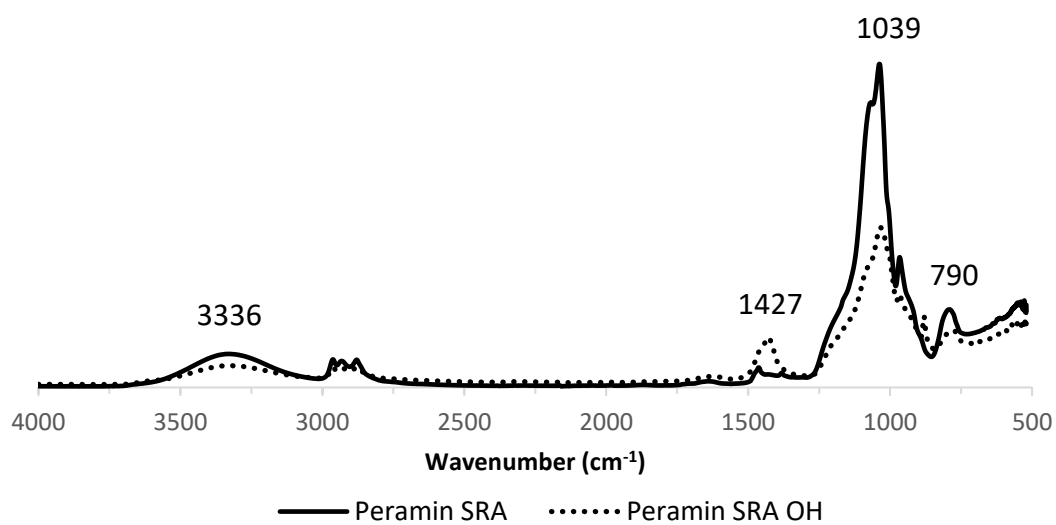


**Fig. 28** Infrared spectra of Peramin SRA and its solution in alkaline media.

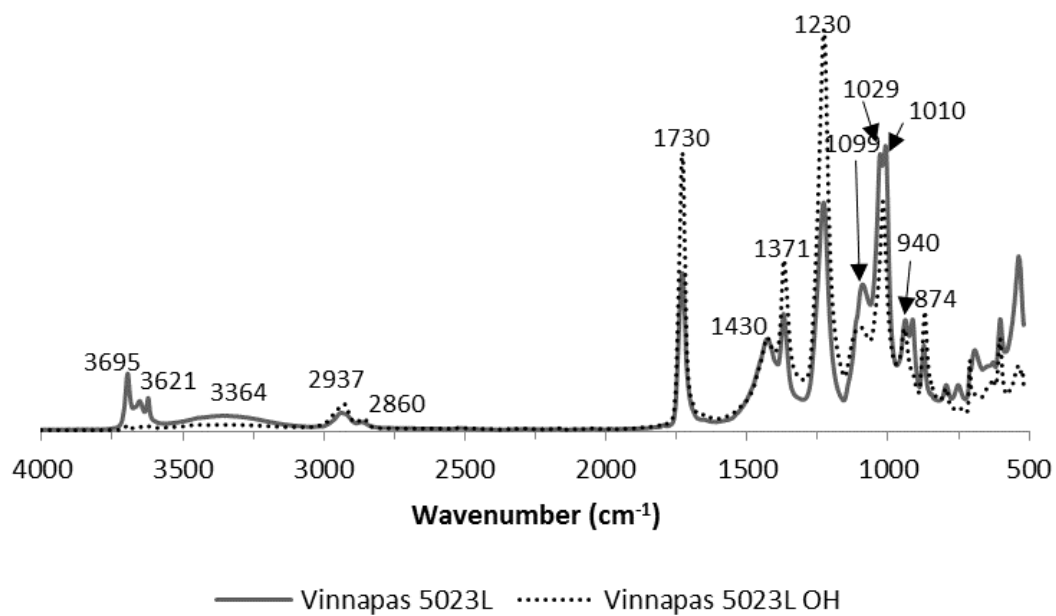


**Fig. 29** Infrared spectra of Vinnapas<sup>®</sup> 5023 L and its solution in alkaline media.

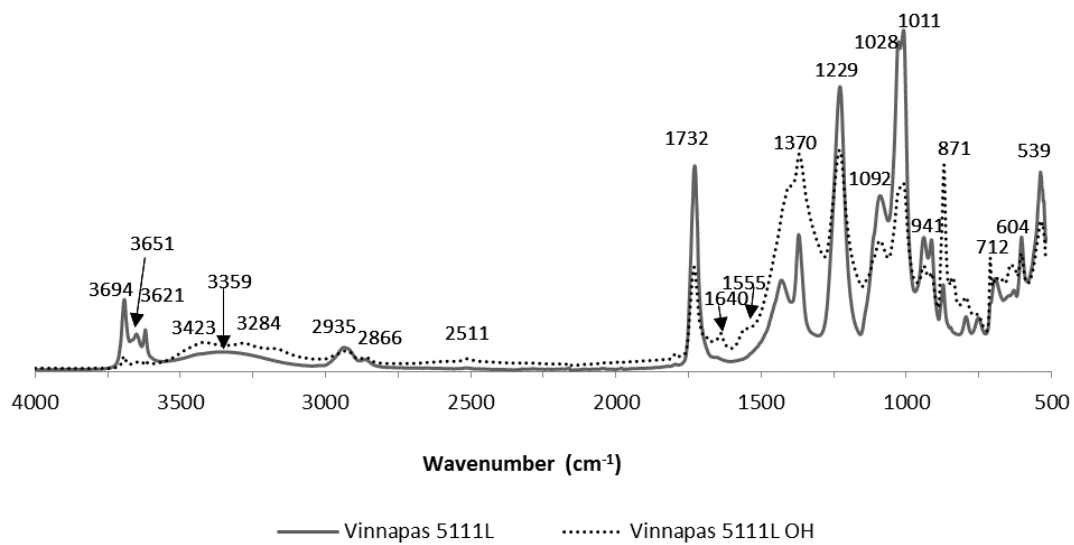


**Fig. 30** Infrared spectra of Vinnapas<sup>®</sup> 5111 L and its solution in alkaline media.

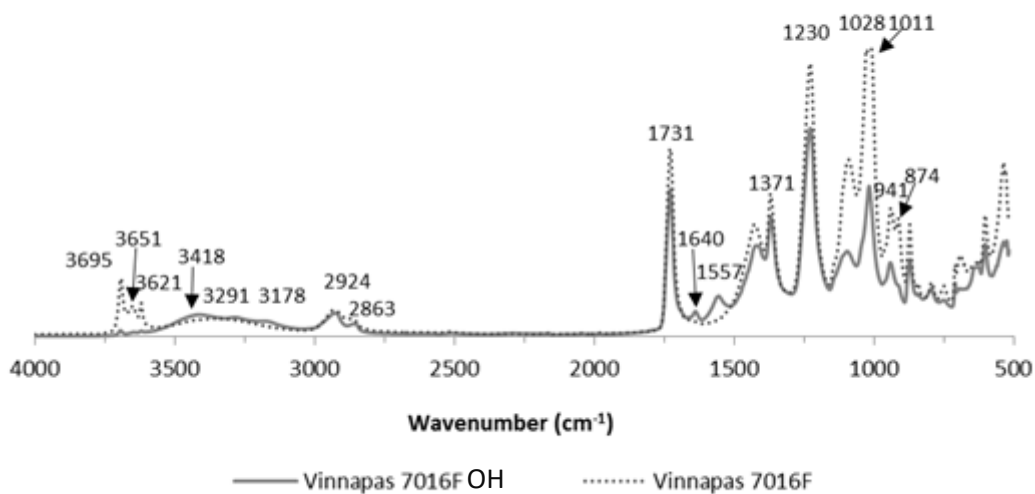


**Fig. 31** Infrared spectra of Vinnapas<sup>®</sup> 7016 F and its solution in alkaline media.

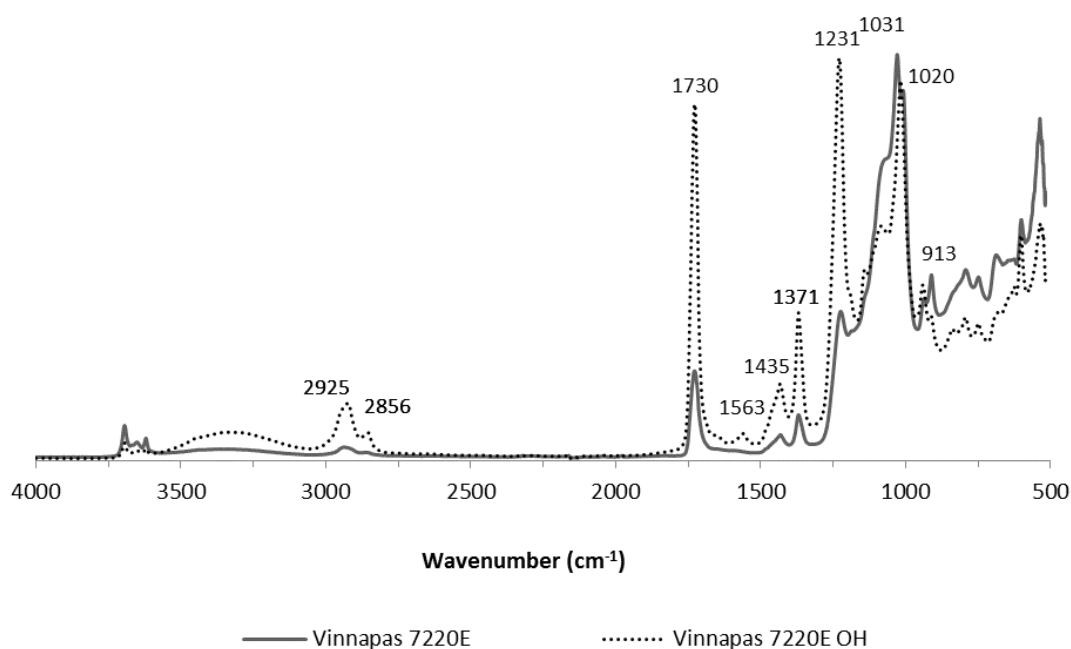


**Fig. 32** Infrared spectra of Vinnapas<sup>®</sup> 7220 E and its solution in alkaline media.

The IR spectra of Vinnapas<sup>®</sup> 5111 L, 7016 F, and 7022 E dissolved in NaOH solution contained new features at 1640 and 1555  $\text{cm}^{-1}$ .

Vibration bands at 1370, 1230 and 941  $\text{cm}^{-1}$  that can be assigned to C–H bending and C–O stretching bands of alcohols and esters are presented in all IR spectra. The band at 1092  $\text{cm}^{-1}$  can be assigned to C–O–C in ethers. Very strong bands C–O at 1029 and 1010  $\text{cm}^{-1}$  can be assigned to C–O in alcohols. The most important observations after the treatment of Vinnapas<sup>®</sup> admixtures in alkaline solution are a simultaneous decrease in intensity of bands around 3600, 1090, 1030 and 1010  $\text{cm}^{-1}$  and the appearance of a new band around 1555  $\text{cm}^{-1}$ , which proves significant structural changes in the chemical composition of these admixtures.

IR spectroscopy was used to study the stability of different commercial polymer admixtures in alkaline media NaOH with pH = 13.47. All PEGs with different molecular mass and PPG are stable in alkaline solution because significant structural changes were not identified. However, structural changes in all types of Vinnapas<sup>®</sup> were observed. Since Vinnapas<sup>®</sup> additives are mainly based on copolymers of vinyl esters and alkyl acrylates, neutralization and probable alkaline hydrolysis occur in a strongly basic environment. However, since the detailed composition of the admixtures is concealed by the manufacturer, it is not possible to reveal all the specific structural changes. However, we can conclude that these admixtures are unstable in highly alkaline media.

#### 4.2.3 Rheological tests

In these experiments, only pastes with Vinnapas<sup>®</sup> admixtures were studied because high shear mixing during viscosimetric experiments caused unexpected segregation of PEG and PPG admixtures from AAS pastes.

Flow curves of the studied alkali-activated slag pastes are shown in Fig. 33.

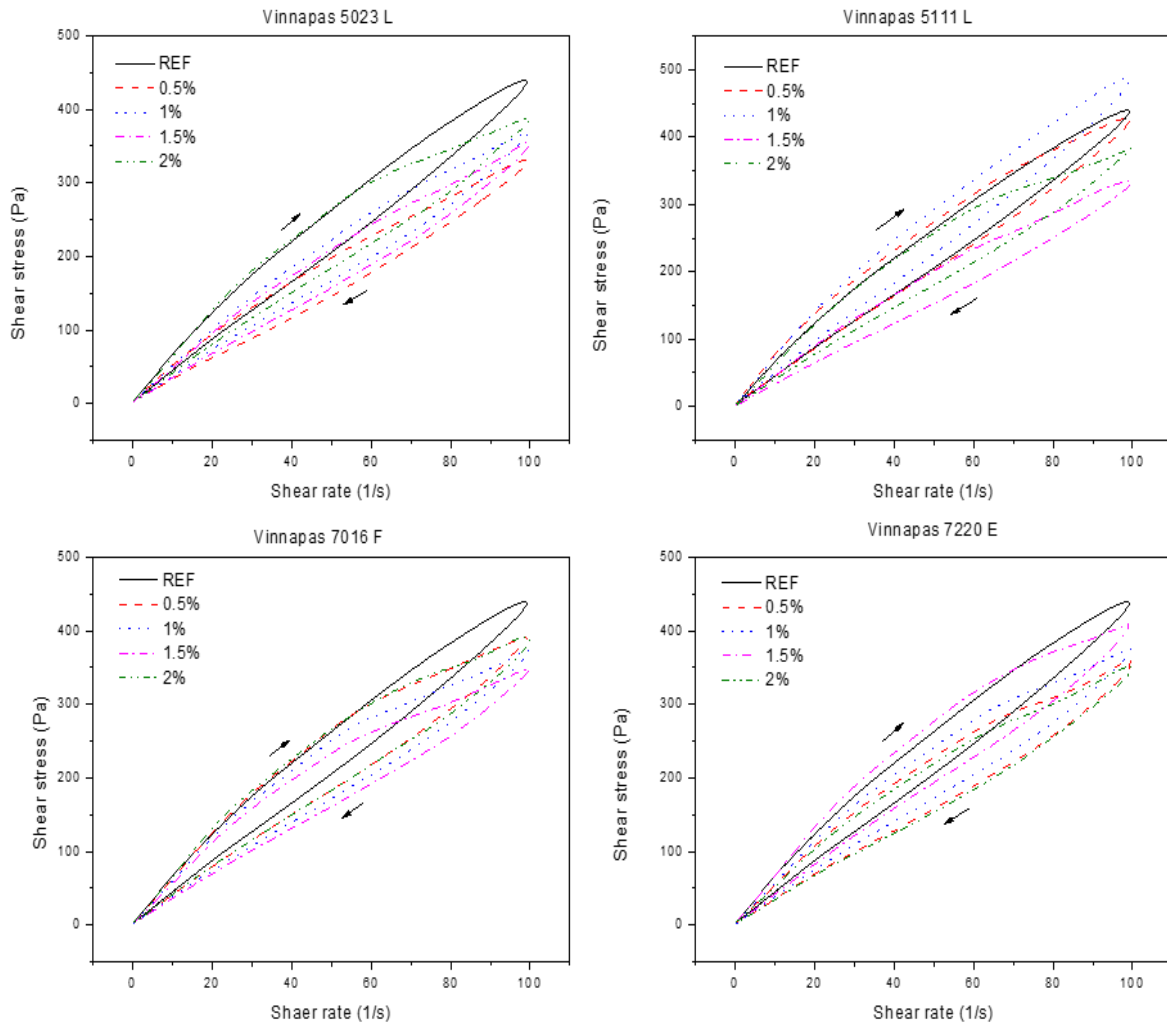


**Fig. 33** Flow curves of AAS paste with different types and dosages of admixtures

The shear stress values found for pastes modified with Vinnapas<sup>®</sup> 5023 L, 7016 F, and 7220 E at different dosages are lower than those observed for REF paste. The only exception was the mixture with adding 1% of Vinnapas<sup>®</sup> 5111 L.

The descending branch of flow curves indicates that these pastes resemble Newtonian to pseudoplastic behavior because practically no yield stress was indicated. The viscosity parameter of tested mixtures was estimated using the Newtonian model (Eq. 1); the calculated values are given in Table 6. The Newtonian flow model is a linear relationship between shear stress  $\tau$  and shear rate  $\dot{\gamma}$ . The proportionality constant  $\eta$  is the plastic viscosity of the fluid. This provides a measure of the resistance to the flow of the fluid.

$$\tau = \eta \cdot \dot{\gamma} \quad (1)$$

**Table 6.** Viscosity of AAS pastes, depending on type and dosage of admixtures.

Type and dosage of admixtures	Viscosity (Pa·s)			
	0.5%	1%	1.5%	2%
REF	4.23	4.23	4.23	4.23
Vinnapas <sup>®</sup> 5023 L	3.09	3.47	3.28	3.71
Vinnapas <sup>®</sup> 5111 L	4.11	4.23	3.16	3.69
Vinnapas <sup>®</sup> 7016 F	3.75	3.52	3.29	3.68
Vinnapas <sup>®</sup> 7220 E	3.29	3.53	3.90	3.23

The results show that adding admixtures slightly decreased the viscosity of the pastes. Increasing the amount of Vinnapas<sup>®</sup> did not affect much shear stress; hence, there was no apparent trend in rheological parameters. The hysteresis of the flow curves indicates the thixotropic behavior of the AAS mixtures, which is not influenced by the type and dosage of admixtures.

Fig. 34 presents the time evolution of the shear stress of tested mixtures determined at maximum shear rate during the initial setting. The measurement was terminated after 30 minutes to prevent the mixture from complete setting and possible damage to measuring geometry.

It can be observed that all types of Vinnapas<sup>®</sup> decreased shear stress of AAS pastes over time due to the thixotropy effect. As the mixture approaches the setting point, the shear stress starts increasing again. Data show that Vinnapas<sup>®</sup> 5023 L, 7016 F and 7220 E tend to prolong slightly the setting time compared to the REF sample. This effect is more pronounced with Vinnapas<sup>®</sup> 7016 F and 7220 E, regardless of the applied dosage.

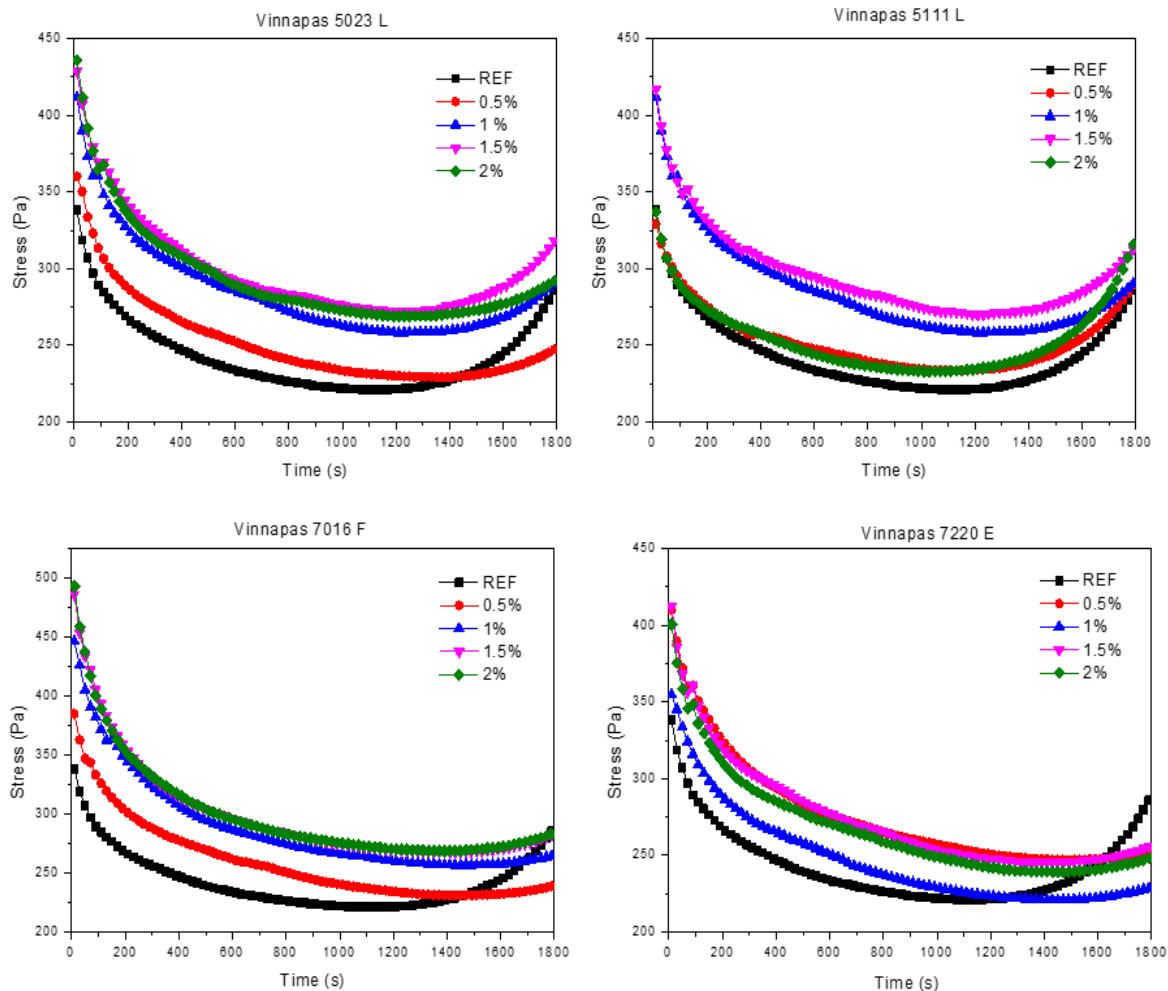


**Fig. 34** Shear stress versus time AAS pastes containing admixtures

#### 4.2.4 Isothermal calorimetry

The results of isothermal calorimetry of AAS with different amounts of Vinnapas<sup>®</sup> are presented in Fig. 35. It shows an initial peak during the first 3 h (Fig. 35 left) and the main hydration peak, which appeared in the period from 40 to 120 h (Fig. 35 right). The initial peak, observed after the first 30 min, is common to water glass-activated systems and consists of two separate peaks. The first one is associated with wetting, dissolution and partial hydrolysis and is also typical for cement-based mixtures [13]. The second additional peak is associated with the reaction of  $\text{Ca}^{2+}$  ions with soluble silicate species from the activator and depends on the composition of the activator [148].

The addition of Vinnapas<sup>®</sup> 5023 L, 7016 F and 7022 E resulted in a decreased heat flow for the additional peak compared to the REF sample. Vinnapas<sup>®</sup> 5111 L appeared to behave reversely. These observations are in accordance with time-controlled rheological measurements, and the maximum of the second peaks may correspond to the initial setting time. Fig. 35 (right) shows that Vinnapas<sup>®</sup> 7016 F and 7220 E shift the main hydration peak towards a longer time, but generally, there is no evident and significant effect of Vinnapas<sup>®</sup> admixtures on the hardening process of AAS.

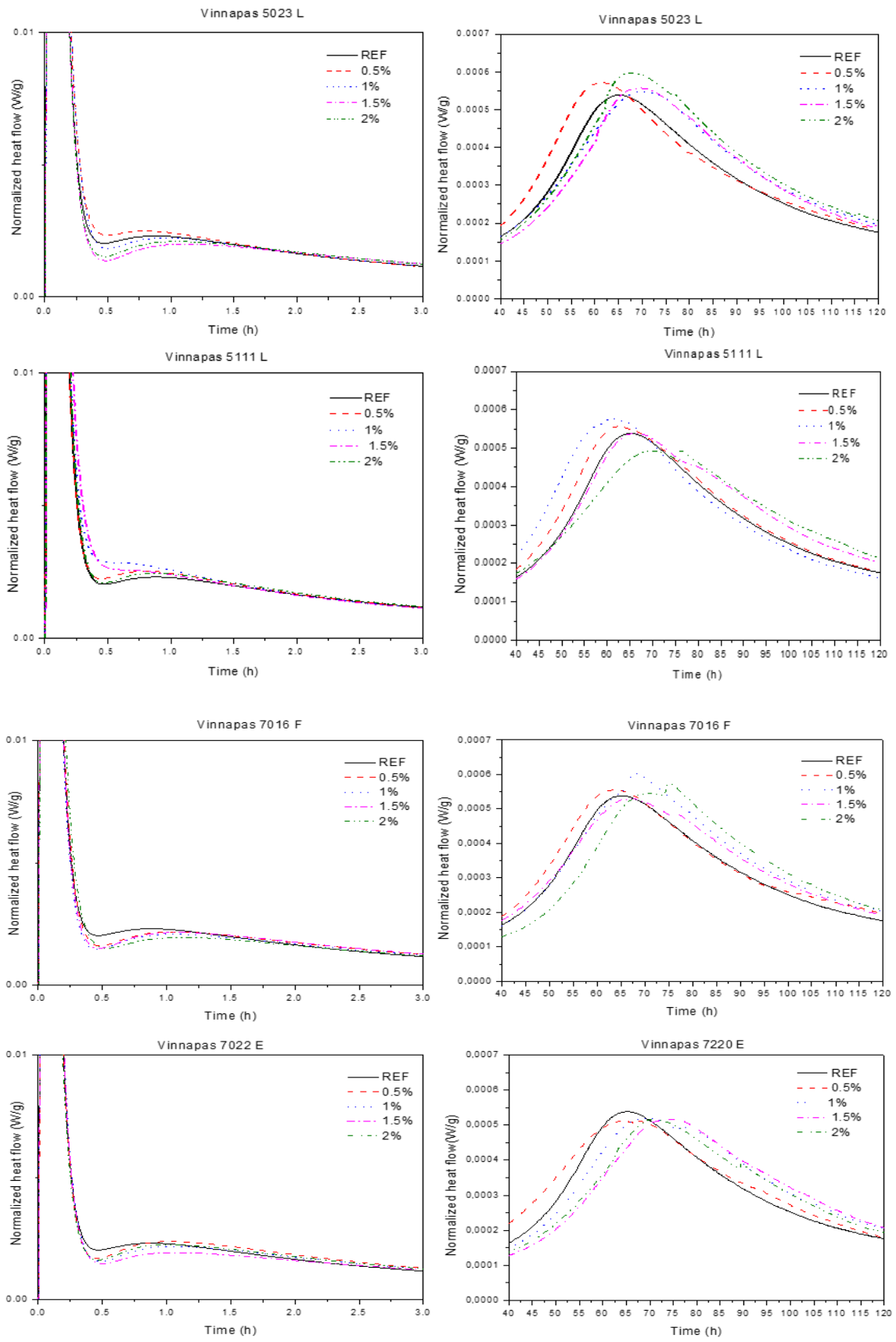


**Fig. 35** Calorimetric major peaks from 0 to 3 h (left), from 40 to 120 h (right).

The effect of polymer admixtures on flow properties and heat evolution of AAS pastes was determined. It was found that all types of Vinnapas<sup>®</sup> admixtures did not significantly modify the rheological parameters (viscosity) of pastes, but Vinnapas<sup>®</sup> 5023 L, 7016 F and 7022 E have a slightly retarding effect on initial setting properties compared to REF.

#### 4.2.5 Mechanical properties

The development of compressive and flexural strengths of reference AAS mortar and AAS mortars with organic additives are given below in Figs. 36-39. The addition of Peramin SRA, PPG and all types of PEGs resulted in a reduction of compressive strength (Fig. 36). More specifically, the compressive strength values decreased with an increasing amount of additives in the composition of the mortar.

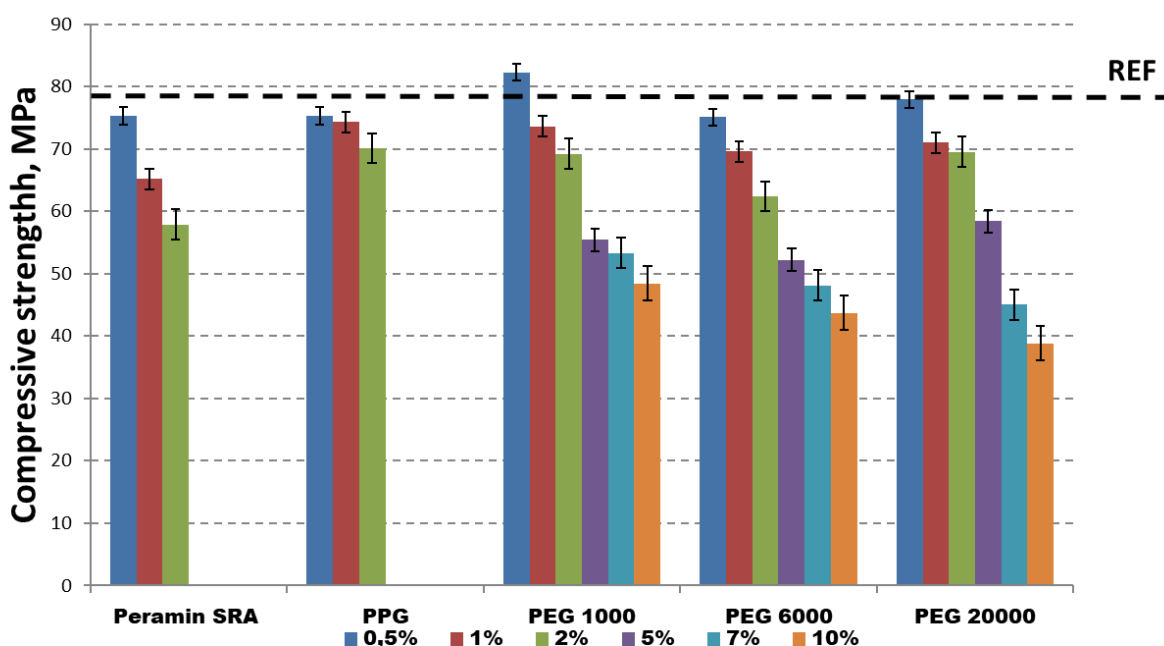


**Fig. 36** Compressive strength of AAS mortars with different dosages of Peramin SRA, PPG and PEG.

The addition of VINNAPAS<sup>®</sup> 5023 L, 7016 F and 7022 E (Fig.37) deteriorated the compressive strength of AAS mortars by 10–15 MPa. However, the increasing addition of VINNAPAS<sup>®</sup> admixtures had little or no effect on the compressive strength values. In the case of Vinnapas<sup>®</sup> 5111 L, adding up to 1 % had almost no effect on the compressive strength, but higher dosages decreased the strength by 10–15 MPa.

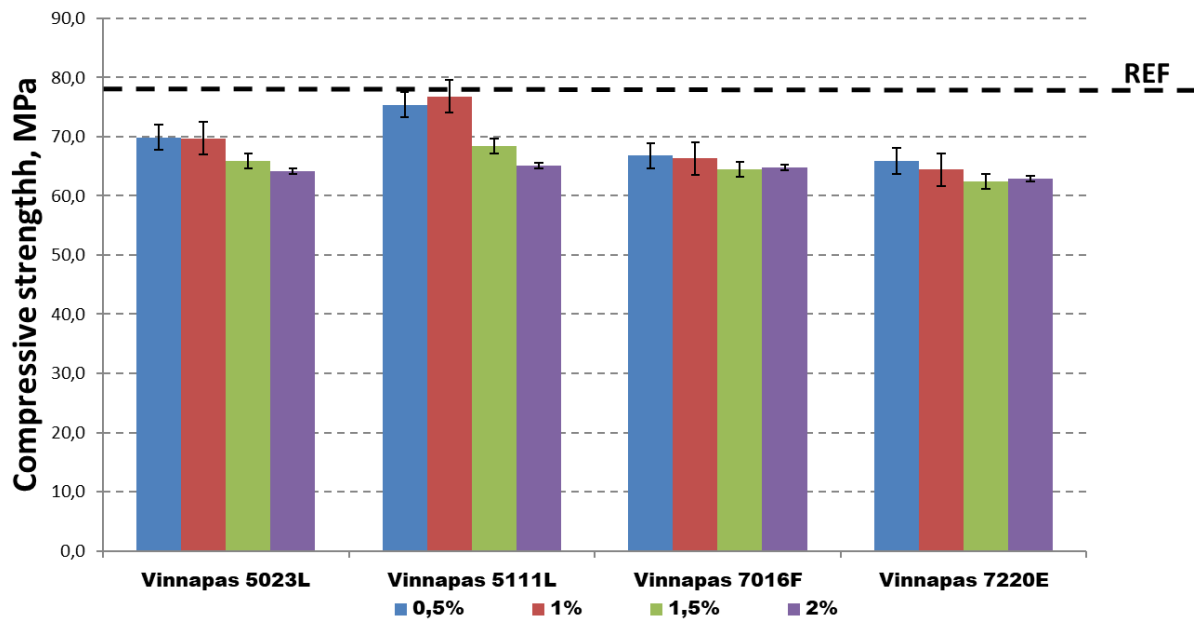


**Fig. 37** Compressive strength of AAS mortars with the various dosage of Vinnapas®.

The effect of each admixture on flexural strength is shown in Figs. 38 and 39. A similar trend in flexural strength can be observed for the AAS mortars modified with polymer admixtures at a dosage of 0.5% and from 2 to 10%. Flexural strengths were reduced as in the case of compressive strength. Only 1% addition of these admixtures had a negligible effect on the flexural strength.

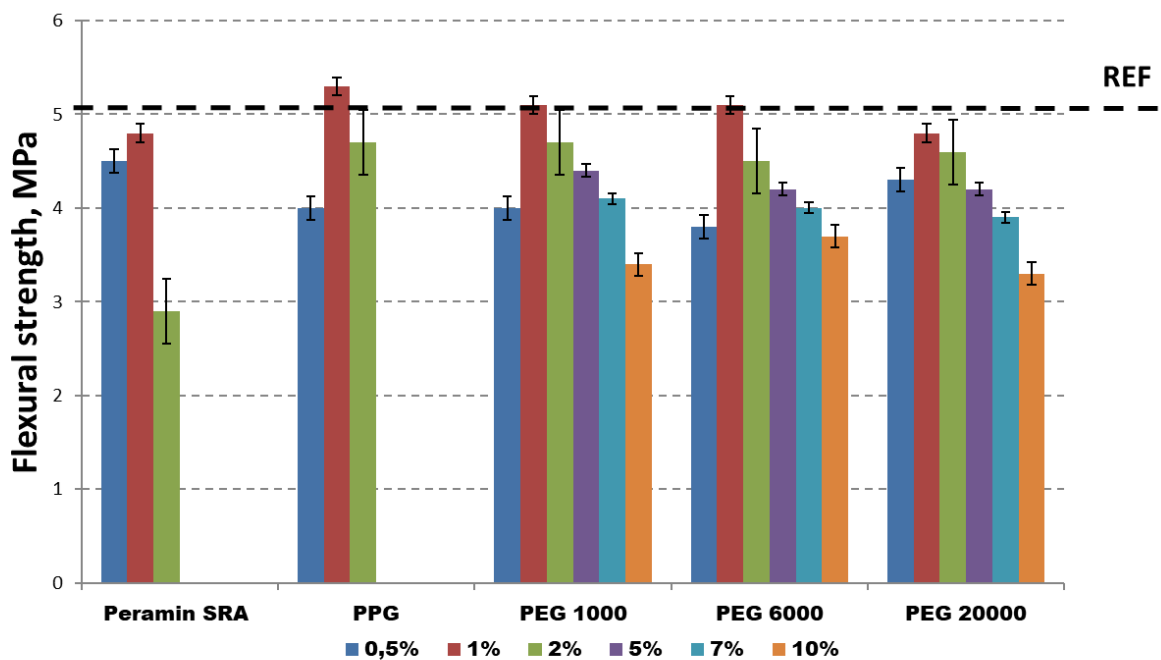


**Fig. 38** Flexural strength of AAS mortars with different dosages of Peramin SRA, PPG and PEG.

All types of Vinnapas® admixtures showed a negative effect on flexural strength (Fig. 39). Samples with Vinnapas® 5011L and Vinnapas® 7220E showed better values of flexural strength than the others, but in any case, none of the Vinnapas® types had the strength values higher than the reference sample.

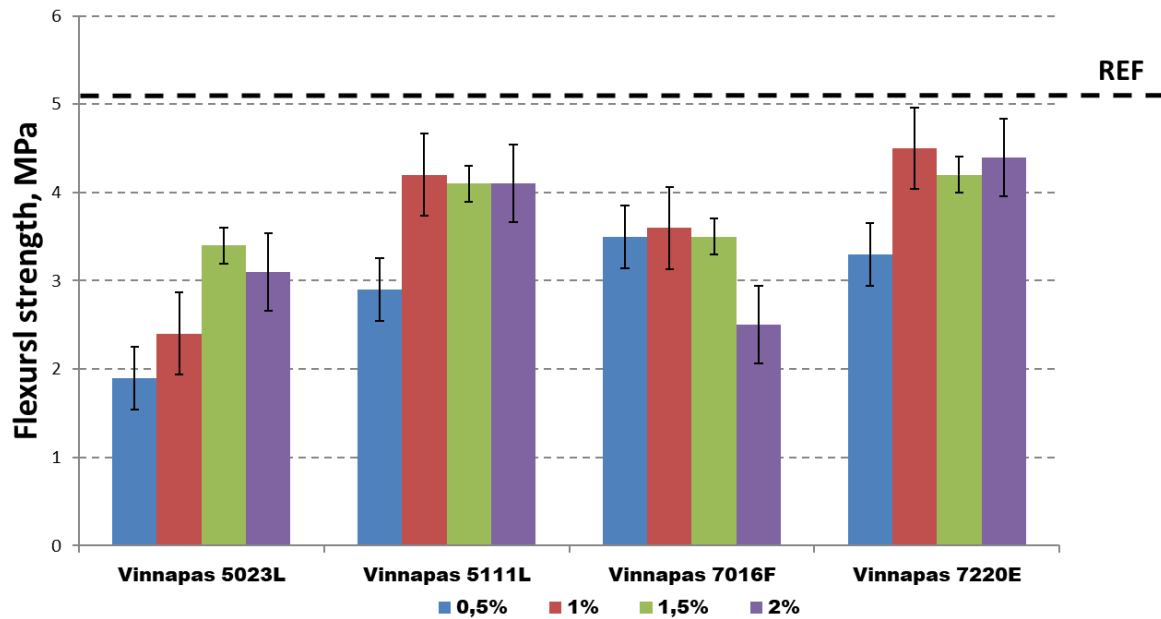


Fig. 39 Flexural strength of AAS mortars with the various dosage of Vinnapas®.

#### 4.2.6 Shrinkage

Due to the segregation problem, only admixtures which were able to dissolve in the AAS mortar were used for shrinkage tests. Shrinkage of AAS mortars with and without different admixtures is shown in Fig. 40. AAS mortars with the addition of 1 and 2% PPG reduced the shrinkage approximately by up to 70%. Adding 1 and 2% PEG 1000 lowered shrinkage by up to 15 and 25%, respectively. The addition of 2% Peramin SRA reduced the shrinkage by 55%, whereas 1% Peramin SRA reduced the shrinkage only by 10%. From this point of view, the most effective shrinkage-reducing admixture is PPG, even at a low dosage.

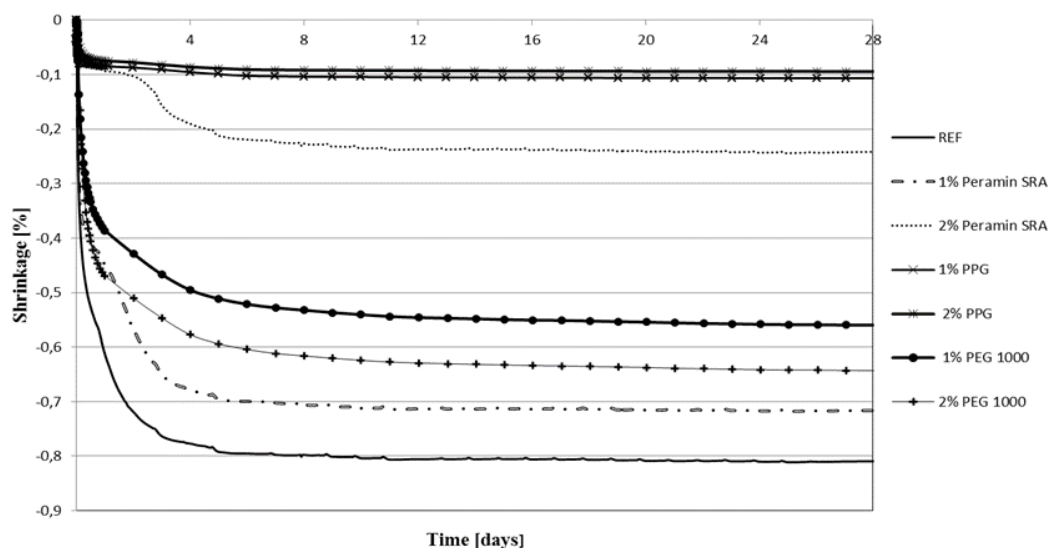
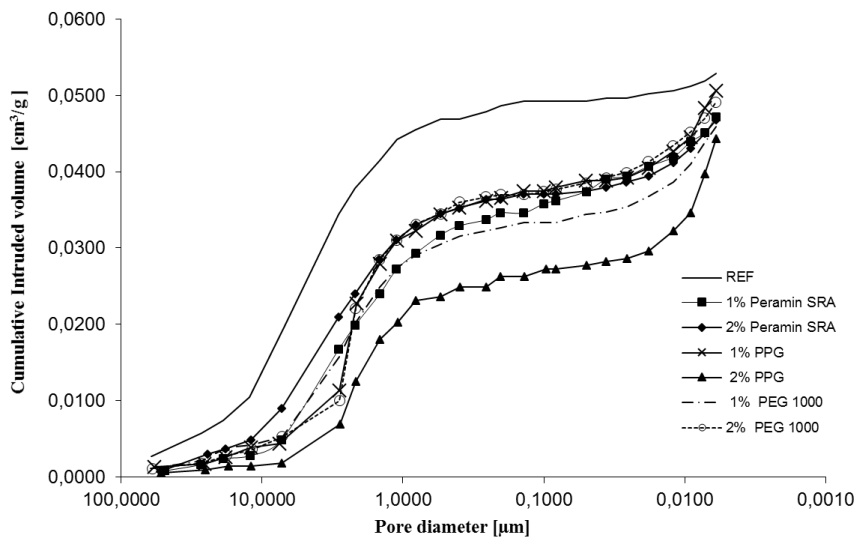


Fig. 40 Shrinkage AAS mortars with different percentages of organic additives.

#### 4.2.7 Porosity

Fig. 41 shows the results of the pore distribution of AAS mortars. The data represent cumulative curves typical for water glass-activated slag. Most pore volume is associated with large capillary pores between 1 and 10  $\mu\text{m}$ . The slightly rising tail also indicates a large number of small gel pores. According to the figure, the most porous material is a REF specimen. The least porous is the specimen with 2 % PPG. The addition of 2 % PPG in AAS mortars decreased the volume of pores with diameters with size ranging from 1.0 and 0.1  $\mu\text{m}$  than REF. 1 % of PEG 1000 and Peramin SRA showed little changes in pore volume than other additives. The addition of admixture caused a decrease in the volume of larger pores, but it increased the volume of pores around 10 nm in diameter. Especially, 2% addition of PPG gives rise to the highest number of gel pores. The admixtures also caused a slight decrease in total intruded volume. Surprisingly, a lower porosity of AAS with additives was not reflected in improved compressive strengths.



**Fig. 41** Porosity of AAS mortars with different percentages of additives.

#### 4.2.8 Fracture tests

The mean values (obtained from three independent measurements) and coefficients of variation of selected material properties were obtained from recorded  $P-d$  diagrams using the academic *StiCrack* software (bulk density  $\rho$ , modulus of elasticity  $E_c$ , effective fracture toughness  $K_{Ic}$  and specific fracture energy  $G_F$ ) are summarized in Table 7. Subsequently, the values of selected parameters calculated relative to the reference specimens without any additive are introduced in Figs. 42–44.

As can be seen from Table 7, the addition of organic additives has almost no effect on bulk density values. Organic additives behaved differently concerning fracture characteristics. The addition of polymer admixtures led to an increase in elastic modulus values. Specimens with 2 % of PEG and 1 % of SRA showed the highest increase of elasticity modulus values up to 14 and 16 %, respectively (Fig.42). 2 % PEG dropped fracture toughness values by 20 % and 2 % SRA – by 18 %, although specimen SRA 1% has a small increase – 3 % (Fig. 43). The most significant decrease

was detected in the case of specific fracture energy, the 2 % amount of PEG and SRA led to a decrease of these values by 46 and 43 %, respectively (Fig. 44).

**Table 7.** Mean values of selected fracture parameters (coefficient of variation in %).

Mixture Parameter	REF	PEG 1000_1	PEG 1000_2	PPG_1	PPG_2	SRA_1	SRA_2
Bulk density $\rho$ [kg/m <sup>3</sup> ]	2250 (0.4)	2248 (0.6)	2232 (0.1)	2234 (0.0)	2228 (0.1)	2261 (0.4)	2254 (0.3)
Modulus of elasticity $E_c$ [GPa]	17.76 (5.4)	18.07 (9.1)	20.32 (12.2)	19.47 (5.6)	18.69 (7.6)	20.65 (13.1)	18.29 (2.3)
Fracture toughness $K_{Ic}$ [MPa·m <sup>1/2</sup> ]	0.832 (5.1)	0.706 (14.8)	0.668 (2.7)	0.803 (6.1)	0.758 (4.9)	0.857 (3.0)	0.684 (7.7)
Fracture energy $G_F$ [J/m <sup>2</sup> ]	30.83 (22.9)	20.27 (31.0)	16.59 (12.9)	28.55 (13.6)	29.10 (20.6)	24.57 (12.3)	17.54 (7.7)

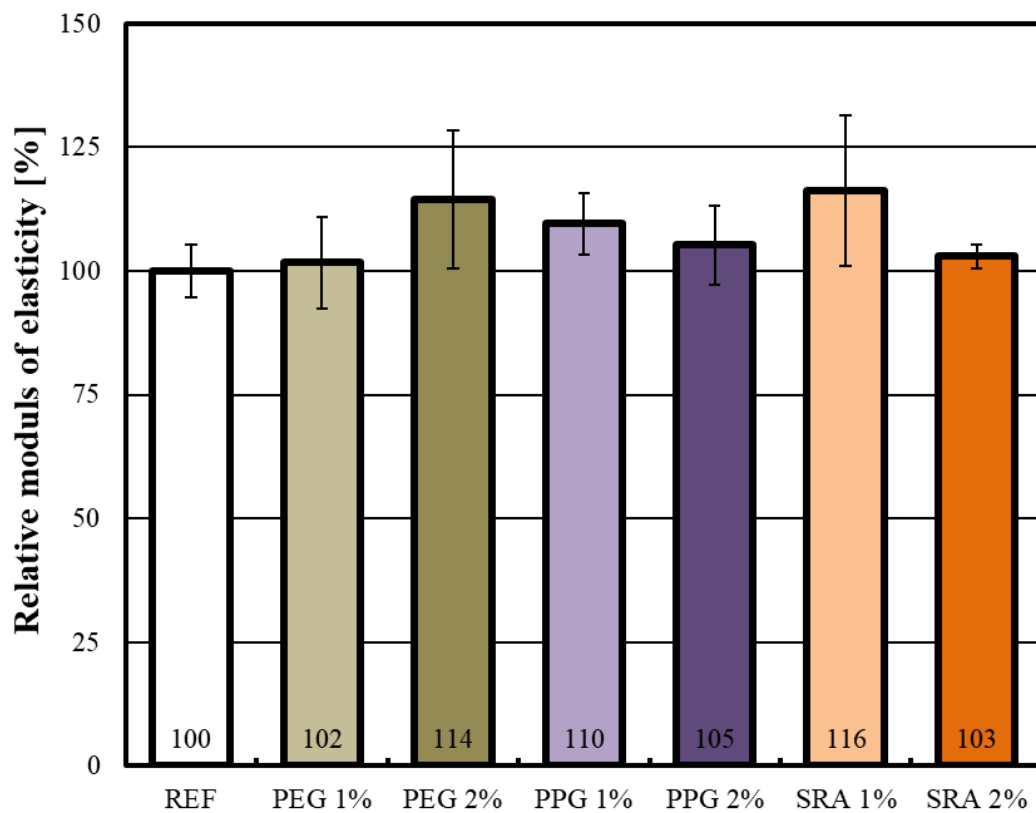


**Fig. 42** Relative values of modulus of elasticity.

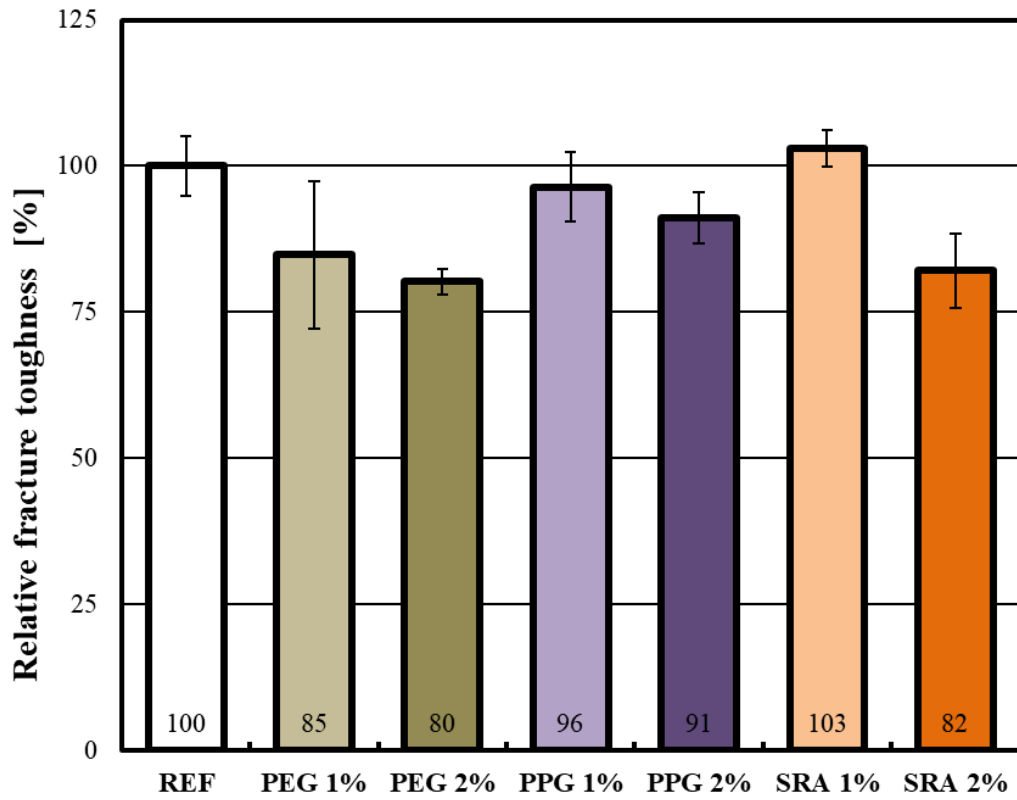


**Fig. 43** Relative values of effective fracture toughness.

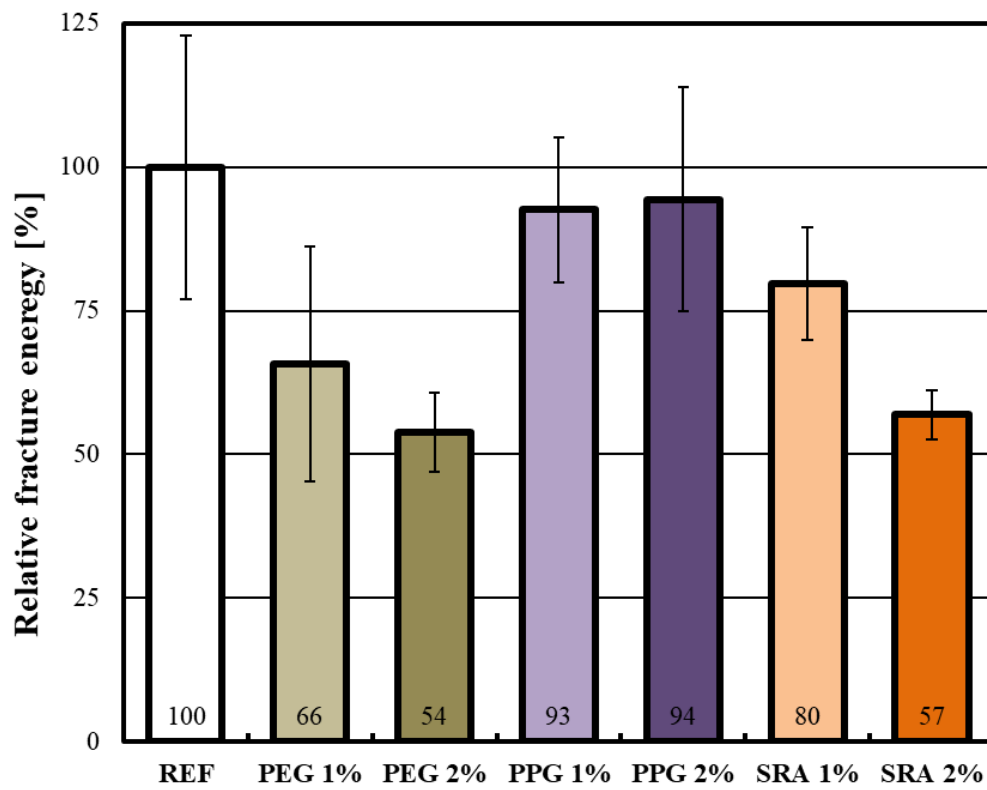


**Fig. 44** Relative values of specific fracture energy.

#### 4.2.9 Acoustic emission

AE activity was recorded during the fracture tests. To describe the origin of microcracks during loading, we focused on the duration of AE signals. Duration represents the time difference between the first and last threshold crossings. Another parameter, AE amplitude, represents the greatest measured voltage in a waveform and is measured in millivolts (mV). The energy of AE signals is the measure of the area under the envelope of the rectified linear voltage-time signal from the transducer. The results of duration, amplitude, and energy of AE signals are presented in Table 8.

The mixture with 2 % of PEG 1000 displayed the most events and had the most extensive variability of the values. However, mixtures with the SRA had a minimum of AE events, which might assume greater brittleness of the material.

A reference mixture had the highest decline from the viewpoint of propagation of AE signals. It can be assumed that the structure of REF had the most defects (microcracks, etc.) and damping signal propagation.

The size of cracks formed during testing was the same for all specimens, except the mixture with 2% of PEG 1000, which had the minimum amplitude, thus obtaining fewer cracks. However, this mixture had a larger number of AE events than the others. Small numbers of large cracks occurred in the specimen matrix with 2 % of SRA, which corresponded to the number of AE events.

From the point of view of energy, previous results confirmed that the specimen with admixture 2 % of SRA was the softest and, therefore, the least cohesive, whereas a large number of small cracks formed a structure with 2 % of PEG 1000. It gradually caused most of the released energy of AE signals.

**Table 8.** Mean values of selected parameters obtained from acoustic emission measurements (coefficient of variation in %).

	REF	PEG 1000_1	PEG 1000_2	PPG_1	PPG_2	SRA_1	SRA_2
Number of AE events [-]	38.0 (7.4)	36.0 (9.0)	71.0 (12.9)	30.0 (8.0)	31.0 (9.0)	27.0 (7.8)	14.0 (4.2)
Duration of AE signals [ms]	1755 (3.7)	1905 (3.8)	1833 (3.4)	1935 (4.9)	1863 (3.8)	1858 (5.8)	2450 (6.9)
Amplitude of AE signals [mV]	2983 (2.5)	2820 (1.7)	2744 (1.8)	2856 (2.5)	2984 (2.5)	2918 (2.1)	3320 (2.2)
Energy of AE signals [mV·s]	40.9 (1.1)	38.3 (7.0)	84.6 (4.4)	53.1 (1.2)	39.7 (8.3)	44.8 (2.4)	14.3 (0.7)

#### 4.2.10 Microstructure

Micrographs of AAS mortars with the addition of 1 % and 10 % of PEG 20000 are shown in Fig. 45. It is obvious that the sample's microstructure with 1 % of PEG is very similar to the sample with 10 % of PEG with approximately the same number of microcracks. Therefore, it can be concluded that PEG does not affect the reduction of microcracks. Similar structures were observed practically for all mixtures, corresponding to the results of mechanical tests.

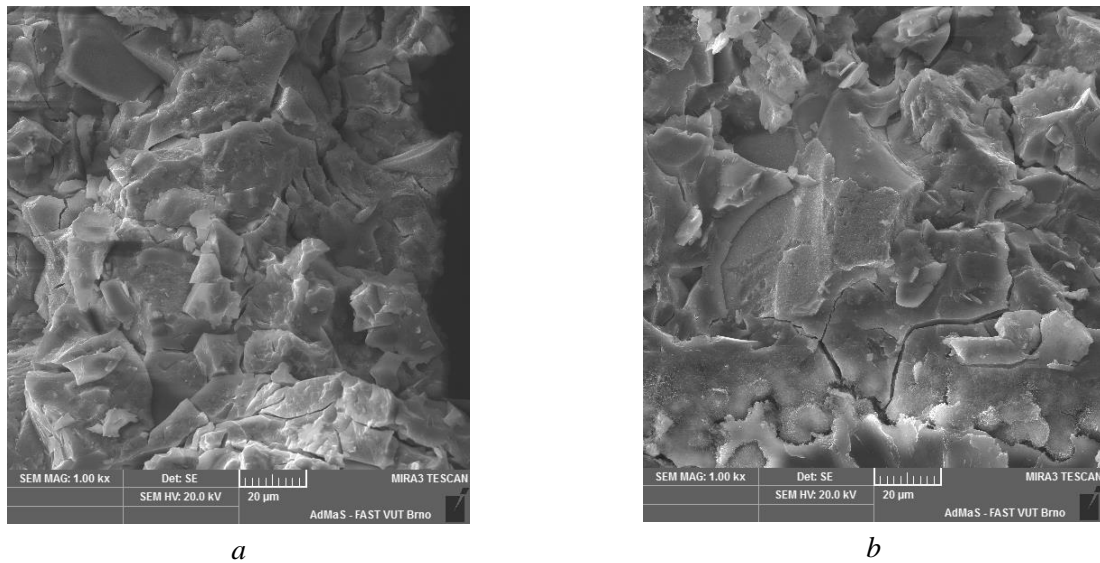


**Fig. 45** SEM microstructure at 1000× magnification of AAS mortars with PEG 20000 at dosage: a) 1 %; b) 10 %.

Micrographs of AAS mortars with Vinnapas<sup>®</sup> admixtures showed that all samples contain plenty of well-shaped crystals of the approximate mean size of 1 µm (Fig. 46a), and also some areas with very porous spongy structures have been observed (Fig. 46b). According to the EDX analysis and also the shape, these crystals belong to calcite. Calcite crystals give proof of enhanced carbonation when Vinnapas<sup>®</sup> admixtures are added. Spongy areas increase the total porosity of the AAS matrix, which results in the deterioration of the mechanical properties.

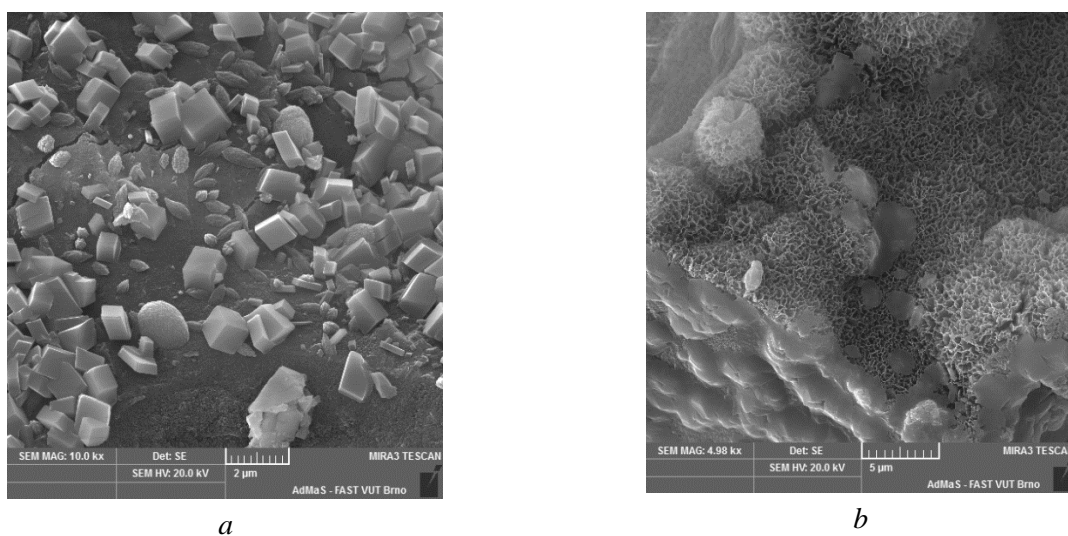


**Fig. 46** SEM microstructure of AAS mortars with Vinnapas<sup>®</sup> admixtures: a) calcite crystals; b) spongy structure.

#### 4.2.11 Efflorescence

Mortar samples with AAS did not show any efflorescence with the addition of any modifiers. That is the opposite of the result obtained with metakaolin geopolymer samples (see chapter 5.5.1).

## 5 METAKAOLIN GEOPOLYMER

### 5.1.1 Mortars preparation

In this part of the research, only different types of Vinnapas<sup>®</sup> and PEG with different molecular mass in metakaolin-based geopolymers were studied to achieve a result as in the experiment of a group of researchers led by Shrotri et al., which was described in the book [89].

For geopolymer mortars metakaolin Mefisto K<sub>05</sub> (České lupkové závody) was used as binder. Metakaolin was produced through a controlled thermal process and grain size adjustments of clay stones and floating kaolin clays. Its chemical composition is given in Table 9. Particle size are  $d_{50} = 3.42 \mu\text{m}$   $6.34 \mu\text{m}$  and  $d_{90} = 11.62 \mu\text{m}$ .

**Table 9.** Chemical analysis of metakaolin, [%]

SiO <sub>2</sub>	Fe <sub>2</sub> O <sub>3</sub>	Al <sub>2</sub> O <sub>3</sub>	CaO	MgO	Na <sub>2</sub> O	K <sub>2</sub> O	TiO <sub>2</sub>	LOI
55.01	0.55	40.94	0.14	0.34	0.09	0.60	0.55	1.57

Geopolymer mortars with PEG and Vinnapas<sup>®</sup> were prepared with an aggregate/binder ratio of 3/1. Each type of PEG was added at dosages of 0.5, 1, 2, 5, 7, and 10 % by mass of metakaolin. Each type of Vinnapas<sup>®</sup> – 0.5, 1, 1.5, and 2 % by mass of metakaolin

The metakaolin was activated with a water glass solution having a SiO<sub>2</sub>/Na<sub>2</sub>O ratio of 1.6. Quartz sand with a maximum grain size of 2.5 mm was used as aggregate.

The activator and PEG were added to water and then mixed with metakaolin. Then quartz sand was added into the fresh mortar during mixing. Geopolymer mortar specimens were cast in prismatic moulds (40 × 40 × 160 mm). The specimens were left in the moulds for 2 hours, then cured in an electric oven at 40 °C for 4 hours to accelerate the hardening process, and finally removed from the moulds after 24 hours. After demolding, the specimens were stored in plastic bags for 27 days at RH = 45 ± 5%.

The effect of the type of PEG on compressive and flexural strength was evaluated at first. The specimens' Flexural and compressive strengths were measured at 28 days. Flexural strengths were determined using a standard three-point bending test, while compressive strengths were measured on both residual pieces obtained from the flexural strength test.

### 5.1.2 Mechanical properties

The development of mechanical strength of the reference metakaolin-based geopolymer mortar (REF) and the polymer-modified geopolymer mortars are given in Figs. 47 and 49 (compressive strength) and Figs. 48 and 50 (flexural strength). The maximum compressive strength was observed for the composition with 10 % of PEG 400, being 57 % higher than that of REF. The composition containing 1% of PEG 1000 showed the minimum compressive strength value, which was 45 % lower than that of REF. Also, one of the lowest values was recorded for the specimen with 7 % PEG 20000. In general, the addition of PEG 20000 resulted in lower compressive strength values compared to REF composition.

On the contrary, PEG 400 added at the amount of 5, 7, and 10 % contributed to a compressive strength increase. Flexural strengths showed the same trend as was observed for compressive strength. The best results were achieved by adding 5, 7, and 10 % PEG 400, whereas the lowest strength showed geopolymer with PEG 20000.

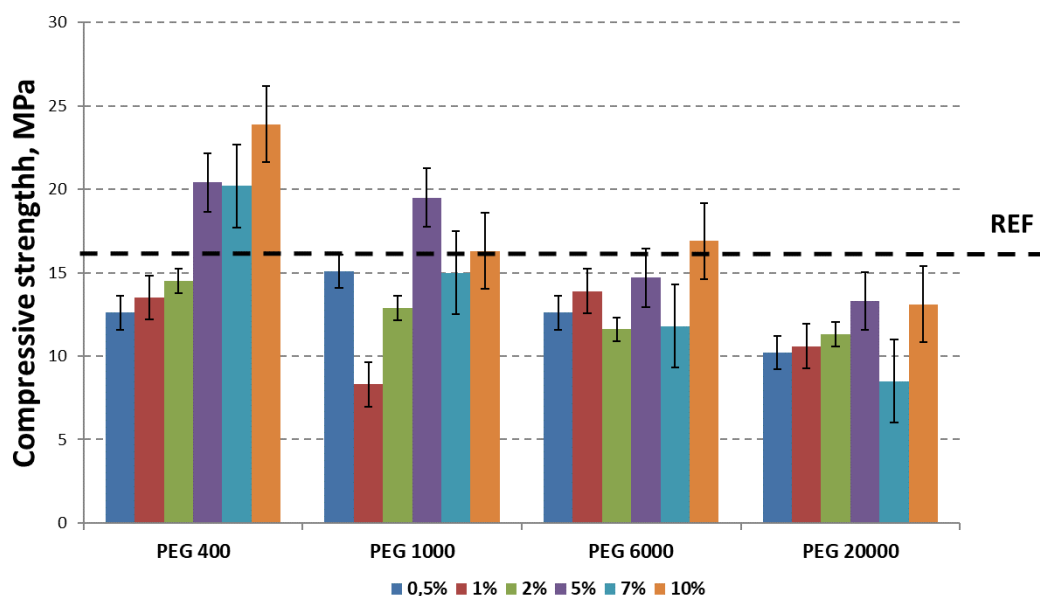


**Fig. 47** Compressive strength of geopolymer mortars with different contents of different types of PEGs.

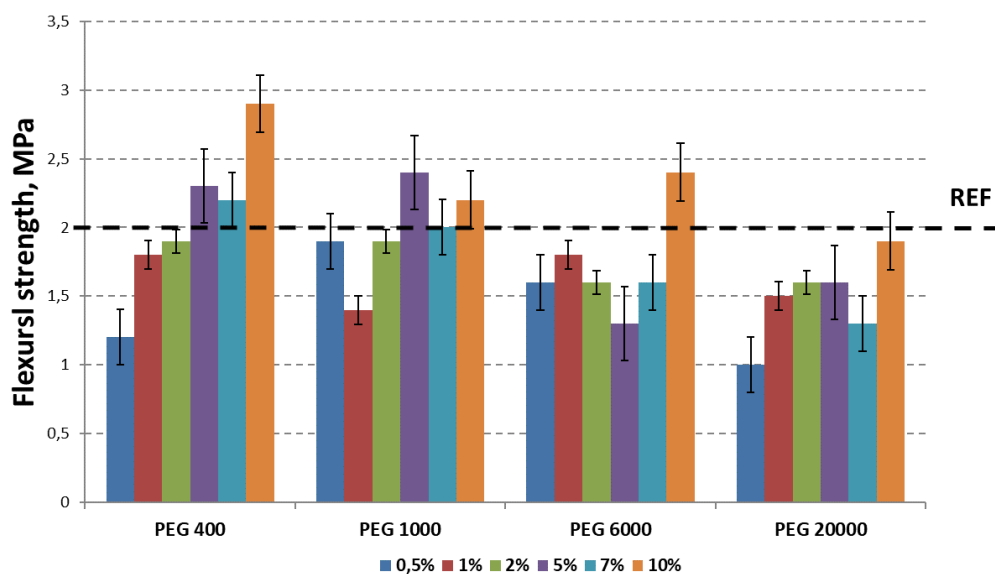


**Fig. 48** Flexural strength of geopolymer mortars with different contents of different types of PEGs.

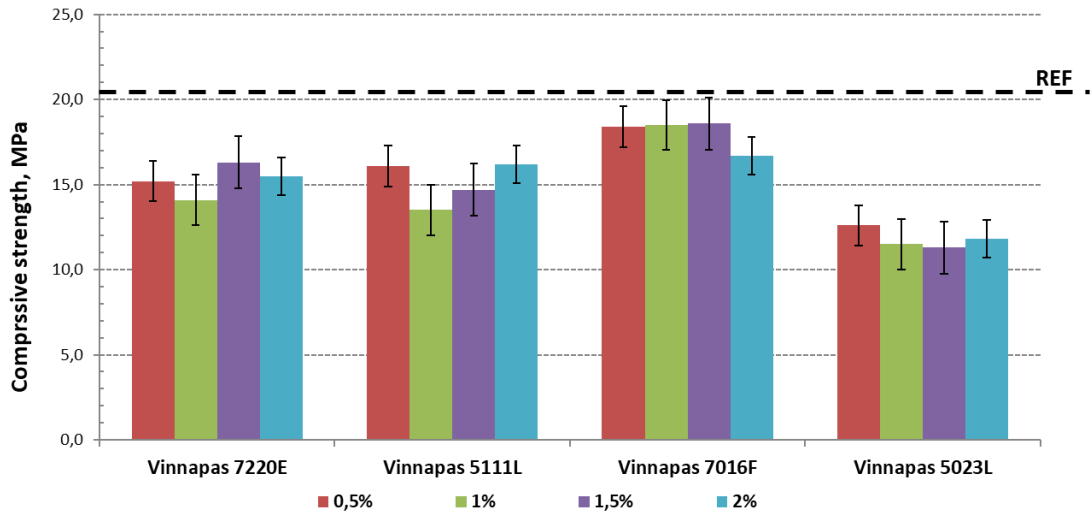


**Fig. 49** Compressive strength of geopolymer mortars with different contents of different types of Vinnapas®.

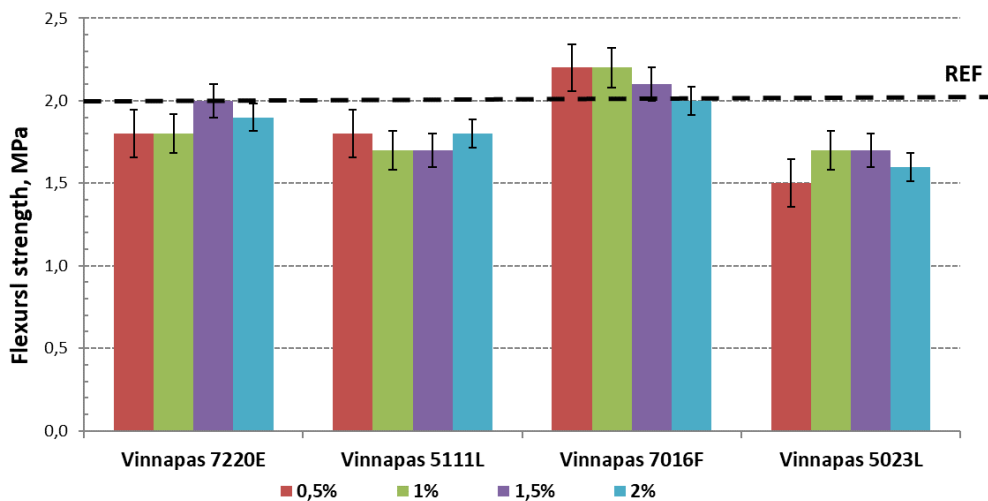


**Fig. 50** Flexural strength of geopolymer mortars with different contents of different types of Vinnapas®.

### 5.1.3 Porosity

Fig. 51 illustrates the pore size distribution of geopolymer mortars. Porosity measurements were performed only on reference specimens and specimens with the highest and lowest strength. According to Fig. 51, the least porous material is the REF specimen, while the mortar with 7 % PEG 20000 was proved as the most porous. The largest pore volume is associated with pores between 0.1–1  $\mu\text{m}$  in diameter. For PEG 1000 and 20000, the curves are shifted to bigger pores, while in the case of PEG 400, smaller pores are predominant. Since porosity strongly influences the material's mechanical properties, these data correspond to the mechanical characteristics of the tested geopolymer.

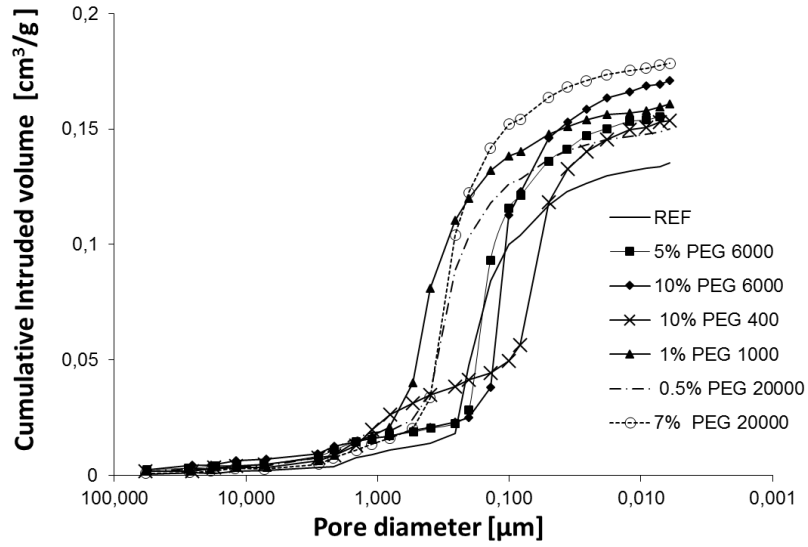


**Fig. 51** The porosity of geopolymer mortars with different content of PEG.

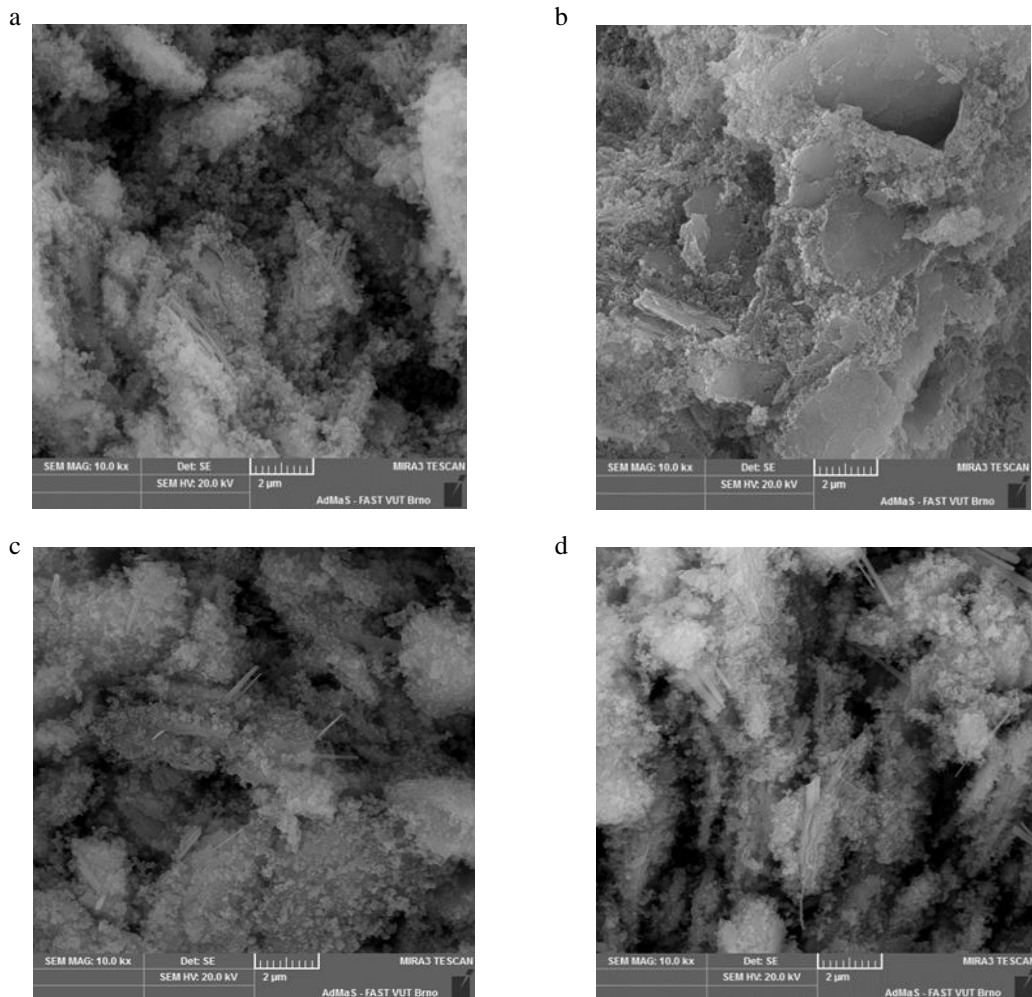


**Fig. 52** SEM photos (10000× magnification) of (a) REF geopolymer mortar, (b) – 10 % PEG 400, (c) - 0.5 % PEG 20000, (d) – 1 % PEG 1000.

#### 5.1.4 Microstructure

Micrographs of samples obtained from the mortars with 10 % PEG 400 showed that the structure is solid and compact (Fig. 52b). In contrast, the structure of REF is a more porous and open grain (Fig. 52a). The structure of the specimens with 0.5 % PEG 20000 and 1 % PEG 1000 (Fig. 52 c, d) is the most porous, therefore showing the lowest compressive strength. It is also apparent that the specimen with 1% of PEG 1000 contains needle-shaped crystals of alkali carbonates. This corresponds to the efflorescence observed in Fig. 53b. However, the structure of geopolymer mortar with 10 % PEG 400 (which had the maximum compressive strength) did not show any efflorescence on its surface (Fig. 52a), which may explain its high strength. SEM analysis proved that the PEGs affect the structure of metakaolin-based geopolymers.

The maximum compressive and flexural strengths were achieved by adding 10 % of PEG 400. The minimum compressive and flexural strength value was obtained for the specimens containing PEG 1000 at dosage 1 % and PEG 20000 at dosage 0.5 %, respectively. SEM observations and porosity measurements confirmed these results. The specimen (10 % PEG 400) with the highest strength had a dense structure and was less porous.

#### 5.1.5 Efflorescence

Fig. 53 shows that intensive efflorescence was observed on the surfaces of the samples with 1 % of PEG 1000, which has the lowest compressive and flexural strength.



**Fig. 53** Geopolymer mortar specimens containing 1% PEG 1000.

No efflorescence was formed on the surfaces of the samples with 2, 5, 7 and 10% of PEG 400. However, the lowest compressive strengths have a specimen with 0.5 and 1 % of PEG 400 (Fig. 54). This corresponds to the mechanical strength results; the specimen with 10 % of PEG 400 has the best mechanical performance.

The most efflorescence also occurred on the surface of specimens with an addition of 0.5 % PEG 6000 and 1 % PEG 20000, which can be seen in Figs. 55 and 56 below.



**Fig. 54** Geopolymer mortar specimens containing 1 and 10 % PEG 400.

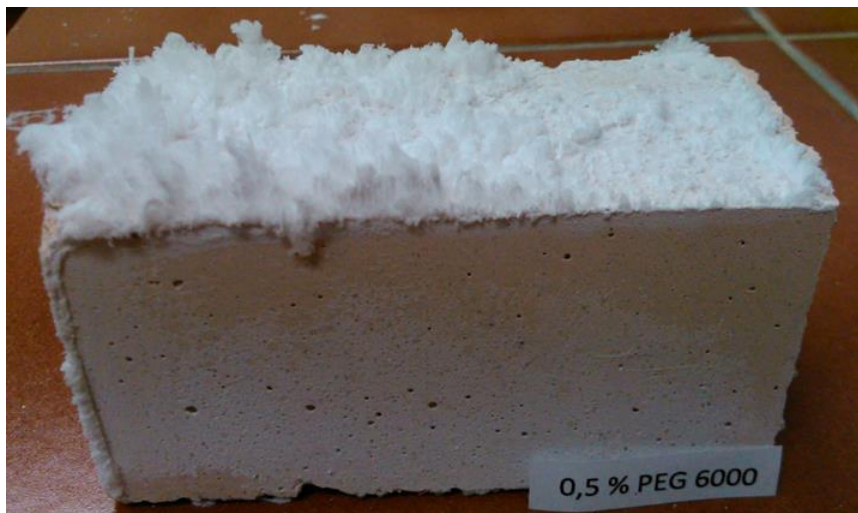


**Fig. 55** Geopolymer mortar specimens containing 0.5 % of PEG 6000.



**Fig. 56** Geopolymer mortar specimens containing 1 % of PEG 20000.

The best mechanical properties showed specimens with Vinnapas<sup>®</sup> 7016 F, which can also be proved by the absence of efflorescence, except for specimens with 2 % of Vinnapas<sup>®</sup>, illustrated in Fig. 57.

The worst mechanical properties showed specimens with Vinnapas<sup>®</sup> 5023 L; all the specimens have a considerable amount of efflorescence (Fig. 58).

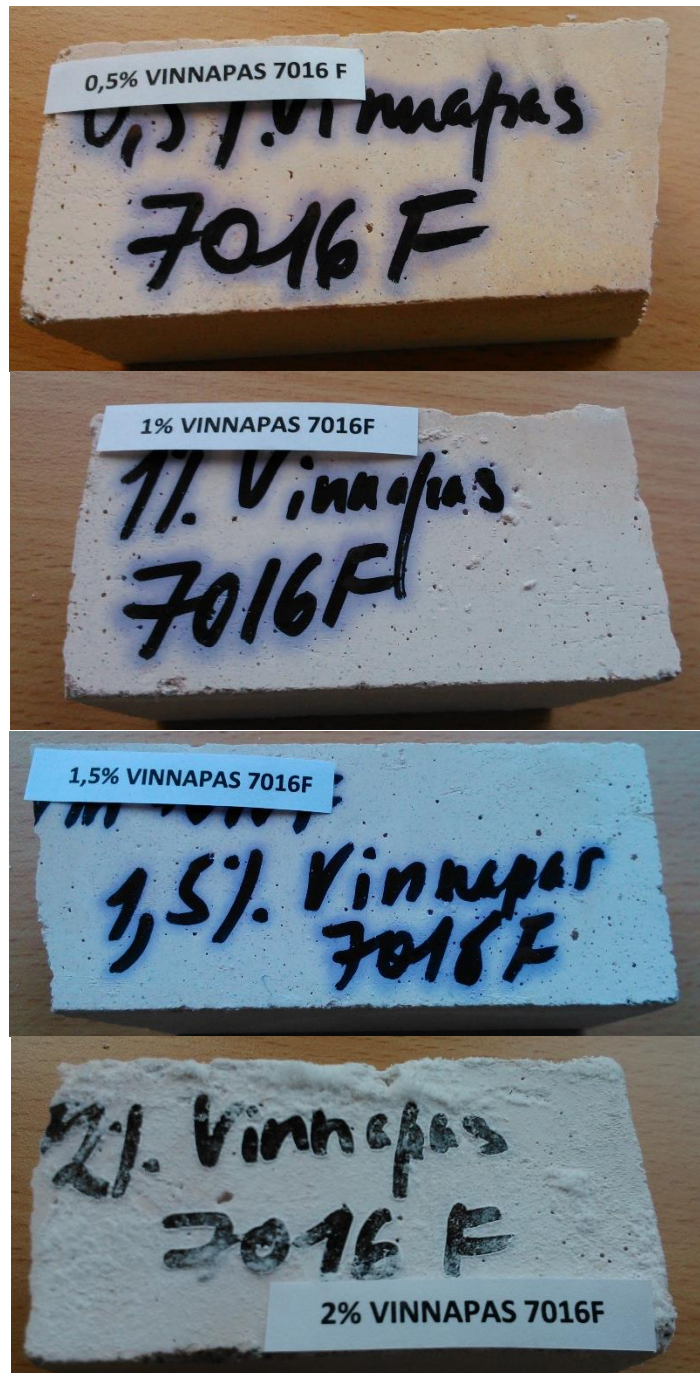


**Fig. 57** Geopolymer mortar specimens containing 0.5, 1, 1.5 and 2 % of Vinnapas<sup>®</sup> 7016 F.



**Fig. 58** Geopolymer mortar specimens containing 0.5, 1, 1.5 and 2 % of Vinnapas<sup>®</sup> 5023 L.

Other specimens have different amounts of efflorescence products on the surface of the specimen increased with Vinnapas<sup>®</sup> content.

## 6 CONCLUSIONS

This work deals with the development, preparation, and study of properties of binder systems based on alkali-activated aluminosilicates. One of the main aims was to find suitable types of polymer admixtures at optimal dosage to produce high-quality composite material having good physical-mechanical properties and high durability and toughness.

In this thesis, two AAA were studied – AAS mortars and metakaolin-based geopolymer; therefore, two main conclusions can be drawn.

Generally, all admixtures had almost no effect on both compressive and flexural strength of AAS mortars. The compressive strength values decreased with an increasing amount of PPG and PEG. The best but slight compressive strength increase was achieved by incorporating 0.5 % PEG 1000. All types of Vinnapas<sup>®</sup> admixtures had a negative effect on both compressive and flexural strength. All results of mechanical tests corresponded to the micrographs of AAS mortars. The most effective shrinkage-reducing admixture was PPG and Peramin SRA, even at a low dosage. Modification by 2 % PPG was the most effective in reducing linear shrinkage by 70 % and modification by 2 % of Peramin SRA by 55 %, respectively.

Nevertheless, in metakaolin-based geopolymer, some admixtures improved its mechanical properties. The best mechanical properties were observed by modification by 10 % of PEG 400. Also, the maximum values of compressive and flexural strengths were obtained by incorporating 1.5 % and 1 % of Vinnapas<sup>®</sup> 7016 H. These results corresponded to SEM observations and porosity results. The structures of these specimens had dense structures and were less porous than REF specimens, which explains their high strength. The rest of the used polymer admixtures had a negligible effect on the mechanical properties, which can be explained by a significant occurrence of efflorescence.

All PEG polymers with various molecular weights, PPG, and Peramin SRA were stable in alkaline media to be used to modify AAM. The opposite result was with all types of Vinnapas<sup>®</sup> admixtures after alkaline treatment; therefore, they are unsuitable for AAM modification.

In order to increase the application of AAM in industry, it is necessary to extend studies in this field of science, which are very limited. One of the thesis's main contributions to building materials engineering is acquiring new knowledge in the field of aluminosilicate alkaline activation. Finding a suitable way of using the type and amount of appropriate admixtures to enable rheology control and optimization of mix designs of AAA materials will increase their application in practice by minimizing the disadvantages (high shrinkage, brittleness) of these materials together with enhancing their benefits. For example, for restoration and renovation of monuments, especially where PC cannot fully meet the requirements of the restorer. Also, the AAMs create environmentally friendly concrete with reduced embodied energy and CO<sub>2</sub> footprint compared to the traditional Portland cement-based concrete.

According to the above, the innovative aspect of the dissertation is modified material, which is low-cost, low carbon, more environmentally friendly and durable than OPC. The second innovation of the thesis is a novel alternative technique for microstructural characterization of hydrating AAM to obtain information about the main reaction product (C-A-S-H gel).

The scientific significance of the study is that it provides information on the use of traditional polymeric additives for concrete in modifying the properties of AAM and their improvement or minimization of their disadvantages.

A further contribution of the thesis is the use of the CRM method as a new alternative characterization technique that illustrates the distribution of the main phases present in the alkali activated system at different ages. Despite the poor crystallinity of the C-A-S-H gel, the hydration of slag at different ages can be easily assessed.

## 7 LITERATURE

1. FLOWER, David J. M. and SANJAYAN, Jay G. Green house gas emissions due to concrete manufacture. *The International Journal of Life Cycle Assessment*. Online. 2 July 2007. Vol. 12, no. 5, p. 282–288. DOI 10.1065/lca2007.05.327.
2. PETROCHE, Daniel M and RAMIREZ, Angel D. A Life Cycle Perspective Study Based on Ecuadorian Data. *Buildings*. Online. 2022. Available from: <https://doi.org/10.3390/buildings12030311>
3. CAO, Yubin, WANG, Yanru, ZHANG, Zuhua, MA, Yuwei and WANG, Hao. Recent progress of utilization of activated kaolinitic clay in cementitious construction materials. *Composites Part B: Engineering*. 15 April 2021. Vol. 211, p. 108636. DOI 10.1016/J.COMPOSITESB.2021.108636.
4. Cement – Analysis - IEA. Online. [Accessed 25 August 2022]. Available from: <https://www.iea.org/reports/cement>
5. ANDREW, Robbie M. Global CO2 emissions from cement production, 1928-2018. Online. [Accessed 25 August 2022]. DOI 10.5281/zenodo.831454.
6. TORRES-CARRASCO, M. and PUERTAS, F. La activación alcalina de diferentes aluminosilicatos como una alternativa al Cemento Portland: cementos activados alcalinamente o geopolímeros. *Revista Ingenieria de Construccion*. 2017. Vol. 32, no. 2, p. 5–12. DOI 10.4067/s0718-50732017000200001.
7. LUUKKONEN, Tero, ABDOLLAHNEJAD, Zahra, YLINIEMI, Juho, KINNUNEN, Paivo and ILLIKAINEN, Mirja. One-part alkali-activated materials: A review. *Cement and Concrete Research*. 1 January 2018. Vol. 103, p. 21–34. DOI 10.1016/J.CEMCONRES.2017.10.001.
8. PACHECO-TORGAL, F., ABDOLLAHNEJAD, Z., CAMÕES, A. F., JAMSHIDI, M. and DING, Y. Durability of alkali-activated binders: A clear advantage over Portland cement or an unproven issue? *Construction and Building Materials*. 1 May 2012. Vol. 30, p. 400–405. DOI 10.1016/J.CONBUILDMAT.2011.12.017.
9. MOHAMED, Osama Ahmed. A Review of Durability and Strength Characteristics of Alkali-Activated Slag Concrete. *Materials (Basel, Switzerland)*. Online. 2019. Vol. 12, no. 8. [Accessed 25 August 2022]. DOI 10.3390/MA12081198.
10. BAŠČAREVČ, Z. The resistance of alkali-activated cement-based binders to chemical attack. *Handbook of Alkali-Activated Cements, Mortars and Concretes*. 1 January 2015. P. 373–396. DOI 10.1533/9781782422884.3.373.
11. AIKEN, Timothy A., GU, Lei, KWASNY, Jacek, HUSEIEN, Ghasan F., MCPOLIN, Daniel and SHA, Wei. Acid resistance of alkali-activated binders: A review of performance, mechanisms of deterioration and testing procedures. *Construction and Building Materials*. 1 August 2022. Vol. 342, p. 128057. DOI 10.1016/J.CONBUILDMAT.2022.128057.
12. RUNCİ, Antonino and SERDAR, Marijana. Effect of curing time on the chloride diffusion of alkali-activated slag. *Case Studies in Construction Materials*. 1 June 2022. Vol. 16, p. e00927. DOI 10.1016/J.CSCM.2022.E00927.
13. BİNGÖL, Şinasi, BİLİM, Cahit, ATİŞ, Cengiz and DURAK, Uğur. Freeze-Thaw Resistance of Blast Furnace Slag Geopolymer Mortars. *Turkish Journal of Engineering*. 2020. Vol. 6, no. 1, p. 10–13. DOI 10.31127/tuje.810937.
14. PENG, Xi, LI, Han, SHUAI, Qin and WANG, Liancong. materials Fire Resistance of Alkali Activated Geopolymer Foams Produced from Metakaolin and Na<sub>2</sub>O<sub>2</sub>. Online. DOI 10.3390/ma13030535.
15. KARAHAN, Okan and YAKUPOĞLU, Aslan. Resistance of alkali-activated slag mortar to abrasion and fire. *Advances in Cement Research*. Online. 1 December 2011. Vol. 23, no. 6, p. 289–297. [Accessed 25 August 2022]. DOI 10.1680/ADCR.2011.23.6.289.

16. KUPWADE-PATIL, Kunal and ALLOUCHE, Erez N. Impact of Alkali Silica Reaction on Fly Ash-Based Geopolymer Concrete. *Journal of Materials in Civil Engineering*. 2013. Vol. 25, no. 1, p. 131–139. DOI 10.1061/(asce)mt.1943-5533.0000579.
17. PUERTAS, F., PALACIOS, M., GIL-MAROTO, A. and VÁZQUEZ, T. Alkali-aggregate behaviour of alkali-activated slag mortars: Effect of aggregate type. *Cement and Concrete Composites*. 1 May 2009. Vol. 31, no. 5, p. 277–284. DOI 10.1016/J.CEMCONCOMP.2009.02.008.
18. UPPALAPATI, Siva, VANDEWALLE, Lucie and CIZER, Özlem. Monitoring the setting process of alkali-activated slag-fly ash cements with ultrasonic P-wave velocity. *Construction and Building Materials*. Online. 2021. Vol. 271, no. xxxx, p. 121592. DOI 10.1016/j.conbuildmat.2020.121592.
19. ADESANYA, Elijah, ALADEJARE, Adeyemi, ADEDIRAN, Adeolu, LAWAL, Abiodun and ILLIKAINEN, Mirja. Predicting shrinkage of alkali-activated blast furnace-fly ash mortars using artificial neural network (ANN). *Cement and Concrete Composites*. 1 November 2021. Vol. 124, p. 104265. DOI 10.1016/J.CEMCONCOMP.2021.104265.
20. ALLAHVERDI, A., NAJAFI KANI, E., HOSSAIN, K. M.A. and LACHEMI, M. Methods to control efflorescence in alkali-activated cement-based materials. *Handbook of Alkali-Activated Cements, Mortars and Concretes*. 1 January 2015. P. 463–483. DOI 10.1533/9781782422884.3.463.
21. CHARITHA, V., ATHIRA, G., BAHURUDEEN, A. and SHEKHAR, Shivang. Carbonation of alkali activated binders and comparison with the performance of ordinary Portland cement and blended cement binders. *Journal of Building Engineering*. 1 August 2022. Vol. 53, p. 104513. DOI 10.1016/J.JOBE.2022.104513.
22. COLLINS, Frank and SANJAYAN, J. G. Cracking tendency of alkali-activated slag concrete subjected to restrained shrinkage. *Cement and Concrete Research*. 1 May 2000. Vol. 30, no. 5, p. 791–798. DOI 10.1016/S0008-8846(00)00243-X.
23. LI, Zhenming, ZHANG, Shizhe, LIANG, Xuhui and YE, Guang. Cracking potential of alkali-activated slag and fly ash concrete subjected to restrained autogenous shrinkage. *Cement and Concrete Composites*. 1 November 2020. Vol. 114, p. 103767. DOI 10.1016/J.CEMCONCOMP.2020.103767.
24. PROVIS, John L. Milestones in the analysis of alkali-activated binders. *Journal of Sustainable Cement-Based Materials*. 2015. Vol. 4, no. 2, p. 74–84. DOI 10.1080/21650373.2014.958599.
25. BUCHWALD, Anja, VANOOTEGHEM, Maarten, GRUYAERT, Elke, HILBIG, Harald and DE BELIE, Nele. Purdocement: application of alkali-activated slag cement in Belgium in the 1950s. *Materials and Structures/Materiaux et Constructions*. 2015. Vol. 48, no. 1–2, p. 501–511. DOI 10.1617/s11527-013-0200-8.
26. KOMNITSAS, Kostas and ZAHARAKI, Dimitra. Geopolymerisation: A review and prospects for the minerals industry. *Minerals Engineering*. 1 November 2007. Vol. 20, no. 14, p. 1261–1277. DOI 10.1016/J.MINENG.2007.07.011.
27. PACHECO-TORGAL, Fernando, CASTRO-GOMES, João and JALALI, Said. Alkali-activated binders: A review: Part 1. Historical background, terminology, reaction mechanisms and hydration products. *Construction and Building Materials*. 1 July 2008. Vol. 22, no. 7, p. 1305–1314. DOI 10.1016/J.CONBUILDMAT.2007.10.015.
28. JANOSEVIC, Natalija, DJORIC-VELJKOVIC, Snezana, TOPLICIC-CURCIC, Gordana and KARAMARKOVIC, Jugoslav. Properties of geopolymers. *Facta universitatis - series: Architecture and Civil Engineering*. 2018. Vol. 16, no. 1, p. 45–56. DOI 10.2298/fuace161226004j.
29. KRIVEN, Waltraud M. 5.9 Geopolymer-Based Composites. *Comprehensive Composite Materials II*. 1 January 2018. P. 269–280. DOI 10.1016/B978-0-12-803581-8.09995-1.

30. KONARIK, J. and BOHACOVA, J. Review of practical applications of alkali-activated systems in construction. *IOP Conference Series: Materials Science and Engineering*. 2018. Vol. 385, no. 1. DOI 10.1088/1757-899X/385/1/012030.
31. ŠKVÁRA, František. Alkali activated materials or geopolymers? *Ceramics - Silikaty*. 2007. Vol. 51, no. 3, p. 173–177.
32. AMER, Ismail, KOHAIL, Mohamed, EL-FEKY, M. S., RASHAD, Ahmed and KHALAF, Mohamed A. A review on alkali-activated slag concrete. *Ain Shams Engineering Journal*. 1 June 2021. Vol. 12, no. 2, p. 1475–1499. DOI 10.1016/J.ASEJ.2020.12.003.
33. PIATAK, Nadine M. and ETTLER, Vojtěch. CHAPTER 1 Introduction: Metallurgical Slags – Environmental Liability or Valuable Resource? Online. 4 August 2021. P. 1–13. [Accessed 25 August 2022]. DOI 10.1039/9781839164576-00001.
34. Lea's Chemistry of Cement and Concrete - Peter Hewlett - Google Книги. Online. [Accessed 26 August 2022]. Available from: [https://books.google.cz/books?id=v1JVu4iifnMC&pg=PA33&lpg=PA33&dq=which+is+defined+as+the+glassy+granular+material+formed+when+molten+blast-furnace+slag+is+rapidly+chilled+by+immersion+in+water&source=bl&ots=Yhw3R2RSuV&sig=ACfU3U2JFdAIXwC1mUbghRRjITYo\\_kMb3g&hl=ru&sa=X&ved=2ahUKEwiP3eLE\\_-L5AhUAxgIHHaWVB-sQ6AF6BAghEAM#v=onepage&q=which+is+defined+as+the+glassy+granular+material+formed+when+molten+blast-furnace+slag+is+rapidly+chilled+by+immersion+in+water&f=false](https://books.google.cz/books?id=v1JVu4iifnMC&pg=PA33&lpg=PA33&dq=which+is+defined+as+the+glassy+granular+material+formed+when+molten+blast-furnace+slag+is+rapidly+chilled+by+immersion+in+water&source=bl&ots=Yhw3R2RSuV&sig=ACfU3U2JFdAIXwC1mUbghRRjITYo_kMb3g&hl=ru&sa=X&ved=2ahUKEwiP3eLE_-L5AhUAxgIHHaWVB-sQ6AF6BAghEAM#v=onepage&q=which+is+defined+as+the+glassy+granular+material+formed+when+molten+blast-furnace+slag+is+rapidly+chilled+by+immersion+in+water&f=false)
35. EMERITUS, Taylor. Cement chemistry Book from Malin. *Cement and Concrete Composites*. Online. 1998. Vol. 20, no. 4, p. 335. [Accessed 26 August 2022]. Available from: [https://books.google.com/books/about/Cement\\_Chemistry.html?hl=ru&id=1BOETtwi7mMC](https://books.google.com/books/about/Cement_Chemistry.html?hl=ru&id=1BOETtwi7mMC)
36. NEWMAN, John and CHOO, Ban Seng. *Advanced Concrete Technology: Concrete Properties*. Online. 2003. [Accessed 26 August 2022]. ISBN 9780750656863. Available from: <http://www.sciencedirect.com/science/article/pii/B9780750656863502950>
37. MANJUNATH, R. and NARASIMHAN, Mattur C. Alkali-activated concrete systems: a state of art. *New Materials in Civil Engineering*. 1 January 2020. P. 459–491. DOI 10.1016/B978-0-12-818961-0.00013-2.
38. CARL, Bo. ECONOMIES OF SCALE AND TECHNOLOGICAL CHANGE: An International Comparison of Blast Furnace Technology. . 1975.
39. TAYLOR, H. F. W. (Harry F. W.). Cement chemistry. . 1997. P. 459.
40. ALDAWSARI, Salem, KAMPMANN, Raphael, HARNISCH, Jörg and ROHDE, Catharina. Setting Time , Microstructure , and Durability Properties of Low Calcium Fly Ash / Slag Geopolymer : A Review. . 2022. P. 1–25.
41. BELLMANN, F. and STARK, J. Activation of blast furnace slag by a new method. *Cement and Concrete Research*. 1 August 2009. Vol. 39, no. 8, p. 644–650. DOI 10.1016/J.CEMCONRES.2009.05.012.
42. NODEHI, Mehrab, VAHID, & and TAGHVAEE, Mohamad. Alkali-Activated Materials and Geopolymer: a Review of Common Precursors and Activators Addressing Circular Economy. *Circular Economy and Sustainability 2021 2:1*. Online. 5 June 2021. Vol. 2, no. 1, p. 165–196. [Accessed 27 August 2022]. DOI 10.1007/S43615-021-00029-W.
43. CHEN, W. Hydration of slag cement: theory, modeling and application. . 2006.
44. ELZEADANI, M., BOMPA, D.V. and ELGHAZOULI, A.Y. One part alkali activated materials: A state-of-the-art review. *Journal of Building Engineering*. Online. 1 October 2022. Vol. 57, p. 104871. [Accessed 27 August 2022]. DOI 10.1016/J.JOBE.2022.104871.
45. PALOMO, A., KRIVENKO, P., GARCIA-LODEIRO, I., KAVALEROVA, E., MALTSEVA, O. and FERNÁNDEZ-JIMÉNEZ, A. A review on alkaline activation: New analytical perspectives. *Materiales de Construcción*. 1 July 2014. Vol. 64, no. 315.

- DOI 10.3989/MC.2014.00314.
46. PACHECO-TORGAL, F., LABRINCHA, J. A., LEONELLI, C., PALOMO, A. and CHINDAPRASIRT, P. Handbook of Alkali-Activated Cements, Mortars and Concretes. *Handbook of Alkali-Activated Cements, Mortars and Concretes*. 3 November 2014. P. 1–830. DOI 10.1016/C2013-0-16511-7.
  47. KRIVENKO, P. Why alkaline activation - 60 years of the theory and practice of alkali-activated materials. *Journal of Ceramic Science and Technology*. 2017. Vol. 8, no. 3, p. 323–333. DOI 10.4416/JCST2017-00042.
  48. ROY, Amitava, SCHILLING, Paul J., EATON, Harvill C., MALONE, Philip G., BRABSTON, W. Newell and WAKELEY, Lillian D. Activation of Ground Blast-Furnace Slag by Alkali-Metal and Alkaline-Earth Hydroxides. *Journal of the American Ceramic Society*. Online. 1 December 1992. Vol. 75, no. 12, p. 3233–3240. [Accessed 27 August 2022]. DOI 10.1111/J.1151-2916.1992.TB04416.X.
  49. PUERTAS, F., PALACIOS, M., MANZANO, H., DOLADO, J. S., RICO, A. and RODRÍGUEZ, J. A model for the C-A-S-H gel formed in alkali-activated slag cements. *Journal of the European Ceramic Society*. 15 October 2011. Vol. 31, no. 12, p. 2043–2056. DOI 10.1016/J.JEURCERAMSOC.2011.04.036.
  50. XING, Jun, ZHAO, Yingliang, QIU, Jingping and SUN, Xiaogang. Microstructural and Mechanical Properties of Alkali Activated Materials from Two Types of Blast Furnace Slags. *Materials* 2019, Vol. 12, Page 2089. Online. 28 June 2019. Vol. 12, no. 13, p. 2089. [Accessed 27 August 2022]. DOI 10.3390/MA12132089.
  51. MYERS, Rupert J., BERNAL, Susan A., SAN NICOLAS, Rackel and PROVIS, John L. Generalized structural description of calcium-sodium aluminosilicate hydrate gels: The cross-linked substituted tobermorite model. *Langmuir*. Online. 30 April 2013. Vol. 29, no. 17, p. 5294–5306. [Accessed 27 August 2022]. DOI 10.1021/LA4000473/SUPPL\_FILE/LA4000473\_SI\_002.ZIP.
  52. KRIVENKO, P. V. and KOVALCHUK, G. Yu. Directed synthesis of alkaline aluminosilicate minerals in a geocement matrix. *Journal of Materials Science* 2007 42:9. Online. 22 February 2007. Vol. 42, no. 9, p. 2944–2952. [Accessed 27 August 2022]. DOI 10.1007/S10853-006-0528-3.
  53. JEGAN, Vasugi. *Strength and Durability Properties of Alkali Activated Slag and Fly Ash-Based Geopolymer Concrete*. Online. 1 January 2009. [Accessed 27 August 2022]. Available from:  
[https://www.academia.edu/925093/Strength\\_and\\_Durability\\_Properties\\_of\\_Alkali\\_Activated\\_Slag\\_and\\_Fly\\_Ash\\_Based\\_Geopolymer\\_Concrete](https://www.academia.edu/925093/Strength_and_Durability_Properties_of_Alkali_Activated_Slag_and_Fly_Ash_Based_Geopolymer_Concrete)
  54. ADAM, Andi Arham. Strength and Durability Properties of Alkali Activated Slag and Fly Ash-Based Geopolymer Concrete the degree of Doctor of Philosophy. *RMIT University Melbourne, Australia*. 2004. No. August.
  55. YI, Yaolin, AL-TABBAA, Abir and LISKA, Martin. Properties and microstructure of GGBS-magnesia pastes. *Advances in Cement Research*. 2014. Vol. 26, no. 2, p. 114–122. DOI 10.1680/adcr.13.00005.
  56. LI, Jing, YIN, Suhong, HUANG, Haoliang, HU, Jie, YI, Chaofan, CHEN, Zheng, MA, Yuwei, YE, Guang and YU, Qijun. Case Studies in Construction Materials Characterizing the effects of Al ( OH ) 3 and Mg ( OH ) 2 on reaction products and drying shrinkage characteristics of alkali-activated slag. *Case Studies in Construction Materials*. Online. 2022. Vol. 17, no. July, p. e01309. DOI 10.1016/j.cscm.2022.e01309.
  57. GENG, Guoqing, MYERS, Rupert J, LI, Jiaqi, MABOUDIAN, Roya, CARRARO, Carlo, SHAPIRO, David A and MONTEIRO, Paulo J M. Aluminum-induced dreierketten chain cross-links increase the mechanical properties of nanocrystalline calcium aluminosilicate hydrate. Online. 2017. DOI 10.1038/srep44032.

58. MOHAMED, Aslam Kunhi, MOUTZOURI, Pinelopi, BERRUYER, Pierrick, WALDER, Brennan J, SIRAMANONT, Jirawan, HARRIS, Maya, NEGRONI, Mattia, GALMARINI, Sandra C, PARKER, Stephen C, SCRIVENER, Karen L, EMSLEY, Lyndon and BOWEN, Paul. The Atomic-Level Structure of Cementitious Calcium Aluminate Silicate Hydrate. *J. Am. Chem. Soc.* Online. 2020. Vol. 142, p. 27. DOI 10.1021/jacs.0c02988.
59. HE, Juan, WU, Yonghua, YANG, Changhui, GAO, Qie and PU, Xiaolin. Effect of carbonation on properties of alkali-activated slag binders. *Revista Romana de Materiale/Romanian Journal of Materials*. 2018. Vol. 48, no. 3, p. 330–337.
60. CUESTA, Ana, SANTACRUZ, Isabel, DE LA TORRE, Angeles G., DAPIAGGI, Monica, ZEA-GARCIA, Jesus D. and ARANDA, Miguel A.G. Local structure and Ca/Si ratio in C-S-H gels from hydration of blends of tricalcium silicate and silica fume. *Cement and Concrete Research*. 1 May 2021. Vol. 143, p. 106405. DOI 10.1016/J.CEMCONRES.2021.106405.
61. TAYLOR, R., RICHARDSON, I. G. and BRYDSON, R. M.D. Composition and microstructure of 20-year-old ordinary Portland cement-ground granulated blast-furnace slag blends containing 0 to 100% slag. *Cement and Concrete Research*. July 2010. Vol. 40, no. 7, p. 971–983. DOI 10.1016/J.CEMCONRES.2010.02.012.
62. BROUGH, A. R. and ATKINSON, A. Sodium silicate-based, alkali-activated slag mortars - Part I. Strength, hydration and microstructure. *Cement and Concrete Research*. 2002. Vol. 32, no. 6, p. 865–879. DOI 10.1016/S0008-8846(02)00717-2.
63. C. SHI, R.L. Day. Day A calorimetric study of early hydration of alkali.pdf. *Cement and Concrete Research*. 1995. Vol. 25, no. 6, p. 1333–1346.
64. MARCHON, D. and FLATT, Robert J. Mechanisms of cement hydration. *Science and Technology of Concrete Admixtures*. 2016. P. 129–145. DOI 10.1016/B978-0-08-100693-1.00008-4.
65. HONG, Sung Yoon and GLASSER, F. P. Alkali sorption by C-S-H and C-A-S-H gels: Part II. Role of alumina. *Cement and Concrete Research*. 2002. Vol. 32, no. 7, p. 1101–1111. DOI 10.1016/S0008-8846(02)00753-6.
66. BERNAL, Susan A, PROVIS, John L, ROSE, Volker and MEJIA DE GUTIERREZ, Ruby. High-Resolution X-ray Diffraction and Fluorescence Microscopy Characterization of Alkali-Activated Slag-Metakaolin Binders. . 2013. DOI 10.1111/jace.12247.
67. JIANG, Tao, JIN, Ying and YE, Hailong. Correlating slag chemistry to setting and mechanical behaviors of alkali-activated slag. *Construction and Building Materials*. 4 July 2022. Vol. 338, p. 127661. DOI 10.1016/J.CONBUILDMAT.2022.127661.
68. KAR, Arkamitra, RAY, Indrajit, HALABE, Udaya B., UNNIKRIISHNAN, Avinash and DAWSON-ANDOH, Ben. Characterizations and Quantitative Estimation of Alkali-Activated Binder Paste from Microstructures. *International Journal of Concrete Structures and Materials*. 2014. Vol. 8, no. 3, p. 213–228. DOI 10.1007/s40069-014-0069-0.
69. RICHARDSON, I. G., SKIBSTED, J., BLACK, L. and KIRKPATRICK, R. J. Characterisation of cement hydrate phases by TEM, NMR and Raman spectroscopy. *Advances in Cement Research*. 2010. Vol. 22, no. 4, p. 233–248. DOI 10.1680/adcr.2010.22.4.233.
70. KIRKPATRICK, R. James, YARGER, J.L., MCMILLAN, Paul F., PING, Yu and CONG, Xiandong. Raman spectroscopy of C-S-H, tobermorite, and jennite. *Advanced Cement Based Materials*. April 1997. Vol. 5, no. 3–4, p. 93–99. DOI 10.1016/S1065-7355(97)00001-1.
71. PILLAY, Deveshan L, OLALUSI, Oladimeji B, AWOYERA, Paul O, RONDON, Carlos, MARÍA ECHEVERRÍA, Ana and KOLAWOLE, John Temitope. A Review of the Engineering Properties of Metakaolin Based Concrete: Towards Combatting Chloride Attack in Coastal/ Marine Structures. Online. 2020. DOI 10.1155/2020/8880974.
72. KHATIB, Jamal M., BAALBAKI, Oussama and ELKORDI, Adel A. Metakaolin. *Waste and Supplementary Cementitious Materials in Concrete: Characterisation, Properties and*

- Applications*. 1 January 2018. P. 493–511. DOI 10.1016/B978-0-08-102156-9.00015-8.
73. LI, Chao, SUN, Henghu and LI, Longtu. A review: The comparison between alkali-activated slag (Si + Ca) and metakaolin (Si + Al) cements. *Cement and Concrete Research*. 1 September 2010. Vol. 40, no. 9, p. 1341–1349. DOI 10.1016/J.CEMCONRES.2010.03.020.
  74. WILSON, I. R. and JIRANEK, J. Kaolin deposits of the Czech Republic and some comparisons with south-west England. *Geoscience in South-West England*. 1995. Vol. 8, no. 4, p. 357–362.
  75. SOURI, Alireza, KAZEMI-KAMYAB, Hadi, SNELLINGS, Ruben, NAGHIZADEH, Rahim, GOLESTANI-FARD, Farhad and SCRIVENER, Karen. Pozzolanic activity of mechanochemically and thermally activated kaolins in cement. *Cement and Concrete Research*. 1 November 2015. Vol. 77, p. 47–59. DOI 10.1016/J.CEMCONRES.2015.04.017.
  76. GEOPOLYMER INSTITUTE, 16 rue Galilée, 02100 Saint-Quentin, France. Geopolymers: Ceramic-Like Inorganic Polymers. *Journal of Ceramic Science and Technology*. 2017. Vol. 8, no. 3, p. 335–350. DOI 10.4416/JCST2017-00038.
  77. ABDELMAWLA, Mohammed. Production of Geopolymer Materials from Solid Wastes of Drinking Water Treatment Plants and Alum Industry Production of Geopolymer Materials from Solid Wastes of Drinking Water Treatment Plants and Alum Industry Submitted by A Thesis Submitted in Partial . . 2021. No. July. DOI 10.13140/RG.2.2.26363.03364.
  78. YAO, Xiao, ZHANG, Zuhua, ZHU, Huajun and CHEN, Yue. Geopolymerization process of alkali–metakaolinite characterized by isothermal calorimetry. *Thermochimica Acta*. 10 September 2009. Vol. 493, no. 1–2, p. 49–54. DOI 10.1016/J.TCA.2009.04.002.
  79. ROCHA, Fernando, ALSHAAER, Mazen, CAO, Rongchuan, FANG, Zheng, JIN, Man and SHANG, Yu. minerals Study on the Activity of Metakaolin Produced by Traditional Rotary Kiln in China. Online. 2022. DOI 10.3390/min12030365.
  80. TCHADJIE, L N and EKOLU, S O. Enhancing the reactivity of aluminosilicate materials toward geopolymer synthesis. *Journal of Materials Science*. Online. 1907. Vol. 53. DOI 10.1007/s10853-017-1907-7.
  81. HA, Miae. MECHANICAL PROPERTIES OF SODIUM AND POTASSIUM ACTIVATED METAKAOLIN-BASED GEOPOLYMERS. . 2010.
  82. ADESANYA, Elijah, PERUMAL, Priyadarshini, LUUKKONEN, Tero, YLINIEMI, Juho, OHENOJA, Katja, KINNUNEN, Paivo and ILLIKAINEN, Mirja. Opportunities to improve sustainability of alkali-activated materials: A review of side-stream based activators. *Journal of Cleaner Production*. 1 March 2021. Vol. 286, p. 125558. DOI 10.1016/J.JCLEPRO.2020.125558.
  83. ZHANG, Xuanhan, LONG, Kaidi, LIU, Wei, LI, Lixiao and LONG, Wu Jian. Carbonation and Chloride Ions' Penetration of Alkali-Activated Materials: A Review. *Molecules (Basel, Switzerland)*. 2020. Vol. 25, no. 21. DOI 10.3390/molecules25215074.
  84. Water Glass - Introduction, Formula, Properties and Uses. Online. [Accessed 31 August 2022]. Available from: <https://www.vedantu.com/chemistry/water-glass>
  85. AYDIN, Serdar and BARADAN, Bülent. Effect of activator type and content on properties of alkali-activated slag mortars. *Composites Part B: Engineering*. 1 February 2014. Vol. 57, p. 166–172. DOI 10.1016/J.COMPOSITESB.2013.10.001.
  86. MITHUN, B M and NARASIMHAN, Mattur C. SELF-Cured Alkali Activated Slag Concrete Mixes- An Experimental Study. *International Scholarly and Scientific Research & Innovation*. Online. 2014. Vol. 8, no. 4, p. 472–477. Available from: <http://waset.org/publications/9998644/self-cured-alkali-activated-slag-concrete-mixes-an-experimental-study>
  87. TORRES-CARRASCO, M. and PUERTAS, F. Waste glass as a precursor in alkaline activation: Chemical process and hydration products. *Construction and Building Materials*.

- 15 May 2017. Vol. 139, p. 342–354. DOI 10.1016/J.CONBUILDMAT.2017.02.071.
88. CRIADO, M., FERNÁNDEZ-JIMÉNEZ, A., PALOMO, A., SOBRADOS, I. and SANZ, J. Effect of the SiO<sub>2</sub>/Na<sub>2</sub>O ratio on the alkali activation of fly ash. Part II: <sup>29</sup>Si MAS-NMR Survey. *Microporous and Mesoporous Materials*. 1 March 2008. Vol. 109, no. 1–3, p. 525–534. DOI 10.1016/J.MICROMESO.2007.05.062.
  89. DAVIDOVITS, Joseph. *Geopolymer Chemistry and Applications. 5-th edition.* . 2020. ISBN 9782954453118.
  90. YANG, Xiaohong, ZHU, Weiling and YANG, Qiao. The viscosity properties of sodium silicate solutions. *Journal of Solution Chemistry*. 2008. Vol. 37, no. 1, p. 73–83. DOI 10.1007/s10953-007-9214-6.
  91. Design and Control of Concrete Mixtures N EB001. Online. Available from: <https://www.cement.org/Learn/concrete-technology/concrete-design-production/design-and-control-mixtures-landing-page>
  92. DRANSFIELD, John. Admixtures for concrete, mortar and grout. *Advanced Concrete Technology*. 1 January 2003. P. 3–36. DOI 10.1016/B978-075065686-3/50280-9.
  93. ČSN EN 206-1 (732403). Online. [Accessed 31 August 2022]. Available from: <https://www.technicke-normy-csn.cz/csn-en-206-1-732403-223199.html>
  94. AÏTCIN, Pierre Claude and FLATT, Robert J. Science and technology of concrete admixtures. *Science and Technology of Concrete Admixtures*. 1 January 2015. P. 1–613. DOI 10.1016/C2015-0-00150-2.
  95. IS 9103. Specification for Concrete Admixtures. *Bureau of Indian Standards, New Dehli*. 1999. P. 1–22.
  96. MYRDAL, Roar. *Accelerating admixtures for concrete*. Online. 2007. ISBN 9788253609898. Available from: [https://www.researchgate.net/publication/288883755\\_Accelerating\\_admixtures\\_for\\_concrete](https://www.researchgate.net/publication/288883755_Accelerating_admixtures_for_concrete)
  97. ALSADEY, Salahaldeen. Effects of super plasticizing Admixture on Properties of Concrete. *Conference on Transport, Environment and Civil*. Online. 2012. No. November, p. 132–134. DOI 10.15242/II.E1213607.
  98. Chemical Admixtures. Online. [Accessed 31 August 2022]. Available from: <https://www.cement.org/cement-concrete/concrete-materials/chemical-admixtures>
  99. SINGH, Surender and UPASANA, Ms. Different Types of Admixtures in Concrete Structure - a Review. *International Conference on Recent Innovations in Science, Agriculture, Engineering and Management*. 2017. P. 1459–1466.
  100. ERDOĞDU, Şakir. Effect of retempering with superplasticizer admixtures on slump loss and compressive strength of concrete subjected to prolonged mixing. *Cement and Concrete Research*. 2005. Vol. 35, no. 5, p. 907–912. DOI 10.1016/j.cemconres.2004.08.020.
  101. DIAB, Ahmed M., ELYAMANY, Hafez E. and ALI, Ali Hassan. Experimental investigation of the effect of latex solid/water ratio on latex modified co-matrix mechanical properties. *Alexandria Engineering Journal*. 1 March 2013. Vol. 52, no. 1, p. 83–98. DOI 10.1016/J.AEJ.2012.11.002.
  102. HILAL, B El, KHUDHAIR, M H and HARFI, A El. Review on different families of polymeric superplasticizers used as adjuvants in the cementitious materials in civil engineering. / *Appl. J. Envir. Eng. Sci*. 2018. Vol. 4, p. 158–170.
  103. OHAMA, Yoshihiko. Polymer-based admixtures. *Cement and Concrete Composites*. 1 January 1998. Vol. 20, no. 2–3, p. 189–212. DOI 10.1016/S0958-9465(97)00065-6.
  104. COMMITTEE, A C I. Report on Polymer-Modified Concrete. .
  105. LI, Z., CHAU, C. K. and LI, F. Effects of the natural polymer-based durability-enhancing admixture on the frost resistance of concrete. <http://dx.doi.org/10.1680/macrc.2001.53.2.73>. Online. 25 May 2015. Vol. 53, no. 2, p. 73–84. [Accessed 31 August 2022].

- DOI 10.1680/MACR.2001.53.2.73.
106. ION, Ioana, BARROSO AGUIAR, José, ANGELESCU, Nicolae and STANCIU, Darius. Properties of Polymer Modified Concrete in Fresh and Hardened State. *Advanced Materials Research*. Online. 2013. Vol. 687, p. 204–212. [Accessed 31 August 2022]. DOI 10.4028/WWW.SCIENTIFIC.NET/AMR.687.204.
  107. KISHORE, Kaushal. Polymer-Modified Mortars And Concrete Mix Design. *Engineer, Materials*. 2012. P. 1–8.
  108. ANDERSON, M., FOWLER, D., SAWANT, S., VIPULANANDAN, C., BALL, J. C., GAUL, R., SCHMIDT, D., VOGT, R., BARTHOLOMEW, J., KHAN, Mohammad S., SHENG, Q., WAHBY, W., BODEA, C., MARUSIN, S., SMOAK, W. G., WALTERS, D., DEPUY, G., MCELROY, J. A., SOLOMON, J., WEBER, H., DIKEOU, J., MENDIS, P., SOUTHWORTH, George L., WHITE, D., DIMMICK, F. E., MILLIRON, R., SPRINKEL, M., WHITNEY, D., WEINBERG, R., FALLIS, PRUSINSKI, R., TIAN, B., YANG, Philip Y., FARRELL, Larry J., TAHA, M., TRAGIANESE, Donald P., ZMIGRODZKI, S., FONTANA, J., KAEDING, A., CHAIR and MAASS, J. Polymer-Modified Concrete ACI 548 . 3 R-03 Reported by ACI Committee 548. *undefined*. 2003.
  109. WAGNER, Herman B. and GRENLEY, Dallas G. Interphase effects in polymer-modified hydraulic cements. *Journal of Applied Polymer Science*. Online. 1 March 1978. Vol. 22, no. 3, p. 813–822. [Accessed 31 August 2022]. DOI 10.1002/APP.1978.070220318.
  110. FELTON, Linda A. Mechanisms of polymeric film formation. *International Journal of Pharmaceutics*. 5 December 2013. Vol. 457, no. 2, p. 423–427. DOI 10.1016/J.IJPHARM.2012.12.027.
  111. KUJAWA, Weronika, OLEWNIK-KRUSZKOWSKA, Ewa and NOWACZYK, Jacek. Concrete strengthening by introducing polymer-based additives into the cement matrix-a mini review. *Materials*. 2021. Vol. 14, no. 20. DOI 10.3390/ma14206071.
  112. BEAN, Dennis L and HUSBANDS, Tony B. TECHNICAL REPORT REMR-CS-3 LATEX ? uJIV11XTURES t-OR PORTLAND CEMENT CONCRETE AND IViORTAR by Waterways Experiment Station , Corps of Engineers US Army Corps of Engineers. . 1986.
  113. JAMSHIDI, M., PAKRAVAN, H. R. and POURKHORSHIDI, A. R. Application of polymer admixtures to modify concrete properties: Effects of polymer type and content. *Asian Journal of Civil Engineering*. 2014. Vol. 15, no. 5, p. 779–787.
  114. *conference\_agm\_1983.pdf*.
  115. JAMSHIDI, Masoud, PAKRAVAN, Hamid Reza and ZOJAJI, Koosha. Correlation between water permeability of latex-modified concrete (LMC) and water diffusion coefficient of latex film. *Iranian Polymer Journal (English Edition)*. 2013. Vol. 22, no. 11, p. 799–809. DOI 10.1007/s13726-013-0179-6.
  116. YANG, Zhengxian, SHI, Xianming, CREIGHTON, Andrew T. and PETERSON, Marijean M. Effect of styrene–butadiene rubber latex on the chloride permeability and microstructure of Portland cement mortar. *Construction and Building Materials*. Online. 2009. Vol. 23, no. 6, p. 2283–2290. [Accessed 31 August 2022]. Available from: [https://www.academia.edu/7496583/Effect\\_of\\_styrene\\_butadiene\\_rubber\\_latex\\_on\\_the\\_chloride\\_permeability\\_and\\_microstructure\\_of\\_Portland\\_cement\\_mortar](https://www.academia.edu/7496583/Effect_of_styrene_butadiene_rubber_latex_on_the_chloride_permeability_and_microstructure_of_Portland_cement_mortar)
  117. MARTIN, J.W. Organic polymeric materials. *Materials for Engineering*. 1 January 2006. P. 159–184. DOI 10.1533/9781845691608.2.159.
  118. LI, Lin, WANG, Ru and LU, Qinyuan. Influence of polymer latex on the setting time, mechanical properties and durability of calcium sulfoaluminate cement mortar. *Construction and Building Materials*. 30 April 2018. Vol. 169, p. 911–922. DOI 10.1016/J.CONBUILDMAT.2018.03.005.
  119. BIN MOBARAK, Mashrafi, HOSSAIN, Md Sahadat, MAHMUD, Monika and AHMED, Samina. Redispersible polymer powder modified cementitious tile adhesive as an alternative

- to ordinary cement-sand grout. *Heliyon*. 2021. Vol. 7, no. 11. DOI 10.1016/j.heliyon.2021.e08411.
120. MAYHOUB, Ola A., ABADEL, Aref A., ALHARBI, Yousef R., NEHDI, Moncef L., DE AZEVEDO, Afonso R. G. de and KOHAIL, Mohamed. Effect of Polymers on Behavior of Ultra-High-Strength Concrete. *Polymers*. 2022. Vol. 14, no. 13, p. 2585. DOI 10.3390/polym14132585.
  121. AFRIDI, M. U.K., OHAMA, Y., IQBAL, M. Zafar and DEMURA, K. Water retention and adhesion of powdered and aqueous polymer-modified mortars. *Cement and Concrete Composites*. 1 January 1995. Vol. 17, no. 2, p. 113–118. DOI 10.1016/0958-9465(95)00007-Y.
  122. GEMERT, Dionys Van. Water-soluble polymers for modification of cement mortars. Online. [Accessed 31 August 2022]. Available from: [https://www.academia.edu/19556092/Water\\_soluble\\_polymers\\_for\\_modification\\_of\\_cement\\_mortars](https://www.academia.edu/19556092/Water_soluble_polymers_for_modification_of_cement_mortars)
  123. FU, Xuli and CHUNG, D. D.L. Effect of methylcellulose admixture on the mechanical properties of cement. *Cement and Concrete Research*. 1996. Vol. 26, no. 4, p. 535–538. DOI 10.1016/0008-8846(96)00028-2.
  124. CHU, T. J., ROBERTSON, R. E., NAJM, H. and NAAMAN, A. E. Effects of poly(vinyl alcohol) on fiber cement interfaces. Part II: Microstructures. *Advanced Cement Based Materials*. 1 March 1994. Vol. 1, no. 3, p. 122–130. DOI 10.1016/1065-7355(94)90043-4.
  125. BALDISSERA, Alessandra F., SCHÜTZ, Marta K., VECCHIA, Felipe D., SEFERIN, Marcus, LIGABUE, Rosane, MENEZES, Sonia C. and EINLOFT, Sandra. Epoxy-modified Portland Cement: Effect of the Resin Hardener on the Chemical Degradation by Carbon Dioxide. *Energy Procedia*. 1 July 2017. Vol. 114, p. 5256–5265. DOI 10.1016/J.EGYPRO.2017.03.1682.
  126. LUKOWSKI, P. and ADAMCZEWSKI, G. Self-repairing of polymer-cement concrete. *Bulletin of the Polish Academy of Sciences: Technical Sciences*. 2013. Vol. 61, no. 1, p. 195–200. DOI 10.2478/bpasts-2013-0018.
  127. SWAMY, R N and BOUIKNI, A. SOME ENGINEERING PROPERTIES OF SLAG CONCRETE AS INFLUENCED BY MIX PROPORTIONING AND CURING. *ACI Materials Journal*. May 1990. Vol. 87, no. 3.
  128. Superplasticizers: Properties and Applications in Concrete. Online. [Accessed 31 August 2022]. Available from: [https://www.researchgate.net/publication/44066467\\_Superplasticizers\\_Properties\\_and\\_Applications\\_in\\_Concrete](https://www.researchgate.net/publication/44066467_Superplasticizers_Properties_and_Applications_in_Concrete)
  129. BAKHAREV, T., SANJAYAN, J. G. and CHENG, Y. B. Effect of admixtures on properties of alkali-activated slag concrete. *Cement and Concrete Research*. 1 September 2000. Vol. 30, no. 9, p. 1367–1374. DOI 10.1016/S0008-8846(00)00349-5.
  130. PALACIOS, M. and PUERTAS, F. Effect of shrinkage-reducing admixtures on the properties of alkali-activated slag mortars and pastes. *Cement and Concrete Research*. 1 May 2007. Vol. 37, no. 5, p. 691–702. DOI 10.1016/J.CEMCONRES.2006.11.021.
  131. BILIM, Cahit, KARAHAN, Okan, ATIŞ, Cengiz Duran and İLKENTAPAR, Serhan. Effects of chemical admixtures and curing conditions on some properties of alkali-activated cementless slag mixtures. *KSCE Journal of Civil Engineering*. 2015. Vol. 19, no. 3, p. 733–741. DOI 10.1007/s12205-015-0629-0.
  132. BÍLEK, Vlastimil, KALINA, Lukáš and FOJTÍK, Ondrej. Shrinkage-Reducing Admixture Efficiency in Alkali-Activated Slag across the Different Doses of Activator. *Key Engineering Materials*. Online. 2018. Vol. 761, p. 19–22. [Accessed 31 August 2022]. DOI 10.4028/WWW.SCIENTIFIC.NET/KEM.761.19.
  133. Fly ash based geopolymers concrete | Request PDF. Online. [Accessed 31 August 2022].

Available from:

- [https://www.researchgate.net/publication/290857231\\_Fly\\_ash\\_based\\_geopolymer\\_concrete](https://www.researchgate.net/publication/290857231_Fly_ash_based_geopolymer_concrete)
134. COLANGELO, Francesco, ROVIELLO, Giuseppina, RICCIOTTI, Laura, FERONE, Claudio and CIOFFI, Raffaele. Preparation and characterization of new geopolymer-epoxy resin hybrid mortars. *Materials*. 2013. Vol. 6, no. 7, p. 2989–3006. DOI 10.3390/ma6072989.
  135. View of Properties of fly ash and metakaolín based geopolymer panels under fire resistance tests | *Materiales de Construcción*. Online. [Accessed 31 August 2022]. Available from: <https://materconstrucc.revistas.csic.es/index.php/materconstrucc/article/view/1794/2194>
  136. GIANNOPOULOU, Ioanna and PANIAS, Dimitrios. Structure, Design and Applications of Geopolymeric Materials. *3rd International Conference on Deformation Processing and Structure of Materials*. Online. 2007. No. 636876, p. 8. Available from: <https://www.researchgate.net/publication/234107877>
  137. FERONE, Claudio, ROVIELLO, Giuseppina, COLANGELO, Francesco, CIOFFI, Raffaele and TARALLO, Oreste. Novel hybrid organic-geopolymer materials. *Applied Clay Science*. 1 March 2013. Vol. 73, no. 1, p. 42–50. DOI 10.1016/J.CLAY.2012.11.001.
  138. KING, Rj. Dynamic mechanical properties of resilin. Online. 2010. Available from: [http://www2.esm.vt.edu/~dmdudek/King\\_RJ\\_Thesis\\_2010.pdf](http://www2.esm.vt.edu/~dmdudek/King_RJ_Thesis_2010.pdf)
  139. CATAURO, Michelina, PAPALE, Ferdinando, LAMANNA, Giuseppe and BOLLINO, Flavia. Geopolymer/PEG hybrid materials synthesis and investigation of the polymer influence on microstructure and mechanical behavior. *Materials Research*. 2015. Vol. 18, no. 4, p. 698–705. DOI 10.1590/1516-1439.342814.
  140. TOMORROW, Creating. CONSTRUCTION I POLYMER POWDERS I MEA PRODUCT OVERVIEW POLYMER POWDERS THE FAST TRACK – .
  141. Peramin® SRA - shrinkage reducers from Imerys. Online. [Accessed 31 August 2022]. Available from: <https://www.imerys.com/product-ranges/peramin-sra>
  142. PUERTAS, F. Cementos de escorias activadas alcalinamente: Situación actual y perspectivas de futuro. *Materiales de Construcción*. 1995. Vol. 45, no. 239, p. 53–64. DOI 10.3989/mc.1995.v45.i239.553.
  143. GUNASEKARAN, S, ANBALAGAN, G and PANDI, S. Raman and infrared spectra of carbonates of calcite structure. *JOURNAL OF RAMAN SPECTROSCOPY J. Raman Spectrosc.* Online. 2006. Vol. 37, p. 892–899. DOI 10.1002/jrs.1518.
  144. KIRKPARTICK, R. James, YARGER, J. L., MCMILLAN, Paul F., YU, Ping and CONG, Xiandong. Raman spectroscopy of C-S-H, tobermorite, and jennite. *Advanced Cement Based Materials*. 1 April 1997. Vol. 5, no. 3–4, p. 93–99. DOI 10.1016/S1065-7355(97)00001-1.
  145. TORRES-CARRASCO, M., DEL CAMPO, A., DE LA RUBIA, M. A., REYES, E., MORAGUES, A. and FERNÁNDEZ, J. F. New insights in weathering analysis of anhydrous cements by using high spectral and spatial resolution Confocal Raman Microscopy. *Cement and Concrete Research*. 1 October 2017. Vol. 100, p. 119–128. DOI 10.1016/J.CEMCONRES.2017.06.003.
  146. BERNAL, Susan A., PROVIS, John L., WALKLEY, Brant, SAN NICOLAS, Rackel, GEHMAN, John D., BRICE, David G., KILCULLEN, Adam R., DUXSON, Peter and VAN DEVENTER, Jannie S.J. Gel nanostructure in alkali-activated binders based on slag and fly ash, and effects of accelerated carbonation. *Cement and Concrete Research*. 1 November 2013. Vol. 53, p. 127–144. DOI 10.1016/J.CEMCONRES.2013.06.007.
  147. HIGL, J., KÖHLER, M. and LINDÉN, M. Confocal Raman microscopy as a non-destructive tool to study microstructure of hydrating cementitious materials. *Cement and Concrete Research*. 2016. Vol. 88, p. 136–143. DOI 10.1016/j.cemconres.2016.07.005.

148. SHI, Caijun, ROY, Della and KRIVENKO, Pavel. Alkali-Activated Cements and Concretes. *Alkali-Activated Cements and Concretes*. Online. 2 April 2003. [Accessed 30 August 2022]. DOI 10.1201/9781482266900.

## **LIST OF USED ABBREVIATIONS**

**AAA** – Alkali activated aluminosilicates

**AAS** – Alkali activated slag

**AAM** – Alkali activated materials

**OPC** – Ordinary Portland Cement

**PEG** – Polyethylene glycol

**PPG** – Polypropylene glycol

**PC** – Portland Cement

**IR** - Infra Red spectroscopy

**FTIR** – Fourier-transform infrared spectroscopy

**GGBS** – Ground Granulated Blast-Furnace Slag

**CRM** – Confocal Ramam Spectroscopy

**REF** – Reference

**XRD** – X-ray diffraction

**DTA** – Thermogravimetry

## LIST OF SELECTED PUBLICATIONS

MIKHAILOVA, O.; ROVNANÍK, P. Effect of polyethylene glycol on the rheological properties and heat of hydration of alkali activated slag pastes. In *Construmat 2018. IOP Conference Series: Materials Science and Engineering*. IOP Publishing Ltd, 2018. p. 1-6. ISSN: 1757-8981.

MIKHAILOVA, O.; ROVNANÍK, P. Effect of polyethylene glycol addition on metakaolin-based geopolymer. In *International Conference on Ecology and new Building materials and products, ICEBMP 2016. Procedia Engineering*. Elsevier, 2016. p. 222-228. ISSN: 1877-7058.

MIKHAILOVA, O.; DEL CAMPO, A.; ROVNANÍK, P.; FERNÁNDEZ, J.; TORRES-CARRASCO, M. In situ characterization of main reaction products in alkali-activated slag materials by Confocal Raman Microscopy. *CEMENT & CONCRETE COMPOSITES*, 2019, vol. 99, no. 1, p. 32-39. ISSN: 0958-9465.

MIKHAILOVA, O.; ROVNANÍK, P. Effect of polymer admixtures on alkali-activated slag mortars. In *Ecological and New Building Materials and Products. Advanced Materials Research*. Switzerland: Trans Tech Publications, 2015. p. 145-150. ISBN: 978-3-03835-587-8. ISSN: 1022-6680.

MIKHAILOVA, O.; ROVNANÍK, P. Effect of polymer admixtures on metakaolin-based geopolymer. In *14th International Conference Silicate Binders, ICBM 2015. Materials Science Forum*. Switzerland: Trans Tech Publications, 2016. p. 67-71. ISBN: 9783038357407. ISSN: 0255-5476.

ROVNANÍK, P.; MIKHAILOVA, O. Influence of polymer admixtures on the rheological properties and heat of hydration of alkali activated slag pastes. In *Solid State Phenomena. Solid State Phenomena*. Switzerland: Trans Tech Publications Ltd, 2018. p. 217-222. ISBN: 978-30-3571-348-0. ISSN: 1662-9779.

MIKHAILOVA, O.; ROVNANÍK, P. Stability of Polymer Admixtures in Alkaline Media. In *Binders, Materials and Technologies in Modern Construction III. Materials Science Forum*. Switzerland: Trans Tech Publications, 2017. p. 145-153. ISBN: 978-3-0357-1157-8. ISSN: 0255-5476.

MIKHAILOVA, O.; ROVNANÍK, P. Study of Metakaolin-Based Geopolymer with Addition of Polymer Admixtures. In *World Academy of Science, Engineering and Technology conference proceedings. World Academy of Science, Engineering and Technology*. 18. Rome, Italy: International Scholarly and Scientific Research & Innovation, 2016. p. 1308-1311. ISSN: 2010-376X.

MIKHAILOVA, O.; ŠIMONOVÁ, H.; TOPOLÁŘ, L.; ROVNANÍK, P. *The Effect of the Organic Additives on the Mechanical Fracture Properties and Shrinkage of Alkali Activated Slag Mortars*. 24th International Conference on materials and Technology. Ljubljana, Slovenia: 2016. p. 155-155. ISBN: 978-961-94088-0-3.

MIKHAILOVA, O.; ROVNANÍK, P. Effect of organic additives on shrinkage of AAS mortars. In *NDT konference v České republice 2015*. Brno: Brno University of Technology and CNDT, 2016. p. 25-30. ISBN: 978-80-214-5315-9.

## ABOUT AUTHOR

### Olesia Mikhailova

Date of birth: January 14, 1989

e-mail: mikhailova.o@fce.vutbr.cz

phone: +420 777959976

Institute of Chemistry, Faculty of Civil Engineering, Brno University of Technology Veveří 331/95  
602 00 Brno · Czech Republic

### WORK EXPERIENCE

**2/2014 – present** Ph.D. Student, Brno University of Technology, Faculty of Civil Engineering, Institute of Chemistry, study field: Physical and Building Materials Engineering (Ph.D. program: Building Materials Engineering);

**8/2022 – present** Office Assistant, Mirai Intex s.r.o.

**7/2018 – 7/2020** Researcher–Technologist, University of Pardubice, Faculty of Restoration, Department of Chemical Technology (part-time), Project “*New composite materials for the restoration of 20th-century architecture*”.

### EDUCATION

**9/2012 - 2/2014** Brno University of Technology, Faculty of Civil Engineering, Institute Of Technology Of Building Materials And Components, Master's degree in Civil Engineering, Thesis “*Research of Effective Use and Activation of Active Concrete Additions*”

**9/2010 – 6/2012** Izhevsk State Technical University, Faculty of Civil Engineering, Bachelor's degree in Civil Engineering, Thesis “*Modification of Portland cement without additives by finely milled dolomitized limestone*”

### INTERNATIONAL and LOCAL ACTIVITIES

**9/2017 – 12/2017** Ceramic and Glass Institute (ICV-CSIC), Madrid, Spain, Erasmus+ Internship

**4/2018 – 5/2018** The Czech Academy of Science – Institute of Theoretical and Applied Mechanics/Centre of Excellence Telč Internship Prague Institute, Internship, Participation in the project 18-26056Y GAČR

### SKILLS

Languages: Russian (native speaker), Czech (advanced), English (advanced), Spanish (basic)

### INTERESTS

Dancing, travelling, languages